ELECTROCHEMICAL STUDY OF ELECTRODE SUPPORT MATERIAL FOR DIRECT METHANOL FUEL CELL APPLICATIONS

A thesis submitted in fulfilment of the requirements for the degree of

Magister Scientiae

Presented to the Department of Chemistry

at the University of the Western Cape (South Africa) by

Andisiwe Bangisa

Supervisor: Dr. Lindiwe Khotseng

November 2013

Declaration

I hereby declare that I am the original author of "Electrochemical Study of Electrode Support Material for Direct Methanol Fuel Cell Applications" with the help of no more than the mentioned literature and auxiliary means.

To the best of the researcher's knowledge, this study has not been published or presented at any other examination office in the same or similar shape.

University of the Western Cape, November 2013

place and date

Signature (Andisiwe Bangisa)

Abstract

This study focused on binary PtRu and PtSn electrocatalyst, synthesized using the polyol approach and supported on MWCNTs, TiO_2 and MoO_2 materials, after synthesis part of the resultant electrocatalyst was heat treated to improve alloying of the secondary metal to the primary platinum metal catalyst and also to enhance the stable distribution and uniform dispersion of the nanoparticles on the support material. Physical characterization of the supported catalyst was done using XRD, HRTEM, HRSEM and EDS for elemental analysis. For electrochemical characterization RDE-CV and RDE-LSV were employed. The home-prepared electro-catalysts were then compared to the Pt/C, PtRu/C and PtSn/C commercial electro-catalysts accordingly.

XRD confirmed that the binary electro-catalyst for both the commercial and home-prepared display characteristic patterns similar to that of the standard Pt/C electro-catalyst, an indication that all catalysts have prevailed the Pt face-centred-cubic (fcc) crystal structure. Particle size and size distribution examined using HRTEM showed that Pt/C and PtSn/C was uniformly dispersed on the carbon support and that all electrocatalyst supported on MWCNTs showed small particle size known to enhance the activity of the catalyst. However, after heat-treatment the particle size increased for all prepared supported electrocatalyst as was expected from literature. SEM micrographs showed that all electrocatalyst were decorated on the support material with agglomerates on some parts of the samples, agglomeration was more pronounced for catalysts supported on MoO_2. The metal loading for the home- prepared electrocatalyst was examined using EDS and it was observed to be closer to that of the commercial catalysts. It was also observed that there were changes on the loading of the electrocatalysts after they were subjected to heat treatment and depending on the support material the metal loading of the catalyst was either more or less.

This study found PtSn/C to be the most active commercial catalyst for methanol tolerant and oxygen reduction. For the home-prepared electrocatalyst supported on MWCNTs, PtSn/MWCNT-HT was found to be the most active catalyst while for catalyst supported on metal oxides $PtSn/MoO_2$ was found to be more active than the rest of the Pt-based electro

Abstract

catalyst supported on metal oxides. Results showed that PtSn is more active than PtRu and could function as a methanol tolerant oxygen reduction electro-catalyst for the cathode of a direct methanol fuel cell. Furthermore, in terms of durability, the home-prepared electro-catalyst proved to be more durable than the commercial electro-catalyst supported on carbon black, with catalyst supported on MWCNTs showing more stability than other supported electro-catalyst. Multi-walled carbon nanotubes have therefore proven in this study to be the best supporting material for electro-catalyst as catalyst supported on them showed to be more stable than commercial catalyst supported on carbon black.

Glossary of terms and abbreviations

A_{geo} [cm^2]

Geometric surface area of an electrode

Ag/AgCl

Silver-silver chloride

b [$mV.decade^{-1}$]

Tafel slope

CV

Cyclic Voltammetry

ECSA (Specific Electrochemical Surface Area) [$m^2.g^{-1}$]

The surface area available for electron transfer, per unit mass of active catalyst material within an electrode.

$$\text{ECSA} = \left[\frac{\text{QH}-\text{adsorption (C)}}{210\mu C cm^{-2} LPt(mgPt.cm^{-2})Ag\ (cm^{2})}\right] 10^5$$

DMFC

Direct Methanol Fuel Cell

EDS

Energy-dispersive Spectroscopy

GCRDE

Glassy Carbon Rotating Disk Electrode

Glossary of terms and abbreviations

HRSEM

High Resolution Scanning Electron Microscopy

HRTEM

High Resolution Transmission Electron Microscopy

J [A.cm^{-2}]

Current density-current per unit geometric surface area of an electrode

J_k [A.cm^{-2}]

Kinetic current density

J_{lim} [A.cm^{-2}]

Diffusion-limited current density

L_{Pt} [mg.cm^{-2}]

Platinum loading per unit geometric electrode area

LSV

Linear sweep voltammetry

MA (Mass activity/ Mass-specific activity) [A.g_{Pt}^{-1}]

Kinetic current per unit mass of the active electrocatalyst (Pt) within an electrode.

MEA

Membrane Electrode Assembly

MOR

Methanol Oxidation Reaction occurs at the anode of the direct methanol fuel cell

$$CH_3OH + H_2O \rightarrow 6H^+ + 6e^- + CO_2$$

Glossary of terms and abbreviations

NASA

National Aeronautics and Space Administration

NHE

Normal Hydrogen Electrode. Potentials throughout this paper are quoted against this reference electrode, unless otherwise stated.

PEMFC

Proton Exchange Membrane Fuel Cell

Polymer Electrolyte Membrane Fuel Cell

ORR

Oxygen Reduction Reaction- occurs at the cathode of fuel cells:

$$\frac{1}{2}O_2 + 2H^+ + 2e^- \rightarrow H_2O \qquad E = 1.23V \text{ vs. RHE}$$

RDE

Rotating Disc Electrode

RPM

Revolutions per minute

RRDE

Rotating Ring-Disc Electrode

SA (Specific activity) [$A.m^{-2}$]

At a given potential, the current density per unit electrochemically-active surface area of the electrode

Glossary of terms and abbreviations

UHP

Ultra high pure (referring to the purity of deionised water with a conductivity of 18.2 mΩ.cm)

UPD

Underpotentially deposited (as in H_{upd}- underpotentially deposited hydrogen)

XRD

X-ray Diffraction

Acknowledgements

This thesis represents the culmination of my research carried out between March 2012 and November 2013 at the Department of Chemistry under South African Institute for Advanced Material Chemistry (SAIAMC) at the University of the Western Cape. I would like to acknowledge several individuals for their contribution, support, guidance, and assistance throughout this period.

Firstly, to God be the glory. I am who I am because of Him. I thank my heavenly Father for the grace which He has bestowed upon me to carry out this work to its completion. I would never have made it without His grace. Indeed His grace has always been sufficient for me.

I am very grateful to my supervisor, Dr. Lindiwe Khotseng for all the support, guidance, and patience she has shown throughout this work.

I want to say thank you to Professor Linkov, Director of SAIAMC, together with the University of the Western Cape, for believing in me and allowing me to conduct my research at the Institute.

The financial assistance from SAIAMC and ESKOM is hereby greatly acknowledged.

This work would not be possible without the assistance from Thobeka Adonisi, Lynwill Martin, and Jonathan Goh. I truly appreciate all the help they have given me. Thank you so much.

To the technical team of SAIAMC, led by Stanford Chidziva, I am thankful to you all for your assistance in technical matters.

I also wish to thank Dr. S. Botha, Dr. F. Cunnings, and Mr A. Josephs (E.M.U, Department of Physics, University of the Western Cape) for assisting me with HRTEM and HRSEM. I also thank

Dr R. Bucher (Materials Research Group, iThemba labs) for assisting me with XRD.

Finally, I wish to thank my dear mother, Esther Bangisa, for your constant support.

Table of contents

TABLE OF CONTENTS

TABLE OF CONTENTS

List of Tables

List of Tables

List of Figures

List of Figures

List of Figures

CHAPTER 1

INTRODUCTION: MOTIVATION AND OBJECTIVES OF THE STUDY

1.1 BACKGROUND TO ENERGY SOURCES

Energy plays a central role in achieving the mutually related economic, social, and environmental aims of sustainable human development [1]. Fuel cells are currently one of the technologies at the fore front of sustainable energy production due to their many benefits and are set to become the main energy power sources of the 21st century. Fuel cells are electrochemical devices that directly convert the chemical energy of a fuel, such as hydrogen, into electrical energy without combustion. They create virtually no pollution when pure hydrogen is used as a source of fuel and have high theoretical efficiency, and hence, they make such an attractive alternative as future energy sources. At present, human population globally depends on fossil fuels as the main source of energy and yet the use of rapidly depleting fossil fuels to meet the increasing global demand for energy is economically and environmentally unsustainable. Greenhouse gas emissions (e.g. CO_2, CH_4 and N_2O) that are linked to the extraction, processing and use of fossil fuels have raised atmospheric concentrations of CO_2 significantly beyond the natural historical maximum of around 300 ppm. The concentration now of ~390 ppm is considered to present a substantial global risk of irreversible climatic changes and yet it still continues to rise [2-4]. Concurrently, the reserves of easily-accessible fossil fuels are declining as they are not produced from renewable sources, resulting in continually escalating financial and environmental costs in utilization, extraction and processing activities, especially as the utilization of non-ideal deposits in complex areas becomes necessary to meet global demand [2-4]. The rate of global oil production currently exceeds the rate at which new reserves are being discovered.

In order to reduce the risk of global temperature increases beyond 1.5^{o} C, greenhouse gas emissions must be reduced dramatically over the next half-decade-starting now. To attain such dramatic emission reductions, whilst at the same time addressing concurrently the issue of increasing energy demand and improving energy security requires a change-over to renewable primary energy sources (e.g. wind, solar, hydro) and the adoption of clean and efficient energy distribution and conversion technologies to replace hydrocarbon fuels and thermo-mechanical engines [3-4].

Hydrogen therefore represents a promising and efficient clean energy vector, that is, a means by which energy can be stored, distributed and converted into useful work at point of use-whose only by-product, when combusted or reacted electrochemically with oxygen is water [4]. The conversion of hydrogen to energy can be achieved through many means including combustion but the most efficient method will be to use a fuel cell where the chemical energy of hydrogen is directly converted into electrical energy. Fuel cells have the ability to fulfil all the global power needs while meeting the efficiency and environmental expectations. Sustainable activities, after all, are about meeting the needs of the current generation without destroying the ability of future generations to meet their own needs, maintaining a balance of course of economic, social and environmental needs [1].

Fuel cells belong to the same class of devices as batteries known as Galvanic cells, which represent the oldest and most direct method for the production of an electrical current via a reaction between chemical substances. While a battery contains a fixed supply of chemical reactants, and thus has a limited life before it can be discarded or recharged. A fuel cell, on the other hand, is supplied by reactants stored externally and will thus go on producing electrical power continuously for as long as reactants are supplied to it, making fuel cells more attractive than batteries. Additionally, fuel cells offer a broad range of applications than any other currently available power source. They can power anything from toys to large power plants, from vehicles to mobile chargers, and from household power to battle field power [2, 5-7].

There are several types of fuel cells, which are classified according to the type of electrolyte they use which governs the operating temperature and the catalyst suitable for those conditions must then be selected. Among the various types of fuel cells, direct methanol fuel

cell (DMFC) is the most attractive, using liquid and renewable methanol as a fuel. DMFCs have been considered to be a very promising alternative in terms of fuel usage and feed strategies. Unlike hydrogen-fed fuel cells, which have safety, storage, and distribution challenges, DMFC uses liquid methanol as a fuel and can easily be stored and transported. This therefore simplifies the fuel cell system [8-9].

1.2 RATIONALE TO THE INVESTIGATION

The focus of this investigation is on direct methanol fuel cell which is a low temperature fuel cell. It has received much attention over the years as a promising technological development that can replace conventional batteries as power sources for portable devices. This is due to their unique features of using liquid methanol as a fuel which offers, high specific energy density, high energy conversion efficiency of 40-50%, low operating temperatures (0 -100^{o} C) and the use of methanol as a fuel allows for easy storage and transportation [8-10], something which simplifies the fuel cell system. Their full commercialization, however, is still hindered by the: 1) use of perfluorosulfonic acid membranes, such as Nafion, which allow methanol, together with water, to permeate through the membrane from the anode to the cathode. This phenomenon is referred to as 'methanol cross-over', the methanol that crosses over reacts with oxygen at the cathode and reduces the cathode potential, with the end results being that less power is generated by the fuel cell and can lead to a waste of fuel; and 2) the sluggish electro-kinetics of the methanol oxidation (MOR) at the anode which is mainly caused by the poisoning of the Pt catalyst by carbon monoxide (CO), a by-product of methanol oxidation which blocks the active site of the platinum catalyst, resulting in slow kinetics [8-10]. The membrane and the electro-catalyst have been identified therefore as two key materials connected with challenges that are inhibiting the full commercialization of DMFC [9].

The cross-over of methanol from anode to cathode is a critical issue that calls for development of novel membranes which are less methanol permeable or alternatively work on the modification of existing membranes since great efforts have already been made in the modification of existing Nafion membranes to limit methanol cross-over, but the measures

taken so far have resulted in undesirable secondary effects that lower the proton conductivity and increases the cell internal resistance, thereby degrading the cell performance. Another strategy in dealing with methanol crossover is the use of oxygen reduction catalysts, which are inactive towards methanol oxidation or have a high methanol tolerance so that the oxygen reduction will not be affected by the adsorption and oxidation of methanol [9]. The crossover of methanol to the cathode results in oxygen reduction and methanol oxidation reactions taking place simultaneously, which is the issue encountered with using Pt as a catalyst, as it is active in catalyzing both reactions. To overcome the sluggish kinetics at the anode, PtRu electrocatalyst is usually employed and is known to be the state of the art anode catalyst, the introduction of ruthenium to platinum is believed to help promote CO to CO_2, which alleviates the poisoning effect of the catalyst and improves the activity [8-10], but still the activity is not high enough to reduce the rate of methanol cross-over, since the cross-over of methanol is directly linked to the sluggish kinetics of methanol oxidation at the anode. The slower the reaction, the more methanol will cross-over, some development is greatly needed to enhance the activity of the anode catalyst as activity improvement of anode catalysts is helpful to reduce methanol cross-over through the electrolyte. The cross-over of methanol from anode to cathode electrode is a challenge for the fuel cell catalyst group (researchers concerned with the development of fuel cell catalysts) and in dealing with the effect of methanol cross-over, much of the research has gone into the development of non-platinum catalyst so as to avoid platinum depolarization and this has led to several transition metal macro-cycles and ruthenium-based chalcogenides being tested for methanol tolerance oxygen reduction because of their inactivity towards the oxidation of methanol [11-15]. Still, the intrinsic catalytic activities of these catalysts towards the reduction of oxygen are lower than that of the platinum-based catalysts and their long term stability under fuel cell operating conditions at high potentials is not as good as the Pt-based catalyst. Thus, it is necessary to develop a novel Pt-based catalyst that can catalyse the oxygen reduction while limiting the oxidation of methanol. Previous studies have proved that the use of some platinum alloy catalyst could be an effective method to deal with methanol cross-over effect. Pt-based alloy catalysts, such as Pt-M (M= Fe, Ni, Cr, Cu, Co etc.), have been recommended before and tested as methanol tolerant cathode catalyst for DMFCs and exhibit an enhanced electro-catalytic activity for oxygen reduction reaction with respect to platinum alone [11-15]. Such an

activity enhancement was elucidated by the structural effect of shortening the Pt-Pt distance in the alloy nanoparticles and weakening the Pt-oxygen bond, the electro-chemical effect for enhancing the electron transfer from oxygen to Pt and the blocking effect, preventing the adsorption of methanol on platinum atom around transition metal [16-18]. Aiming to increase the catalytic activity of the oxygen reduction reaction and to lower the cost of the catalyst, this study chose to employ platinum-based alloys as a cathode catalyst for DMFC application.

Another hurdle faced with in realizing the full commercialization value of DMFC is the durability and high cost of the fuel cell system. The catalyst is known to be the major contributor to both these factors hampering full commercialization of DMFC. The catalyst of choice currently used in DMFC application is the expensive platinum metal as it is the only material known to show good activity and stability under the operating conditions of the DMFC [21]. Efforts, therefore, need to be made to reduce the loading of the expensive platinum metal, thereby reducing the cost without compromising the performance of the fuel cell catalyst. One of the effective ways frequently employed in reducing the loading of the expensive platinum metal and concurrently improving the activity of the catalyst is to increase the electro-chemical surface area [$m^2.g^{-1}$] by reducing the catalyst particle size down to a nanometre scale and supporting them on high surface area and electron conductive materials such as carbon materials. This will increase the surface area of the electro-catalyst, which is the most active component of the electro-catalyst. In this way, the surface area per unit weight or the utilization of platinum is improved. Alternatively, the electro-chemical surface area can be increased by increasing the proportion of the catalyst that is electro-chemically active within the catalyst layer. Another approach of reducing the Pt loading is through increasing the specific activity [A. m^2] which can be achieved by alloying Pt with other metals so as to modify the intrinsic activity of the catalyst surface. This study aims to apply these two approaches, that is, increasing the electro-chemical surface area and by also increasing the specific activity in order to realize the improvements in mass activity.

Another effective approach in enhancing the activity and durability of electro-catalyst is the use of good support material. Support material, which is the main point of focus of this study, play a vital role in influencing the cost, activity and durability of the catalyst, which are the major challenges facing the catalyst group and more importantly the commercialization of low temperature fuel cells, with emphasis on DMFC. Traditionally, carbon black has been

used as the support material of choice in DMFCs as it offers high electronic conductivity, high surface area and is cost effective. Recently, carbon-based nanomaterial with high graphitic structure, such as carbon nanotubes (CNTs), and carbon nanofibers (CNFs) are being extensively studied as new generation of catalyst support [19]. This is due to their distinctive characteristics as they offer more crystalline structure with high electrical conductivity, excellent corrosion resistance and high purities compared to conventional carbon black powders. CNTs are particularly of great interest due to their unique structural, electrical and mechanical properties. Carbon-based support, however, generally suffers from corrosion in different levels depending on the carbon material used, carbon blacks being the most affected by corrosion under fuel cell conditions. The instability of carbon based support material under fuel cell conditions, is a major concern and accordingly a drawback in the performance of electro-catalyst supported on these materials because the corrosion of the carbon support leads to Pt sintering and lowers the electro-chemical active surface area of the catalyst and ultimately results in the undesired degradation of the fuel cell system. Thus, a new class of support material is needed that will be extremely resistant to corrosion under fuel cell conditions. Non-carbon materials, especially conductive oxides, are now being extensively studied as possible support materials due to their high resistance to corrosion under fuel cell conditions and many have been used to modify the carbon-based support material in order to improve the durability of the catalyst. They can also be used in their own right independently so as support materials [20].

1.3 OBJECTIVES OF THE STUDY

The main objective of this study was to investigate the influence of the support material on the performance of the cathode electro-catalyst in terms of activity and durability for DMFC applications. Electro-catalysts that were chosen for the research were binary PtRu and PtSn. They were synthesized and supported on multi-walled carbon nanotubes (MWCNTs), titanium oxide (TiO_2) and molybdenum oxide (MoO_2) and compared with carbon black (CB) currently used on the market. They were then investigated for their physical-chemical properties and their applicability in the cathode of a DMFC system. The aim was to investigate the behaviour of the electro-catalyst in terms of activity and durability when

supported on different materials (MWCNTs, TiO_2, and MoO_2) with the focus on oxygen reduction reaction (ORR), methanol tolerance of the supported electro catalysts and durability. This was done using the rotating disk electrode (RDE). The main sub-objectives included:

- Synthesis of PtRu and PtSn and deposition of these electro-catalysts on the support material, forming supported electro-catalyst.
- Heat treatment of the prepared supported binary electro-catalyst.
- Physical characterization of the supported catalyst and support material using X-ray diffraction spectroscopy (XRD), high resolution scanning electron microscopy (HRSEM), high resolution transmission electron microscopy (HRTEM) and elemental dispersive spectroscopy (EDS).

1.4 FRAME-WORK OF THE INVESTIGATION

PtRu and PtSn electro-catalysts were synthesized using the modified polyol method and deposited on MWCNTs, TiO_2 and MoO_2 support material. Before deposition of the electro-catalyst on MWCNTs, the MWCNTs were purified and functionalized using acid treatment. The metal oxide support materials were used as received without any further treatment. The synthesized electro-catalysts were then subjected to heat treatment. The commercial and synthesized electro-catalysts were then physical-chemical characterized using different techniques as mentioned above. The commercial Pt/C, PtRu/C and PtSn/C were characterized and bench-marked as standards to which they were compared to the synthesized supported electro-catalysts with. Figure 1.1 below illustrates a process scheme of the research frame-work.

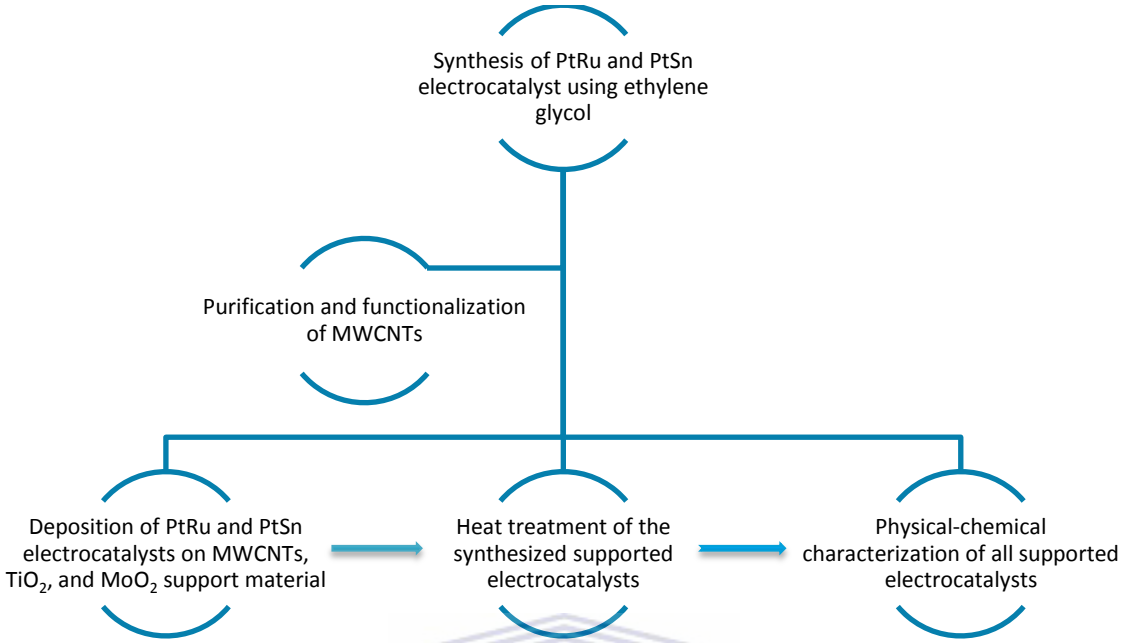

Figure 1.1: *Process scheme of the research frame work*

1.5 RESEARCH OUTLINE

CHAPTER 2: LITERATURE REVIEW

Chapter 2 focuses on the introduction to fuel cells, types and operating conditions. The fuel cell of interest for this research is the direct methanol fuel cell and it is discussed in detail, bringing out its advantages, principle of operation and the challenges. The main focus of this study is examining the influence of the support material on the cathode electro-catalyst for DMFC applications. Therefore, the support material will be discussed giving emphasis on the ones used in this study (MWCNTs, TiO_2, and MoO_2); the cathode electro-catalyst will also be discussed with emphasis on binary catalysts. Binary PtRu and PtSn will be discussed as they were used as the cathode electro-catalyst for this investigation.

CHAPTER 3: METHODOLOGY

Chapter 3 outlines the method used in this study, emphasis being on the techniques used to characterize the supported catalyst.

CHAPTER 4: RESULTS AND DISCUSSION OF PtRu ELECTROCATALYST

The results of PtRu electrocatalyst supported on different materials with commercial Pt/C and PtRu/C are presented in this chapter to give insight into the structural physical and electrochemical properties of the supported electro-catalyst.

CHAPTER 5: RESULTS AND DISCUSSION OF PtSn ELECTROCATALYST

The results of PtSn electro-catalyst supported on different materials are presented and discussed in this chapter with commercial Pt/C and PtSn/C used as standards for comparison purposes.

CHAPTER 6: CONCLUSION AND RECOMMENDATIONS

The conclusion of the behaviour of electro-catalyst under various support materials is given together with recommendations.

CHAPTER 2

LITERATURE REVIEW

2.1 FUEL CELLS

2.1.1 Introduction

A fuel cell is an electro-chemical device that directly converts the free energy of a chemical reaction of a fuel (e.g. hydrogen, natural gas, methanol, gasoline, and formic acid) and an oxidant (air or pure oxygen) into electrical energy. The most attractive characteristic of fuel cells is that their thermodynamic efficiencies are not restricted by the Carnot cycle as is the case with combustion engines. Instead, fuel cell efficiency is directly related to the overpotential, the difference between the experimental voltage and the thermo-dynamically recommended voltage of the half reactions at each electrode, hence, a fuel cell has the potential to operate at much higher efficiency than combustion engines [22, 23]. Burning hydrogen in an internal combustion engine gives efficiencies ranging from 10-20%, while the thermodynamic efficiency of a hydrogen fuel cell theoretically can be greater than 90%. However, in real practice, such high efficiencies are never achieved [23]. In spite of their high modern day technology *aura,* fuel cells are not a new technology. In fact, fuel cells have been known to science for more than 170 years now [24]. Their origin can be traced back to an English lawyer turned scientists Sir William Grove in 1839. Sir William Grove (often referred to as "father of fuel cells") was the first person to demonstrate the fuel cell principle. Using apparatus depicted in Figure 2.1, Grove was able to demonstrate that the hydrogen and oxygen evolved by electrolysis at platinum electrodes immersed in dilute sulphuric acid solution could be consumed at the same electrodes, with the production of an electrical current, a process which Grove termed 'reverse electrolysis' [24, 25]. The current density of Grove's device, however, and the amount of platinum black required made it impossible then to be even considered for general use [26] as primary energy sources were abundant, unrestricted and inexpensive. Things began to change at the beginning of the 20th century as human population increased as it continues to grow at a very rapid pace, making electricity

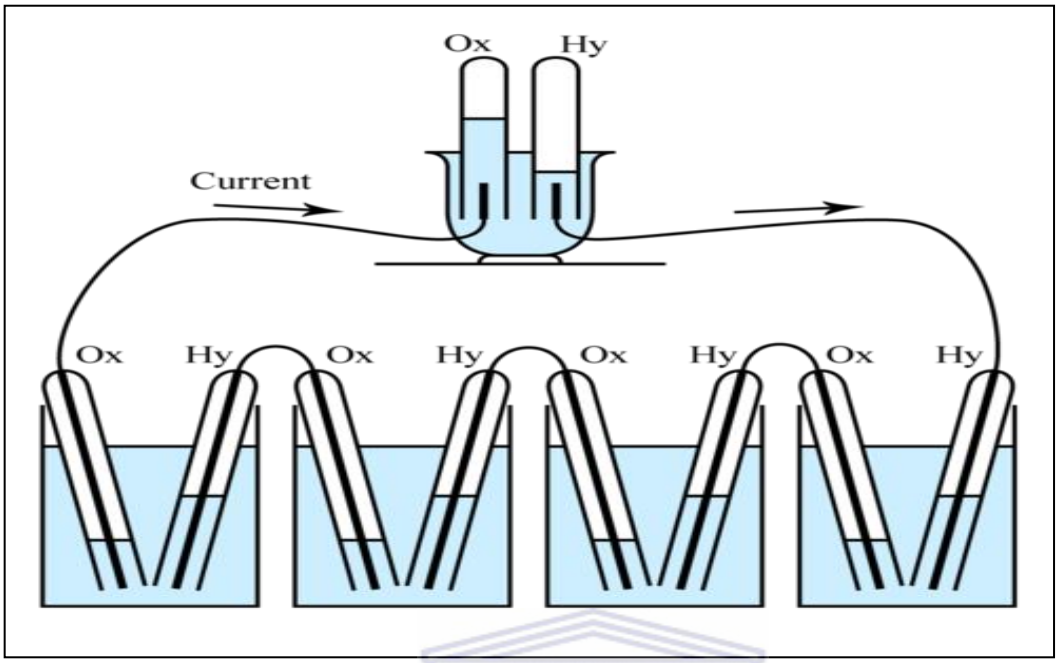

Figure 2.1: *Sir William Grove's gaseous voltaic battery, demonstrated in 1839, consisted of platinum electrodes contained within sealed glass test tubes, in contact with a sulphuric acid solution* [27].

consumption in great demand more than ever before, and hence the conversion of chemical energy into electrical energy is becoming more and more important today [24]. The increased demand for energy has led to an increase in the cost of fuels. In addition to it, the reserves of easily-accessible fossil fuels are dwindling very fast, resulting in rising financial and environmental costs in fuel exploration, extraction and processing activities, as the exploitation of non-ideal deposits in sensitive areas becomes necessary to meet global demand. In response to the pressing global concerns relating to sustainable generation and increasing population therefore, a strong research drive has been mounted globally is to develop environmentally clean and efficient alternatives to fossil fuel [28], and fuel cells are proving to be an interesting and very promising alternative, which can realize the promise of clean reliable electric power generation with high efficiency [24]. They are believed by many to be the ideal energy source for the future generations.

2.1.2 Advantages of Fuel Cells

Fuel cells offer a unique combination of benefits that make them to be such a vital technology that is ideally suited for a number of applications. Below are just some of the few benefits that make fuel cell technology to be attractive as energy power source of the 21st century.

a. Low-to-zero emissions

A fuel cell operating on pure hydrogen emits zero emissions at the source, giving off only electricity, water and heat. Even when the fuel source used is natural gas or hydrocarbons, the emission produced from these sources is still lower than conventional power plants. The ability of fuel cells, therefore, to provide zero or near zero emissions has been the driving force in the development of the technology over the past decades and is increasingly attracting more and more attention to this technology today [29, 30].

b. High efficiency

Because there is no combustion involved in fuel cells, energy is created electro-chemically. Therefore, fuel cells are essentially more efficient than combustion systems. Fuel cell systems today deliver 40-50% fuel-to-electricity efficiency using hydrocarbon fuels such as natural gas [29, 30].

c. Reliability and high quality power

There are no moving parts in fuel cell stack, making them more reliable and quieter than present generators. Unlike batteries that must be discarded once the chemicals are used up, fuel cells can run indefinitely as long as fuel is supplied [29].

2.1.3 Limitations of Fuel Cells

Below are some of the limitations common to all fuel cell system that actually hinder fuel cells from reaching their full commercialization stage.

a. High costs

Indeed at present, fuel cells are more expensive than conventional power systems, owing to the requirement for materials with specific properties. The challenge is to develop low cost replacements, including the need for Nafion membrane and platinum metal as a catalyst that is used in low temperature fuel cells such as PEMFC and DMFC [31]. Extensive research has gone into the modification of Nafion membranes and also great efforts have gone into developing binary and ternary platinum-based alloy electro-catalyst to reduce cost by equally reducing the amount of platinum loading without compromising the performance of the fuel cell catalyst.

b. Storage and transportation issues

Distribution and storage of hydrogen in large volumes for commercial, domestic and automotive purposes represent a significant challenge that is compounded by its low volumetric energy density-but is debatable, no more a challenge than was the establishment of the existing infrastructure for the transportation, distribution and storage of hydrocarbon fuels [29].

c. Stability issues

Stability and durability of the fuel cell is a major concern for fuel cell technology and consequently a drawback. To offer a reliable power generator for portable devices and automotive applications, fuel cell systems have to meet the present US Department of Energy lifetime specified target of 5 000 hours; 20 000 hours for bus application and 40 000 hours of continuous operation for stationary applications, which to date, has yet to be achieved [29, 31], though much progress has been made over the years.

2.1.4 Basic Operation of Fuel Cells

The structure of a simplified fuel cell is shown in Figure 2.2 below. The basic principle of operation is the same in all fuel cells. They all consist of an electrolyte layer in contact with two electrodes (anode and cathode electrode) on either side.

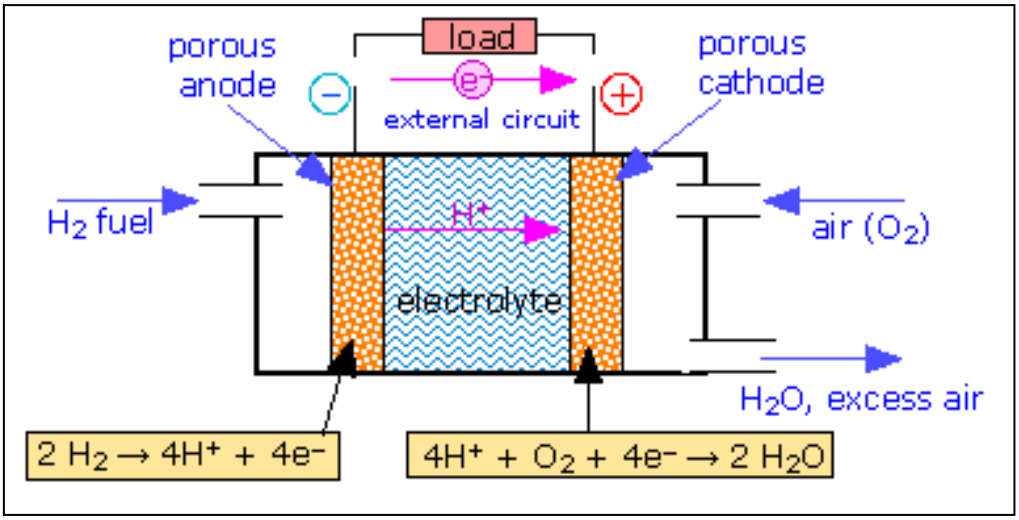

Figure 2.2: Schematic diagram of a hydrogen fuel cell [33]

Hydrogen is fed continuously to the anode electrode where it is electro-chemically oxidized into positive ions and negative ions while oxygen is fed into the cathode electrode. The positive ions will migrate into the cathode using an electrolyte membrane which permits only positive ions to pass through from the anode to the cathode and simultaneously serve as an insulator for electrons. For the system to become stable, the electrons have to recombine with protons at the cathode and, therefore, travel via the external electrical circuit generating electricity on their way to the cathode electrode. At the cathode terminal, a reduction process occurs, where protons, electrons and the oxidant recombine to form water. All these reactions take place in the presence of a suitable catalyst. The chemical reactions involved in the anode and cathode and the overall reactions are given below as [33, 34d]:

Anode reaction: $2H_2 \rightarrow 4H^+ + 4e^-$ (2.1)

Cathode reaction: $O_2 + 4H^+ + 4e^- \rightarrow 2H_2O$ (2.2)

Overall reaction: $2H_2 + O_2 \rightarrow 2H_2O$ (2.3)

2.1.5 Classification of Fuel Cells

Fuel cells are primarily classified according to the electrolyte material they use which governs the operating temperature and at that temperature a suitable catalyst is to be chosen [35, 36]. The type of electrolyte material employed governs their performance characteristic, making each type of fuel cell suitable for specific applications. Currently, six major types of fuel cells are available as summarised in Figure 2.3 below. The first four are categorized by their low to medium temperature of operation (50-120^o C). The latter two types are categorized by their high temperature of operation (600-1000^o C) and their ability to use methane directly in the fuel cell [35, 37].

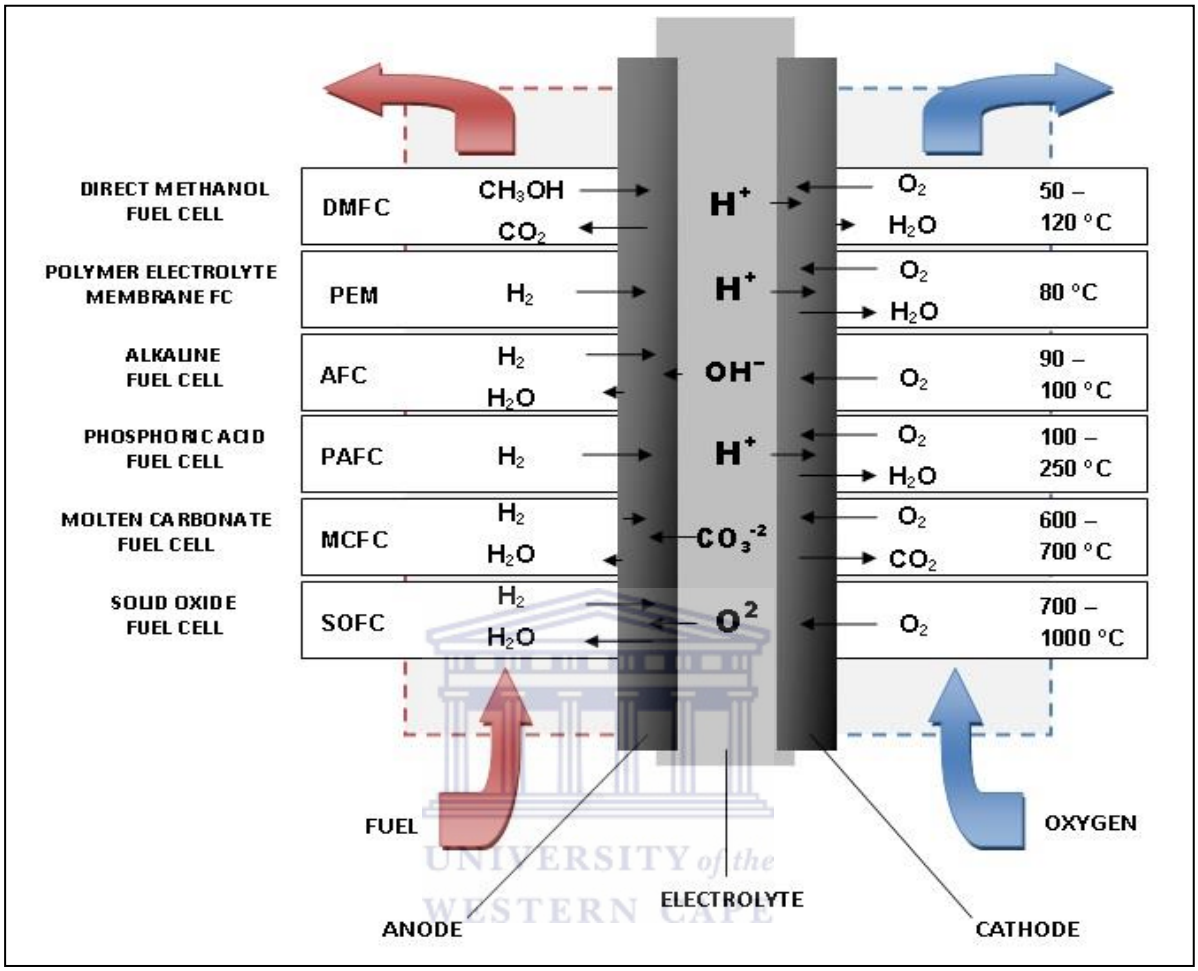

Figure2.3: Schematic showing the operating temperatures, anode and cathode and electrolyte charge carriers for several types of fuel cell: direct methanol fuel cell (DMFC), proton exchange membrane fuel cell (PEMFC), alkaline fuel cell (AFC), phosphoric acid fuel cell (PAFC), molten carbonate fuel cell (MCFC) and solid oxide fuel cell (SOFC) [38]

Proton exchange membrane fuel cell (PEMFC) uses a polymeric membrane as its electrolyte, which transports protons produced by oxidation of hydrogen at the anode to the cathode, where they participate together with electrons in the reduction of oxygen, with pure water as the only by-product. The advantages of PEMFC are its higher power density and quick start-up qualities for automotive vehicles and its low operating temperature. This makes the PEM fuel cell competitive in transportation and commercial applications like in laptop computers, cars and mobile phones. The need to use expensive platinum as catalyst and their low operating efficiency (40-50%) are currently the major obstacles for full commercialization of the PEMFC [34].

Alkaline fuel cell (AFC) is one of the earlier fuel cell systems employed for NASA's space mission. It is a low temperature fuel cell that uses aqueous solution of potassium hydroxide (KOH) as an electrolyte and transports electrons from the anode to the cathode electrode while it releases water as its by-product. One of the advantages of AFC is that it gives a quick start. Its sensitivity to CO_2 is, however, one of its major disadvantages. AFC finds wide application in the transportation industry, such as in fleet vehicles, boats and space shuttles [24, 34].

Phosphoric acid fuel cell (PAFC) utilizes liquid phosphoric acid as an electrolyte. PAFC is very tolerant to impurities in the reformed hydrocarbon fuels compared to AFC and PEMFC [39]. The slightly high operating temperature allows for the possibility of co-generation and the potential for hot water supply as well as electricity available, processes that are dependent on heat and electricity load profile [40, 41]. The major drawback in PAFC is the cost which increases due to the use of expensive platinum metal as catalyst [34].

Molten carbonate fuel cell (MCFC) operates at high temperatures (650-700^{o}C) and has internal reforming capabilities. It separates the hydrogen from carbon monoxide fuel and decomposition of hydrogen is taken through the water shift reaction in order to produce hydrogen. The result of the reaction is the same as in PEM fuel cell in producing electricity. Higher efficiencies (50-60%), non-use of metal catalyst and a separate reformer due to high operating temperatures are some of the major advantages of the MCFC. The slow start-ups and the intolerance to sulfur are the drawbacks of the cell. The MCFC is mainly used for medium to large power generation applications [24].

Solid oxide fuel cell (SOFC) is a high temperature fuel cell using dense yttria-stabilized zirconia as an electrolyte. Oxygen combines with hydrogen to generate water and heat. The main advantages of SOFCs is that they can operate at high efficiency levels of 50-60% and a separate reformer is not required to extract hydrogen from the fuel due to its internal reforming capability. Waste heat can be recycled to make additional electricity by co-generation [39, 41]. Slow start ups, high cost, and intolerance to sulfur content of the fuel cell are some of its drawbacks. Since it is not suitable for larger fluctuations in load demands, it is therefore mainly used for medium to large power applications [34].

Direct methanol fuel cell (DMFC), which is the main focus of this study, will be discussed in detail below. It operates like the PEM fuel cell which uses the polymer electrolyte instead of the reformed hydrogen. DMFC, as the name indicates, uses liquid methanol as the source of fuel. One of its main advantages is that the anode catalyst itself draws hydrogen from the methanol and reduces the overall cost due to the absence of a reformer. Major limitations of the fuel cell are the slow kinetics of the electro-chemical oxidation of methanol and the cross-over of methanol from anode to cathode which lowers the system's efficiency [34]. This study is concerned with the development of cathode (oxygen reduction and methanol tolerant) catalysts for the direct methanol fuel cell.

2.2 DIRECT METHANOL FUEL CELL (DMFC)

Direct methanol fuel cell is one of the most promising devices in the nearest future for energy sources. It offers several advantages over other types of fuel cells in that it is a dependable and long lasting portable power source that can replace batteries in a number of electronic products, including laptop computers and cellular phones. Some of the unique features that make DMFC to be viewed by many as a key enabling technology for this century include [42-45]:

- High energy density of liquid methanol (6100 $Whkg^{-1}$ at 25^{o} C);
- High energy conversion efficiency (40-50%);
- Ease of delivery and storage of liquid methanol;
- Low temperature of operation (0-100^{o} C);
- Simple and compact structures;
- Availability of liquid methanol

Liquid methanol can be sourced from fossil fuels, such as natural gas or coal, as well as from sustainable sources through fermentation of agricultural products and biomasses [42-45]. Methanol is easily available. The low cost of liquid methanol and the fact that it can be distributed using the present infrastructure for liquid fuels eliminates the need to build new infrastructure and accordingly, it reduces the high cost that goes with building new infrastructure.

Although DMFC is a promising technology, it is still facing some technical challenging issues that must be resolved in order to make DMFCs commercially and practically usable.

These challenges include the sluggish electro-kinetics of methanol oxidation reaction at the anode and oxygen reduction reaction at the cathode which both limit the DMFC performance. And also the Nafion membrane, which allows methanol together with water to permeate through it from anode to the cathode terminal, the effect of which is termed 'methanol cross-over', is highly detrimental to the cell performance [42-45]. The high cost of the fuel cell system is also a limiting factor and is mainly due to the expensive materials that are needed such as Nafion membranes and platinum metal as a catalyst.

2.2.1 Working Principle of the Direct Methanol Fuel Cell (DMFC)

The basic working principle of a liquid feed direct methanol fuel cell is presented in Figure 2.4 below. Electro-chemical reactions occur in the catalyst layers (CLs), which are attached to both sides of the membrane. They are designed in such a manner as to facilitate the transport of protons, electrons and reactants. The function of the membrane is to conduct protons from the anode to the cathode and simultaneously serve as an insulator for electrons. The membrane that is used in DMFCs is a per-fluorinated sulfonic acid ion exchange membrane that was developed by DuPont and trade-marked as Nafion®. Reactants enter the cell through the flow channels [42-46].

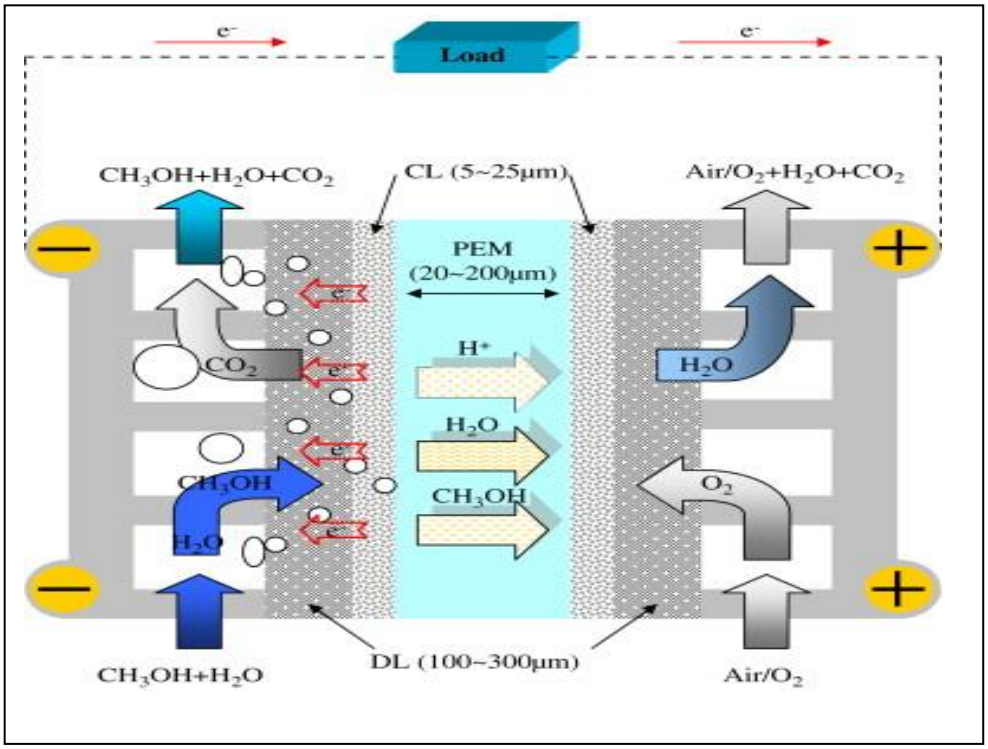

Figure2.4: Schematic diagram of a liquid feed methanol fuel cell [10]

The methanol solution is supplied as a fuel to the anode flow channel and transfers from the anode diffusion layer (DL) to the anode catalyst layer (CL) where it is electro-chemically oxidized in the presence of a catalyst typically binary PtRu/C to form protons, electrons and carbon dioxide and the remaining methanol solution is transported to the cathode catalyst layer through the polymer electrolyte membrane as shown in Figure 2.4 above. The permeation of methanol from anode to cathode is referred to as methanol cross-over, which creates mixed potential and decreases the cathode potential. The produced carbon dioxide in the anode CL then moves backward through the anode diffusion layer to the flow channel as shown in Figure 2.4 above and from there it is vented out by a stream of liquid solution toward the exit of the flow channel. The protons, formed at the anode catalyst layer, are transported through the polymer electrolyte membrane to the cathode CL. Since the membrane serves as an insulator for electrons, therefore, electrons commence their journey across the external circuit (Figure 2.4) arriving at the cathode, depleted from having performed external work. On the cathode, oxygen/air is supplied through the cathode flow channel and is transferred from the cathode DL to the cathode CL. This is where the majority of oxygen reacts with electrons and protons in the presence of a catalyst, typically pure Pt on highly conductive carbon support to form water while the remaining part of oxygen electro-chemically reacts with the permeated methanol [42-46]. The reactions that take place are given below as:

The overall half-cell reaction at the anode is

$$CH_3OH + H_2O \rightarrow CO_2 + 6H^+ + 6e^- \qquad E_0 = 0.046V \quad (2.4)$$

At the cathode the overall half-cell reaction is

$$6H^+ + 6e^- + 3/2O_2 \rightarrow 3H_2O \qquad E_0 = 1.23V \quad (2.5)$$

Thus, the overall cell reaction in the DMFC is

$$CH_3OH + 3/2O_2 \rightarrow CO_2 + 2H_2O \qquad E_0 = 1.184V \quad (2.6)$$

Equation 2.6 simply means that methanol reacts with oxygen to produce the desired electric energy with carbon dioxide and liquid water as by-products. The standard cell voltage for a DMFC at 25^o C is 1.184V. However, this potential is never achieved practically. Instead, the open circuit potential is usually about 0.6 to 0.8V in the best case.

Figure 2.5 below illustrates the key components of a DMFC. The major components of the direct methanol fuel cell include: 1) the membrane electrode assembly (MEA) and, as the name indicates, is the assembly of the membrane and electrodes. MEA is widely known as the heart of the fuel cell owing to the fact that all reactions within the fuel cell occur in the MEA. It is made up of the electrodes (anode and cathode), catalyst layers and polymer electrolyte membrane; 2) the second key component of the fuel cell is the catalyst, which will be discussed in detail latter in this chapter. The catalyst is usually made to be rough and porous and this is to allow for the maximum surface area of the platinum to be exposed to the methanol or oxygen.

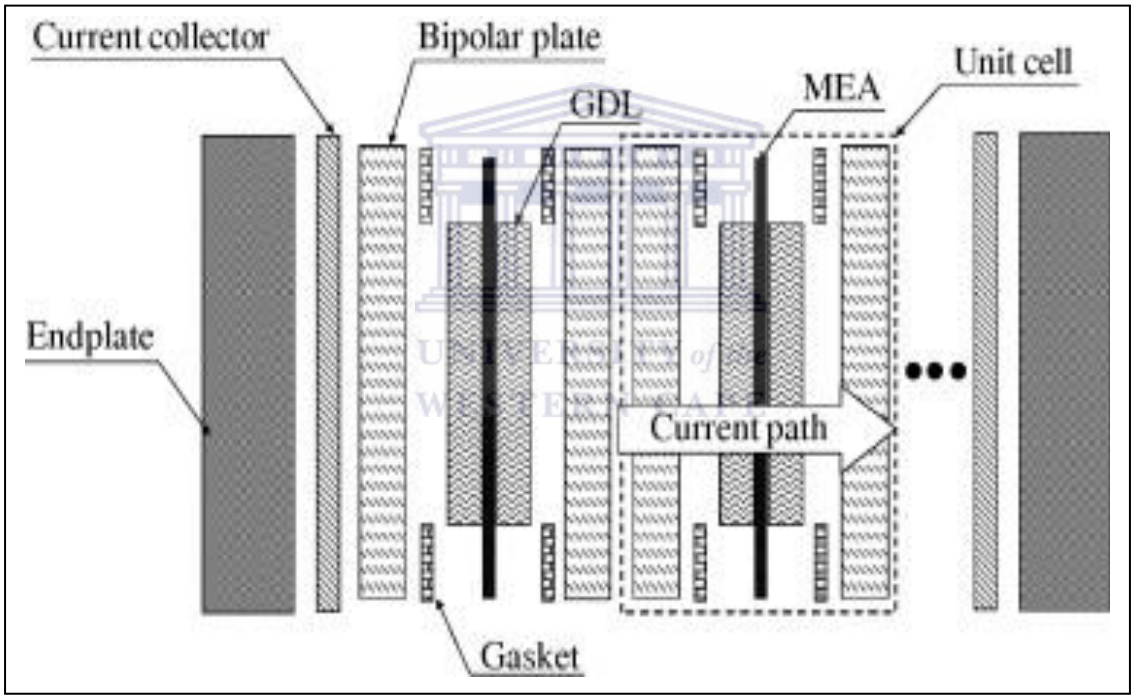

Figure2.5: Key components of DMFC [48]

The platinum coated side of the catalyst faces the polymer electrolyte membrane; 3) the gas diffusion layer (GDL) ensures that the reactants effectively diffuse to the catalyst layer and minimize mass transport overpotential, and also provide an electrical connection between the CL and the current collector that is the bipolar plate; furthermore they also assists in water management by allowing an appropriate amount of water to reach, and be held at the membrane for hydration. GDLs are typically constructed from a porous carbon paper or carbon cloth with thickness in the range of 100-300 µm; and 4) is the hardware, which is made up of backing layers, flow fields and current collectors and is designed in such a way

that it can maximize the current from the MEA [28, 49]. The bipolar plate (BP) functions as a flow field to deliver reactants and remove products and also collects current generated in the cell [50-53].

2.2.2 Challenges Facing the Commercialization of DMFC

The commercialization of direct methanol fuel cell is hindered mainly by the high cost and low reliability and durability of the cell, the catalyst has been identified as the main contributor to these issues that DMFC is faced with. Although a great deal of effort has been put into the synthesis of cost-effective, active and stable fuel cell catalysts, no real break-through can be reported. Therefore, exploring break-through catalysts, improving catalyst activity, stability and durability and reducing catalyst cost are some of the major tasks in realizing fuel cell commercialization [54]. Below are some of the key challenges that have hampered DMFC from reaching full commercialization stage and, unless dealt with, the DMFC cannot be made commercially viable.

i. Slow Electro-oxidation Reaction

Indeed, methanol oxidation is an important step and accordingly a limiting factor, in the performance of a DMFC [32]. The reactions involved in methanol oxidation are very complex with many intermediate steps which in turn form many chemical intermediates. Figure 2.6 below illustrates the reaction paths and possible intermediates in the electro-oxidation of methanol [55]. Green arrows indicate indirect mechanism for the formation of CO_2. Some of these intermediates formed during methanol electro-oxidation are not readily oxidizable and they remain strongly adsorbed on the surface of the catalyst, and consequently prevent fresh methanol molecules from adsorbing and undergoing further reaction. Thus, electro-oxidation of these intermediates becomes the rate limiting step [56]. Methanol is mainly decomposed to CO which is further oxidized to CO_2. The poisoning of platinum catalyst surface by carbon monoxide results in sluggish electro-kinetics of methanol electro-oxidation and increases the rate of methanol cross-over from anode to cathode through the Nafion membrane [54-57]. Unfortunately CO is the most stable intermediate formed during methanol electro-oxidation.

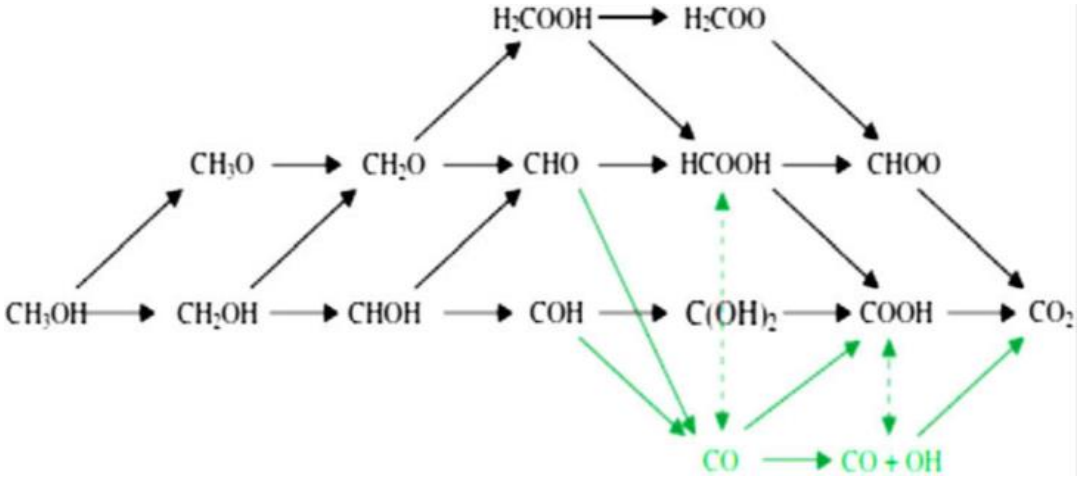

Figure2.6: Schematic representation of reaction paths and possible intermediates in MOR [58]

To overcome the issue of CO poisoning, platinum is usually alloyed, together with other metals such as Ru, Sn, Mo, and Cr, to help promote the catalytic activity and the oxidation of the chemisorbed CO [59]. PtRu has been identified through studies as the most active Pt-based alloy catalyst among all other platinum-based alloyed catalysts for enhanced activity and CO tolerance. It is, therefore, known as the state of the art DMFC anode catalyst.

ii. Methanol Crossover

The issue of methanol cross-over in DMFC that is linked to the use of Nafion membranes has been extensively studied and is one of the major drawbacks in the commercialization of DMFC [46, 60]. Methanol adsorbs on Pt sites in the cathode catalyst layer (CL) for the direct reaction between methanol and oxygen. The simultaneous oxidation of methanol and the reduction of oxygen reaction results in mixed potential on the cathode and reduces the cell voltage. The cross-over of methanol also leads to a waste of fuel which lowers fuel efficiency. In addition to this, the Pt surface gets poisoned by CO which is an intermediate of methanol oxidation. This poisoning effect ultimately results in instability as well as a reduction in cell performance [60]. Extensive efforts have gone into the modification of existing Nafion membranes and the development of new ones with a lower rate of methanol cross-over, but to date, no real break-through have been reported. The most common

approach used to lower the rate of methanol cross-over through the membrane is the use of thicker Nafion membranes, because when the thickness of the membrane is increased it can greatly decrease the methanol diffusion flux. However, a thicker membrane leads to an increase in the internal cell resistance, thereby degrading the cell performance. The compromise between the two effects is to employ Nafion 115 or 117 membranes, which by far have been proven to exhibit the best performance [46, 61-63]. Another approach that is commonly used is reducing methanol concentration in the anode CL, presently dilute methanol solutions (0.5-2.0 M) are usually fed to the DMFC so that the rate of methanol crossover can be minimized. It is crucial to maintain adequate methanol concentration in the anode CL such that both the rate of methanol crossover and the mass-transport loss can be minimized, for if the concentration of methanol is too low the low rate of methanol transfer can cause the methanol concentration in the anode catalyst layer to be too low, resulting in a large mass-transport loss and thus lower cell voltage. Hence, it is vital that a balance be achieved [43].

2.3 ELECTROCATALYSTS

2.3.1 Overview of Electrocatalysts

The concept of electro-catalysis is rather recent and has emerged since the advent of research in fuel cells as a practical means of energy conversion [64]. An electro-catalyst is a catalyst that participates in electro-chemical reactions and is used to modify the rate of chemical reactions without being consumed in the process. After the reaction, it can theoretically be recovered from the reaction mixture chemically unchanged. Electro-catalysts are a specific form of catalyst that function at the electrode surface or may be the electrode surface itself. They assist in transporting electrons between the electrode and reactants and/or facilitate an intermediate chemical transformation described by an overall half-reaction. An electro-catalyst can be heterogeneous, such as platinum surface or nanoparticles or homogeneous, like a coordination or enzyme [64]. The presence of a catalyst in a reaction lowers the activation energy required as shown in Figure 2.7 below, allowing the reaction to proceed more quickly or at a lower temperature.

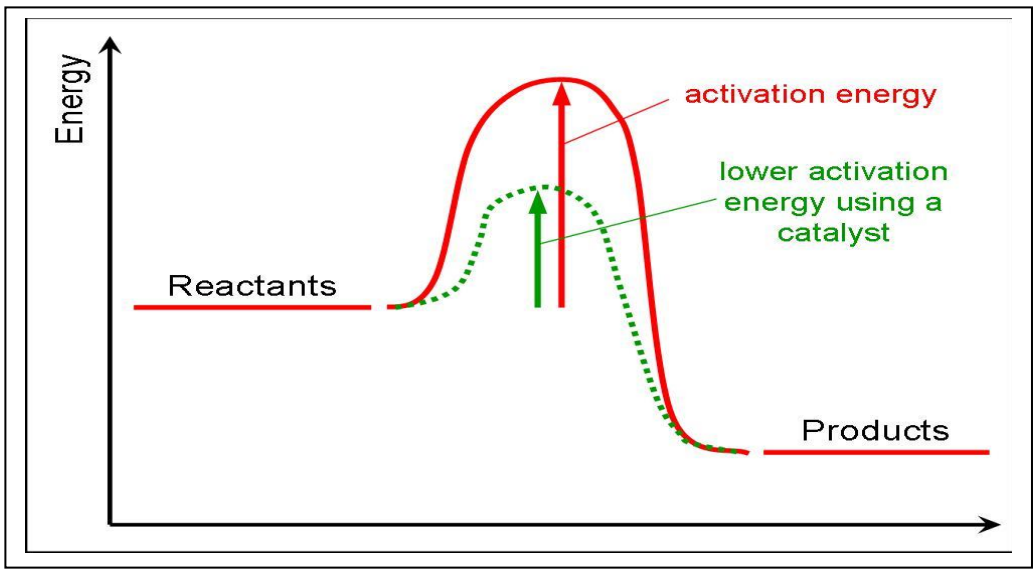

Figure2.7: Energy diagram showing the effect of a catalyst in a reaction [65]

For low temperature fuel cells, platinum is considered to be the catalyst of choice for both anode and cathode fuel cell reactions. The ORR at the cathode is a sluggish and complexed two/four electron reaction, even on pure platinum; the overpotential for ORR is in excess of 300 mV [28, 49]. Countless efforts have been made by researchers towards developing applicable catalyst materials, particularly for the ORR. In pursuit of improving the ORR catalyst activity, platinum is usually alloyed with a second transition metal forming binary electro-catalyst (PtFe, PtNi, PtCu, etc.) which will be discussed in detail in the following sections or use ternary electro-catalysts (PtNiFe, PtWFe, etc.). The introduction of a third metal to the alloy is expected to yield a combination of effects such as the reduction of the Pt-Pt lattice distance, the addition of surface sites for the formation of metal-oxygen bonds, the adsorption of OH^- and the modification of *d*-band centre [28, 49]. Thus, alloying Pt with transition metals is expected to increase the ORR catalyst activity greatly than monometallic Pt catalyst according to the following trend ternary> binary> monometallic Pt electro-catalysts. On the anode catalyst, most of the studies have focused on addressing the poisoning matter of the Pt catalyst mainly by CO. In the following sections the anode and cathode catalyst for DMFC applications will be discussed in detail, with emphasis on the ORR catalysts.

2.3.2 Electrocatalysts in Direct Methanol Fuel Cell

The key objective in DMFCs research and development is to develop low-cost, high-performance and durable electrocatalyst. However, the DMFC systems at present have high intrinsic costs and fairly poor durability [41]. The durability of a DMFC mainly depends on the characteristics of the MEA, while the reduction in cost critically relies on maximizing the performance of the MEA while minimizing the Pt content [49]. The lowering of the Pt loading on the electrodes has become the subject of much research as Pt covers a large portion of the DMFC's cost due to its high price and limited supply. The catalyst accounts for about 55% of the total stack cost (not including the balance of the plant) [49]. Hence, developing low-cost, high-performance and durable electrocatalyst is the number one priority for DMFCs research and development. Electro-catalysis in DMFC involves simultaneous occurrence of the methanol oxidation reaction at the anode and the oxygen reduction reaction at the cathode. Both these reactions require highly active electrocatalysts. At the current technical stage the most practical catalyst of choice is highly dispersed platinum and platinum based nanoparticles. These Pt nanoparticles are normally supported on high surface area carbon particles in order to increase the active Pt surface and enhance the catalyst utilization [54]. The major limitations with using platinum nanoparticles however, is the high intrinsic cost of metal platinum, the sensitivity of Pt to contaminants (especially to CO poisoning), intolerance of the metal catalyst to methanol oxidation at the cathode catalyst layer, and the dissolution of platinum [54]. The catalytic activity of Pt nanoparticles is hugely affected by a number of factors including:

a. Effect of particle size on electrochemical activity of the catalyst

The size of nanoparticles plays a significant role in the activity and durability of the electro-catalyst. Catalysis requires the use of nanoparticles possessing high electro-active surface area that must be controlled to maximize their activity and the most obvious route to improving the catalyst mass activity (mA/mg_{Pt}) and reduce the amount of Pt used is to obtain smaller particles by finding better ways to disperse them on carbon support [54, 66]. Studies have shown that small particle sizes in the range of (3-10 nm) show maximum mass specific activity for the methanol electro-oxidation [59]. However, Pt particles with smaller sizes are

more likely to grow and lose surface area, leading to durability concerns of DMFC. Therefore, Pt particle size is one of the key factors that determines the activity and durability of the Pt-based catalyst in DMFC. Up to now, there still remains some debate on the effect of particle size on the kinetics of ORR. Literature proposes that catalytic activity might be dependent on the relative concentrations of the Pt surface atoms, the coordination numbers of the localized atoms and the ratio of desirable crystal planes on the crystallite surface [67].

b. Effect of heat treatment on electrochemical activity of the catalyst

The electro-catalytic performance is known to depend strongly on preparation procedures including the addition of metal and its precursor, the support type and supporting strategy and the heat-treatment strategy [54]. Various heat-treatment techniques, such as traditional oven /furnace heating, microwave heat treatment and ultrasonic spray pyrolysis have been employed to prepare PEM fuel cell electro-catalysts. The traditional oven/ furnace heating technique has been one of the most popular and widely used techniques. Basically, it involves heating the catalyst under an inert (N_2, Ar, or He) or a reducing (H_2) atmosphere in the temperature range of 80^o C -1200^o C for 1-4 hours [54, 66]. The benefits of heat treatment are to remove any undesirable impurities that results from early stages of preparation. Heat treatment also allows for uniform dispersion and stable distribution of the metal on the support and therefore improves the electro-catalytic activity of the synthesized catalyst [54, 66]. The heat treatment has a prominent effect on the metal particle size and size distribution, particle surface morphology and metal dispersion on the support. The particle growth of the catalyst during heat treatment of Pt and its alloys can result in both higher activity and durability [66]. Jalan *et al* [68] reported that heat treatment of Pt catalyst lowers the dissolution rate in addition to reducing the initial surface area. Heat treatment also affects the fundamental properties of the catalyst and its support, including, the number of catalytic sites, distribution of the catalyst particle on the support, the loading level of the catalyst on the support and the acid-base properties of the support [54, 66]. The role of heat treatment on catalyst properties is significant in terms of improving the activity and durability of the catalyst and has been recognized as an important or at times a necessary step for the catalytic improvement of ORR synthesized catalyst [54]. For the benefits mentioned above resulting from heat treatment, the synthesized supported electro-catalysts used in this study were subjected to heat treatment to enhance their ORR catalytic activity.

c. Effect of degradation of the catalyst on its electrochemical activity

The size of Pt-based catalyst used in DMFC is in nm scale, typically in the range of 2-6 nm. Nanoparticles inherently show a strong tendency to agglomerate owing to their high specific surface energy. For nanoparticles, the smaller the size, the higher the specific surface area, and the easier it is to agglomerate [66]. Thus when Pt nanoparticles agglomerate to bigger ones; the electrochemical surface area of Pt catalysts decreases and consequently the performance of the DMFC degrade. The oxidation of the carbon support also accelerates Pt degradation, and when the carbon support is oxidized, Pt or Pt alloy falls off the support resulting in a decline in the electrochemical surface area [66].

2.3.3. Anode Electrocatalyst for Methanol Oxidation Reaction (MOR)

Indeed very few electrode materials have been shown to be capable of adsorbing methanol in acid media and, of these only Pt based materials display enough stability and activity to be attractive as fuel cell electro-catalysts [67]. The main challenge with using platinum metal as a catalyst is the sensitivity of the metal catalyst to carbon monoxide poisoning. CO, an intermediate of methanol oxidation which is adsorbed strongly on the surface of Pt (equation 2.7) and blocks the catalytically active area of Pt, and in so doing significantly decreases its reactivity, resulting in sluggish electro-kinetics and low catalytic efficiency [22, 69]. Various Pt based alloys such as PtRu, PtMo, PtW, PtSn, and PtOs have been investigated in order to improve the efficiency of methanol [55, 66, 67, and 69]. Among them, PtRu alloy with the atomic ratio of 1:1 has been found to have better performance because of its suitable structural composition, alloying degree, particle size and morphology [69]. Ru, which alloys with platinum, promotes the adsorption of the oxygen containing species at lower potentials (0.25 V vs. NHE) and facilitates the oxidation of CO to CO_2, thereby, reducing the effect of platinum poisoning [45]. The use of alloying platinum with less noble metal is also useful in terms of cost reduction as alloying reduces the loading of the expensive platinum metal [46]. The MOR, catalysed by PtRu catalyst, is assumed to follow through two mechanisms, namely: the bifunctional effect and the ligand effect. The bifunctional effect [59] involves de-hydrogenation of the adsorbed methanol molecule to form poisonous intermediate CO, which further becomes adsorbed on the Pt surface (equation 2.7). The Ru atoms provide sites for

water adsorption and dissociation, thus, forming oxygen-containing species on Ru sites (equation 2.8) and this promotes the oxidative removal of CO_{ads} to CO_2 (equation 2.9) [59].

$$CH_3OH + Pt \rightarrow Pt\text{-}CO_{ads} + 4H^+ + 4e^- \quad (2.7)$$

$$Ru + H_2O \rightarrow Ru\text{-}OH_{ads} + H^+ + e^- \quad (2.8)$$

$$Pt\text{-}CO_{ads} + Ru\text{-}OH_{ads} \rightarrow Pt + Ru + CO_2 + H^+ + e^- \quad (2.9)$$

The ligand effect assumes that the change of Pt electronic properties, brought by the presence of ruthenium, makes Pt atoms more susceptible to OH adsorption, even for dissociative adsorption of methanol [59]. It was observed that the threshold potential, where the decomposition of methanol proceeds by creating products other than CO_{ads} depends on the catalyst surface and electronic structure [59- 61]. A fundamental understanding of the effects of structural parameters on the catalytic activity has been found to be necessary for the design of high performance DMFC catalysts [61].

2.3.4 Cathode Electrocatalyst for Oxygen Reduction Reaction (ORR)

The cathode accounts for about one third of the performance losses in a PEMFC, mainly due to the limitations of the ORR catalyst [49]. The ORR on the cathode is a key reaction in the fuel cell system, specifically those operating at low temperatures such as PEMFC and DMFC [32]. The ORR is universally sluggish, even more so for the cathode of a DMFC, as the cathode catalyst layer experiences the cross-over of methanol, making the cathode electro-catalyst having to simultaneously catalyse the oxygen reduction and the undesired methanol oxidation reactions. This results in mixed potentials at the cathode and leads to a loss of fuel efficiency. ORR is also a challenging reaction to catalyse, in the sense that it requires catalyst material to be: 1) stable under the extreme corrosive conditions at a DMFC cathode; 2) chemically active so as to be able to activate O-O bond; and 3) noble enough to be able to release the oxygen from the surface in the form of H_2O [49]. Pt at the moment seems to be the best metal catalyst for ORR in DMFCs that meets the requirements stated above and is therefore widely employed and known to be the state of the art cathode catalyst for low temperature fuel cells [55]. The ORR has been known to proceed along two parallel pathways in aqueous electrolytes according to the following reactions [70]:

$O_2 + 4H^+ + 4e^- \rightarrow 2H_2O$ $E_0 = 1.23$ V vs. NHE (2.10)

$O_2 + 2H^+ + 2e^- \rightarrow H_2O_2$ $E_0 = 0.70$V vs. NHE (2.11)

$2H_2O_2 + 2H^+ + 2e^- \rightarrow 2H_2O$ $E_0 = 1.76$V vs. NHE (2.12)

The first possible pathway (equation 2.10) is referred to as the direct four-electron pathway, where oxygen adsorbs to the surface of platinum to generate a species that undergoes further steps that include accepting protons and electrons and cleaving the oxygen-oxygen bond to eventually produce water [71-72]. The second possible pathway is referred to as the indirect two-electron pathway (equation 2.11), where oxygen combines with two protons and two electrons to give hydrogen peroxide. The formed H_2O_2 gets further reduced to water (equation 2.12). It is commonly accepted that the 4-electron pathway is faster than the 2-electron pathway hence, it is the most preferred pathway reaction in fuel cells [70, 73]. The two electron pathway reaction is highly undesired in fuel cells. Not only does it reduce the efficiency of the system, but also the strong oxidation that is linked with the produced hydrogen peroxide can degrade the catalytic activity of the catalysts and membrane, thereby resulting in significant fuel cell degradation or even failure [23].

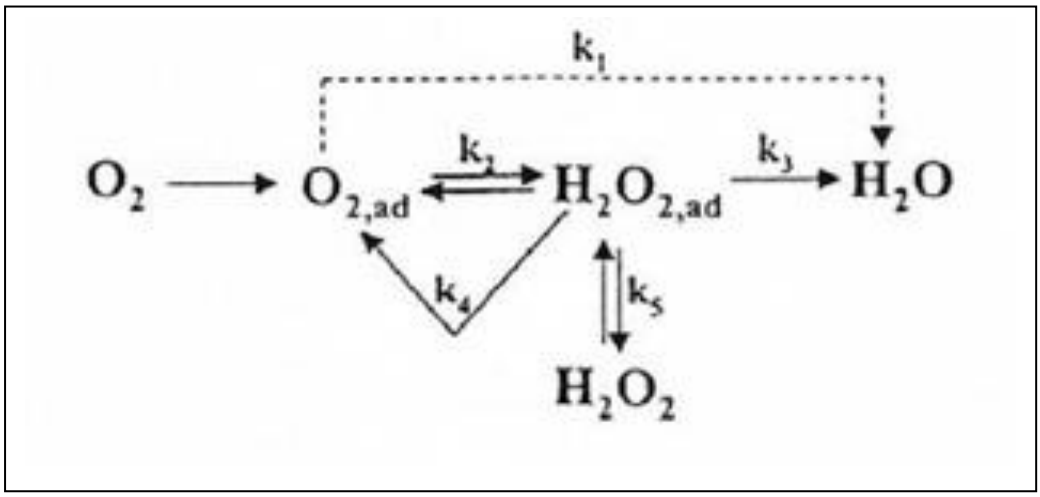

Figure2.8: The oxygen reduction reaction mechanism on Pt surface electrodes [74]

As explained above, the ORR is a multi-electron reaction that involves a number of elementary steps involving different reaction intermediates [70]. The overall reaction mechanism still remains unsolved. Figure 2.8 above illustrates the simplified version of the

mechanism involved in the ORR to produce the only two products of the reaction that is water and/or hydrogen peroxide [70]. The mechanism shown in Figure 2.8 indicates that O_2 can be reduced either directly to water (direct 4-electron reduction) electrochemically with the rate constant k_1, or to adsorbed hydrogen peroxide with the rate constant k_2 (2-electron reduction). H_2O_2 can be further reduced to water with the rate constant k_3, chemically decomposed on the electrode surface k_4, and/or desorbed into the electrolyte solution k_5 [70].

The catalytic activity of Pt towards ORR is known to strongly depend on its O_2 adsorption energy, the dissociation energy of the O-O bond and the binding energy of OH on the Pt surface. The electronic structure of the Pt catalyst (Pt d-band vacancy) and the Pt-Pt interatomic distance (geometric effect) can strongly affect these energies [70]. To enhance the catalytic activity of Pt towards ORR, Pt is usually alloyed with transition metals forming Pt-M where (M= Fe, Co, Ni, etc.), the Pt-M electro-catalyst has been projected to have higher electro-catalytic activity than pure platinum [70]. The enhancement of activity that takes place when Pt is alloyed with other metals can be elucidated by the change in the electronic structure of Pt (the increased Pt d-band vacancy) and in the geometric effect (Pt-Pt interatomic distance). Alloying of Pt with other metals is known to cause lattice contraction, which leads to a more favourable Pt-Pt distance for the dissociative adsorption of O_2. The d-band vacancy can be increased after alloying, creating a strong metal-oxygen interaction and then weakening the O-O bonds thereby improving the kinetics of ORR [70].

2.3.5 Binary Catalyst

Indeed Pt/C electro-catalyst is currently the best material to be used in low-temperature fuel cells. However, platinum is costly and the world's supply of Pt is limited [75] as South Africa and Russia are the only two countries that produce Pt on a large scale, South Africa accounting for 80% of that production. Therefore, reducing the platinum loading in fuel cell applications and still maintain the catalytic activity has become the subject of most research. Efforts have been made to reduce the Pt loading through: 1) increasing the Pt catalytic activity by incorporating transition metals; and 2) improving the Pt utilization by increasing the surface area and dispersion of Pt nanoparticles using high surface area supports. Other approaches made include developing Pt-free catalyst and non-noble metal catalyst for ORR [49]. Platinum in DMFCs is used as an anode and cathode electro-catalyst.

At the anode, methanol oxidation occurs and it is a slow reaction that requires active multiple sites for the adsorption of methanol and sites that can donate OH species for the desorption/oxidation of the adsorbed methanol residue [71-72]. As is well-known, pure platinum at room or moderate temperatures is easily poisoned by CO, an intermediate in the oxidation of methanol [36, 49]. To date, the approach to overcome this problem has been to alloy Pt with transition metals including, Ru, Sn, Mo and Cr, where the second metal is believed to assist in the promotion of CO to CO_2, and accordingly improve the catalytic activity and CO tolerance of the alloyed electro-catalyst [60].

It is well-known that the cell voltage of DMFC is limited by sluggish kinetics at the cathode electrode (ORR). The search for ORR catalysts that are more active, less expensive and more stable than Pt has led to the development of Pt alloys [75]. Some Pt-based binary alloys, including PtFe, PtCo, PtNi and PtCr, exhibit higher catalytic activity for the ORR in pure acid electrolytes than pure Pt [75]. The cause for the higher catalytic activity of Pt based binary catalysts have been reported to be due to: 1) an increase in the resistance to particle sintering; 2) surface roughening due to the removal of some base metal, increasing the Pt surface area; 3) preferred crystallographic orientation; 4) geometric factors (*i.e.* decreased Pt-Pt bond distance); 5) electronic factors (i.e. increased Pt d-band electron vacancy of the Pt skin layer originating from the bulk alloys) and 6) oxygen adsorption differences due to modified anion and water adsorption [28, 49, 76-79]. Toda *et al*. [80] have explained the enhancement in the Pt-M catalytic activity based on an increase in the d-orbital vacancy, promoting a stronger metal-oxygen interaction and the formation of a stronger Pt-O_2 bond with the adsorbed O_2 species. The stronger Pt-O_2 can cause a weakening and lengthening of the O-O bond and an easier scission of the O-O bond, resulting in an increased reaction rate. Mukerjee *et al*. [81] explain the enhanced Pt-M alloy activity based on the decrease in the Pt-Pt distance and Pt-Pt coordination numbers. The improved electro-catalytic activity can be explained by an electronic factor, that is, the change of the d-band vacancy in Pt upon alloying and/or by geometric effects (Pt coordination number and Pt-Pt distance) [75]. Thus, the alloying of Pt with a second metal, whether for methanol electro-oxidation or oxygen electro-reduction, has proven to be a necessary path, not only in reducing the use of the expensive Pt metal catalyst, but also in enhancing the activity of the electro-catalyst. Thus, this study has focused on using binary Pt-based electro-catalyst.

2.3.6 Catalyst Used in this Study

The following electro-catalysts were investigated in this study for their applicability in the cathode of a direct methanol fuel cell.

2.3.6.1 PtRu Electrocatalysts

PtRu electro-catalyst supported on high surface area carbon has been extensively studied as an anode catalyst owing to the presence of ruthenium which promotes the CO to CO_2, alleviating the Pt catalyst of the CO. Supported PtRu was used as a cathode electrode in this study to suppress methanol effects (CO poisoning). Namgee *et.al* [134] reported on PtRu black as a cathode catalyst mainly employed to suppress the effect of methanol on the primary catalyst (Pt/C) by helping with the oxidation of CO-like species nearby the poisoned Pt surfaces; supported PtRu, however has not been reported according to the author's knowledge as a cathode catalyst. Thus, it was of interest to examine the catalytic activity of PtRu alloy towards ORR and was therefore chosen for this research as a cathode catalyst for direct methanol fuel cell application.

2.3.6.2 PtSn Electrocatalyst

Sn electro-catalysts have so far been less employed for the ORR in comparison with other metals such as Fe, Co, Cu, and Ni *etc*. Indeed, very few studies have reported on PtSn alloy as oxygen reduction and methanol tolerant cathode catalyst. Hence, it was of interest to examine if PtSn alloys could be ORR active and methanol tolerant cathode catalyst for DMFC applications. PtSn was therefore employed in this study as a cathode electro-catalyst for ORR. It has been reported by some studies that Sn improves the catalytic activity of Pt towards methanol oxidation [23, 82-83]. There are reports of low or no improvement of methanol oxidation by Sn when PtSn alloy systems are used. In actual fact, such improvements were later found to be due to other superseding factors than the effect of Sn on methanol oxidation, typically involving "ensemble" effects [84]. Colmati *et.al* [85] reports that adsorption-de-hydrogenation of methanol becomes more difficult due to alloying of Sn with Pt and methanol oxidation occurs only at moderate alloying. Jehabharathi *et.al* [23] used PtSn/C as a cathode electro-catalyst for DMFC and reported that PtSn/C catalyst showed much higher

methanol tolerance during the oxygen reduction reaction process than Pt/C catalyst, to the extent that it has been concluded that PtSn/C bimetallic catalyst may function as oxygen reduction and methanol tolerant cathode catalyst in a direct methanol fuel cell. PtSn catalysts have also been used for carbon monoxide oxidation, ethanol oxidation, hydrogenation reaction and dehydrogenation of isobutene.

2.3.7 Preparation Methods of Electrocatalysts

The common criteria for high performance catalysts include a narrow nanoscale size distribution, a uniform composition throughout the nanoparticles, a fully alloyed degree and high dispersion on supporting material. All these elements depend on the preparation stage, making the synthesis of Pt nanoparticles of practical importance as it influences greatly the performance of the resultant electro-catalyst. There are three major methods for preparing supported Pt-based nanoparticles. They include [86]: 1) the impregnation method; 2) the colloidal method and 3) the micro-emulsion method.

Impregnation method is the most used method of the three. It is a relatively simple and straight forward chemical preparation technique for catalyst preparation that can produce small particles in the range of 3-7 nm with controlled loading [86, 87]. The impregnation method includes an impregnation step, where Pt and Ru precursor salts are mixed with the support material typically high surface area carbon black to form a homogenous mixture. The chemical reduction can be carried by liquid phase reduction using $Na_2S_2O_3$, $NaBH_4$, $Na_4S_2O_5$, N_2H_4 or formic acid as a reductive agent, or gas phase reduction using a flowing hydrogen stream as a reductive agent under elevated temperatures. The major drawback in the impregnation method is the difficulty in controlling nanoparticle size and distribution [86, 87].

Colloidal method which was employed in this study has been extensively explored as a preparation method for Pt [86, 88]. Usually the colloidal method includes the following common steps: 1) preparation of Pt containing colloids; 2) deposition of the colloids onto the support; and 3) chemical reduction of the mixture. Other colloid methods using several reducing agents, organic stabilizers or shell-removing approaches have also been developed in recent years. The colloidal method using ethylene glycol (EG) as a reducing agent and solvent was employed in this work as a method of synthesis for PtRu and PtSn electro-

catalysts. In this process (polyol reduction) ethylene glycol acts as both reducing agent and solvent for the Pt precursor. During the reduction step the solution of EG and Pt precursor salt is heated to 120-170^{o}C. In this step EG is decomposed and produces the reducing species (CH_3CHO-acetaldehyde, equation 2.15) [89].

$$CH_3OCH_2OH \rightarrow CH_3CHO + H_2O \quad (2.15)$$

$$2CH_3CHO + (PtCl_6) + 6OH^- \rightarrow 2CH_3COO^- + Pt + 6Cl^- + 4H_2O \quad (2.16)$$

The acetaldehyde reduces the Pt ions to metallic Pt particles as presented in equation 2.16. The main advantage of this polyol synthesis is that the acetate can also serve as a stabilizer for Pt colloids through the formation of chelate-type complexes through its carbonyl group. The application of stabilization agents to protect Pt particles from agglomeration is therefore not necessary. Consequently, the preparation of carbon-supported catalyst with smaller noble metal sizes and narrow size distribution is possible.

Microemulsion method is a relatively new method for synthesizing catalysts that has been developed in recent years [86, 90-91]. The microemulsion is a nanoscaled aqueous liquid droplet containing a noble metal precursor. The droplets are engulfed by surfactant molecules and uniformly in an immiscibly continuous organic phase. The first step in this method is the formation of Pt nanoparticles through water-in-oil microemulsion reaction, followed by a reduction step. The microemulsion here serves as a nanoscaled reactor in which the chemical reactions take place. The reduction step can be carried out by either adding a reducing agent (e.g., N_2H_4, HCHO, and $NaBH_4$) into the microemulsion system, or by mixing it with another reducing agent-containing microemulsion system. As a result the reaction is kept into the inside of the nanoscale microemulsion, and the formed particle sizes can be easily controlled by the magnitude of the microemulsion size. The removal of surfactant molecules can be easily carried out by heat-treating the high surface area carbon support nanoparticles. The main advantage of the microemulsion method is its ease in controlling metallic composition and particle size within a narrow distribution by varying the synthetic conditions, however, using this method is expensive as it uses costly surfactants molecules and another drawback to employing the microemulsion method is that it requires a number of separation and washing steps, which may be suitable for large-scale production [86, 90-91].

2.4 SUPPORT MATERIAL

Supporting strategies have been explored in order to obtain fine dispersion, high utilization, and stable nanoscale metallic particles [86]. The supporting material for the functioning of the electrocatalyst is very crucial and it should be a combination of high surface area, high electronic conductivity, and good corrosion resistivity. It has been proven through research that supported catalysts show improved catalytic activity and stability in comparison to unsupported bulk metal catalysts [86, 92]. For low-temperature fuel cells, Pt and Pt alloys are employed as anode and cathode catalysts and are supported on a high surface area substrate; and the structure and proper dispersal of these metal particles on the support material allows for low loading catalyst to be possible for fuel cell operation [93]. When a catalyst is dispersed to the support material, it bonds to the support material and that creates an interaction between the metal catalyst and the support material and, as a result of this interaction, the support material is able to influence enormously the activity and durability of the electro-catalyst [68]. The effect of the interaction can be elucidated in two distinctive ways: 1) the support material could modify the electronic character of the catalyst particle which in turn could affect the reaction sites present on the surface of the catalyst; and 2) the support material could also modify the shape of the catalyst particles and this effect is termed the geometric effect [68]. Both these effects (electronic and geometric effect) could change the activity of catalytic sites on the metal surface and modify the number of active sites present, thereby improving the catalytic efficiency. Moreover, the support can also help in sufficiently enhancing the catalyst performance and durability by reducing catalyst poisoning [92, 93]. Hence, the choice of support material is vital and highly influential in determining the behaviour, performance, longetivity and cost effectiveness of the catalyst and the overall fuel cell. The main requirements needed from a support material to be able to achieve a high performing fuel cell catalyst are as follows [86, 92,-94]:

- High surface area to obtain high metal dispersion;
- Sufficient electrical conductivity so that the support can act as a path for the flow of electrons;
- Suitable porosity to boost gas flow;
- Electrochemical stability of the catalyst support in fuel cell environment which is key in the development of new substrates;
- Good catalyst support interaction;

- Easy recovery of the catalyst [66-68].

Support materials are categorized in to two that is: 1) the primary supports such as novel nanostructured carbon and 2) the secondary supports such as oxides, which have been used mainly to modify and promote the primary supports, even though they are capable of being used as independent supports. This study focuses on carbon nanotubes as possible supports to replace the conventional carbon black. With regards to conductive metal oxides, the study will examine the applicability of titanium oxide and molybdenum oxide as support materials. The interest on the metal oxides is more on improving the stability and durability of the catalyst than catalytic activity.

2.4.1 Carbon Support Materials

To reduce the amount of precious metal used, Pt is usually supported on a high surface area carbon in the form of nano-dispersed particles. The dispersement of these nanoparticles on the carbon support allows for high-catalyst surface area at low-catalyst loadings. Carbon black is the typical catalyst support material of choice for DMFC applications. There are various types of carbon support materials including the conventional carbon black, nanostructured carbon such as carbon nanotubes and carbon nanofibers, mesoporous carbon, nano-diamonds and doped diamonds, as well as graphene [86, 94]. The carbon support boasts of essential fuel cell properties such as: high surface area, high electrical conductivity compared to other supporting material, well-developed pore structure, as well as availability and cost effectiveness of the carbon material. Unfortunately, with all those outstanding advantages, carbon support suffers from electrochemical instability in the fuel cell environment which is a major drawback in using them as support materials. The carbon support, especially at the cathode, undergoes oxidation in the presence of water and is usually termed as carbon corrosion, according to the following reaction:

$$C + 2H_2O \rightarrow CO_2 + 4H^+ + 4e^- \qquad E_0 = 0.207 \text{ vs. NHE} \quad (2.14)$$

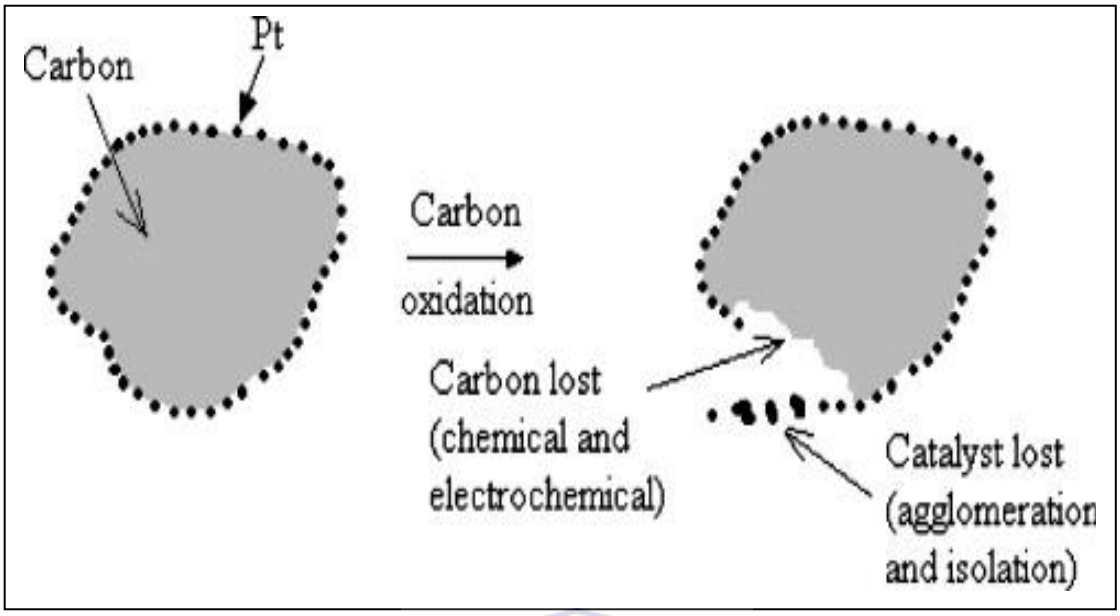

Figure2.9: Schematic representation of carbon oxidation [95]

Carbon corrosion causes the performance of the catalyst to degrade quickly, resulting in it creating a short life-time for the fuel cell that is inadequate for most of its projected applications. Agglomeration of a platinum catalyst on the carbon surface is inevitable as carbon corrosion becomes more severe [49]. Corrosion of the carbon support also results in separation of Pt particles from the support material as shown in Figure 2.9 above and ultimately a loss of catalytic performance. These separated Pt particles would become electronically isolated and the isolation would lead to a low Pt utilization as well as degrading fuel cell performance. The standard potential for the oxidation of carbon to CO_2 is 0.207V vs. NHE at 25^o C. This implies that under typical DMFC cathode operating conditions, carbon corrosion is not only thermo-dynamically possible because of high potentials (0.6-1.2V) and high concentration of oxygen, but it is also kinetically boosted by the elevated temperatures (50-90^o C) [86, 92-94]. The carbon support materials used in this study include:

2.4.1.1 Carbon Black

Carbon black is the most commonly used support material for Pt and Pt-alloy catalysts for fuel cells in many studies and commercial applications. There are various types of carbon blacks, such as Acetylene Black, Vulcan XC-72, Ketjien Black, etc. [96-97]. They are generally manufactured by pyrolysing hydrocarbons such as natural gas or oil fractions taken from

petroleum processing [96]. They exhibit a three dimensional structure of micro-crystalline primary particles (20-50 nm in diameter) aggregated to amorphous clusters. As a result of their heterogeneous structure, the primary particles exhibit a high density of surface defects. These defects represent crystallographic sites of different activity for the adsorption of surface species, mainly hydrogen and oxygen functional groups. In the literature, phenol, carboxyl, carbonyl, quinone and lactone groups are identified [96-97]. Carbon oxidation also starts at the edges and corners of basal planes since these exhibit unsaturated valence and free б electrons [69]. Carbon black (CB) possess necessary properties such as high surface area ($\backsim$250 m^2/g for Vulcan XC-72), high electronic conductivity, ease of recovery of the expensive metal catalyst from the support, low cost and the availability of CBs which helps to reduce the overall cost of the fuel cell. These unique properties have made them to be a popular choice to support fuel cell electro-catalysts [92, 96]. With all their benefits, carbon black has some undesired limitations such as thermo-chemical instability, which is a requirement under acidic conditions of DMFC to enhance the life-time of the fuel cell. The absence of it leads to corrosion of the carbon support resulting in disintegration of catalyst layer [43]. Hence, new support materials are being sought after to replace the conventional carbon black and among them are the carbon nanotubes [86, 92-94].

2.4.1.2 Carbon nanotubes

Carbon nanotubes were first imaged by Iijima in 1991 and have since generated an interest amongst a lot of scientists and engineers that exceeds almost any material known to man [98]. Carbon nanotubes have stimulated a great interest for several applications, including hydrogen storage, field emission, super-conductivity and heterogeneous catalysis. The unique structural, mechanical and electrical properties of CNTs have made them to be proposed as a replacement for traditional carbon black, as an alternative support for fuel cell catalysts [99]. Carbon nanotubes consist of rolled up graphene hexagonal sp^2 carbon layer, which forms cylinders with diameters of nanometre sizes and length of up to millimetres [100]. They are synthesized as single wall carbon nanotubes (SWCNT) or multi-walled carbon nanotubes (MWCNT) [86, 92]. The structure of SWCNT can be conceptualized by wrapping one-atom thick layer of graphite into a seamless cylinder and the MWCNTs are a collection of concentric SWCNTs (Figure 2.10 below) [100]. SWCNTs have been found to have more

surface area (typically 400 and 900 m^2/g) and are often reported as metallic or semiconductors, while the surface area of as produced MWCNTs have been reported in values ranging between (200 and 400 m^2/g) and have relatively high electronic conductivity and high chemical stability [86, 92]. It is because of their high electronic conductivity and chemical stability that MWCNT have been chosen as support material for this study.

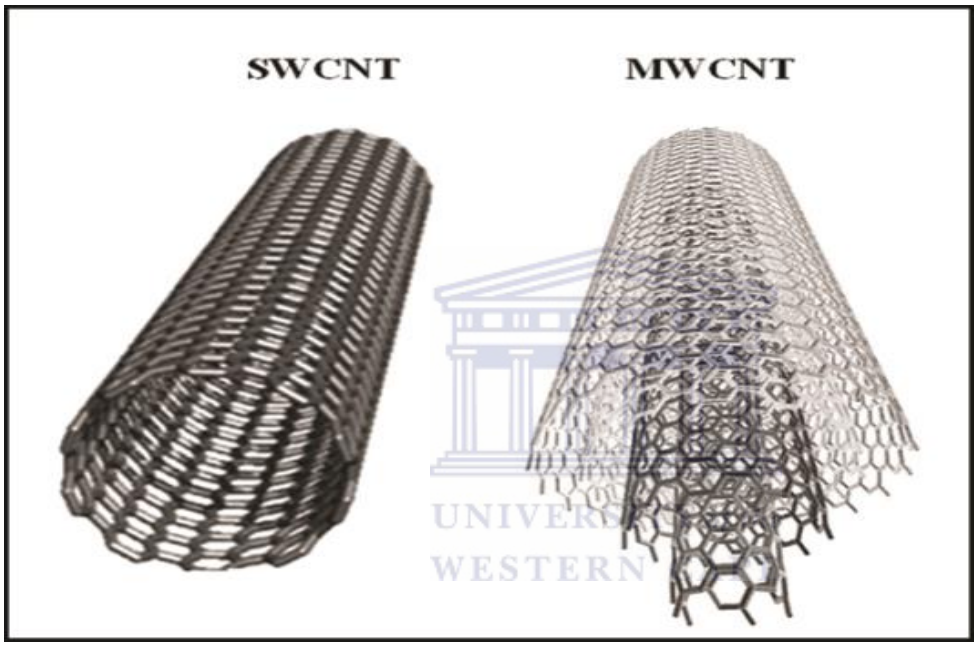

Figure 2.10: Schematic diagram of SWCNT and MWCNT [86]

MWCNTs are usually synthesized by various methods such as arc discharge, laser ablation, plasma enhanced chemical vapour deposition (PECVD), and catalytic chemical vapour deposition (CCVD). The synthesis of CNTs via CCVD has been widely used, as it offers a promising route for bulk production of CNTs, which can possible lead to commercialization [100]. MWCNTs are chemically inert by nature and thus make it difficult to attach metal nanoparticles on them. As a result of their inertness, surface modification of MWCNTs before metal deposition was found to be necessary for achieving optimal interaction between the support and the catalyst precursor. Surface modification introduces surface oxygen groups (using strong acid such as HNO_3, H_2SO_4, etc.) in order to make the surface more hydrophilic and thus improve the catalytic support interaction. The most commonly used pre-treatment is that of refluxing CNTs in a nitric acid solution (chemical treatment) to create acid site on the surface, which can act as nucleation centre for metal ions, making it possible to obtain better

dispersion of metal nanoparticles, better size control and distribution. The other method used is called dry treatment using DBD plasma under air. Chemical treatment of MWCNT was used in this study based on the success of the method from literature [86, 92, 99-100]. MWCNTs have been used to support a wide variety of mono, binary (e.g. PtRu, PtFe, and PtCo) as well as ternary catalyst (e.g. PtRuPd, PtRuOs, and PtRuNi) systems using both noble and non-noble metals [86, 92]. The advantages of MWCNTs include, fewer impurities when compared to CBs, are more resistant towards corrosion than CBs whilst at the same time they are free from the deep cracks that exist in CBs in which the Pt nanoparticles deposited will lose catalytic activity because the electro-chemical triple phase boundary (TPB) does not form [92]. It is because of these advantages already stated above, that MWCNTs have been chosen as support material for this study. They have been used in this study to improve catalyst activity and durability of the binary electro-catalysts.

2.4.2 Inorganic Oxides as Supports

Traditionally, carbon materials have been extensively employed as electro-catalyst support for fuel cell applications owing to their high surface area, high electrical conductivity, high availability and low cost. Unfortunately, the corrosion of carbon support under fuel cell environment is a major hindrance in using these materials. Although some improvements have been achieved in reducing the undesirable reaction by employing nanostructured carbon like having carbon nanotubes in place of the conventional carbon blacks, however, complete elimination of carbon oxidation has yet to be attained [92]. Furthermore, the functionalization done to improve the anchorage of the catalyst nanoparticles on the support and reduce agglomeration, make the carbon support more inclined to electro-chemical oxidation, leading to a loss of active surface area. There is therefore, an urgent need to explore other non-carbonaceous supports to address these issues [92]. Conductive oxides such as titanium oxides, tin-based oxides, tungsten oxides, ruthenium oxides, silicon dioxide and indium tin oxide etc. have been greatly investigated because of their extreme resistance to corrosion character [94]. This work will be focusing on titanium oxide and molybdenum oxide as support materials for PtRu and PtSn electro-catalysts.

2.4.2.1 Titanium oxide (TiO_2)

Titanium dioxide, also known as titania is the naturally occurring oxide of titanium. Titanium oxide materials have been used in many applications that depend on its photo-electrochemical and catalytic properties and its excellent resistance to corrosion in various electrolytic media [94]. The high corrosion resistance and electrochemical stability demonstrated by these oxides even in acids media have encouraged studies of these oxides as catalyst support in fuel cells [92]. Titania exists in three main crystallographic forms e.g. anatase, rutile, and brookite. Each structure exhibits different physical properties which lead to their different applications [67, 69]. It is generally accepted that anatase titania is more efficient as photo-catalyst than rutile titania [92, 94]. TiO_2 has a hypo-d- electron character which interacts with inert noble metals, like Pt, changing additional the catalytic activity of the Pt. Furthermore, TiO_2 may improve the Pt oxygen reduction activity through facilitating mechanisms, such as reactants surface diffusion and oxygen spill-over. These properties together with the fact that they are easily available, non-toxic, and cost effective recommend consideration of TiO_2 as an alternate fuel cell catalyst support [92, 102]. Thus, anatase titania was chosen as support material for this study.

2.4.2.2 Molybdenum oxide (MoO_2)

Molybdenum oxide has been used in low-temperature fuel cells as a co-catalyst with Pt forming platinum alloys. But, for this study, it will be employed as support material. According to the author's knowledge, molybdenum oxide has not been used as support material for PtRu and PtSn electro-catalyst for the cathode of a DMFC. Thus, it became of great interest to study the potential of molybdenum oxide as a support material. The high corrosion stability of molybdenum oxides in alkaline and acidic media and the relatively high electronic conductivity have also hugely encouraged the study of this oxide as a possible support material. Nonstoichiometric lower valence molybdenum oxides, called the Magneli phases, which have composition between MoO_2 and MoO_3, have a rutile-type structure with short metal-metal distance along the direction of the edge sharing, which accounts for the high electronic conductivity of these materials [103]. Thus molybdenum was chosen as the support material for this study.

2.5 SUMMARY

Currently DMFCs are attracting much attention as the fuel cell of choice and find appealing applications in portable devices owing to their unique features. Despite progress made in the development of DMFCs; their performance is limited because of poor kinetics of the anode and cathode reaction, poisoning of catalyst material and methanol cross-over from anode to cathode through the polymer electrolyte membrane. Developing high performance, cost-effective and durable electro-catalysts, is thus, the number one priority for DMFC's research and development. The catalytic activity of Pt-based catalyst has been found to strongly dependant on the composition, structure, morphology, particle size, alloying degree and support material. The synthesis of these metal particles as electro-catalytic materials with uniform size and good dispersion on the support material has become of great importance. Thus, alloying and supporting strategies enable both performance increase and cost reduction for DMFCs by dramatically reducing the Pt content in the catalyst without performance compromise. Hence, this project has been dedicated to studying the effect of different support material to improve the activity and durability of the electro-catalyst, thereby lowering the over-all cost of the DMFC system.

CHAPTER 3

METHODOLOGY

This chapter provides a detailed description of the methods, materials and techniques that were employed in the characterization of the electro-catalysts (commercial and/or synthesized) used in this study. The pivotal role played by the physical-chemical properties of the electro-catalyst in enhancing the performance and cost reduction of the catalyst cannot be overstated. Literature reveals that the decreased particle size of an electro-catalyst leads to some change in the properties of the electro-catalyst. Upon decreasing the particle size and uniformly dispersing the nanoparticles on the supporting material, the activity of the catalyst is increased and the loading of the catalyst used is greatly reduced. Hence, an improvement in the performance of the fuel cell catalyst and the much desired cost reduction can be achieved. Literature also reveals that heat treatment of the synthesized supported electro-catalysts also results in some change in the properties of the supported electro-catalysts, leading to a uniform dispersion and stable distribution of the metal nanoparticles on the support. This, therefore, improves the electro-catalytic activity of the synthesized catalyst. Pt-based nanoparticles can be dispersed as small particles when the supporting material has a high surface area and, ideally, it should be a conductive material. It is therefore crucial to gain better understanding and be able to measure the enhanced properties of these materials as their physical-chemical characteristics play a vital role in their use as catalysts for DMFC applications.

In this study, binary PtSn and PtRu electro-catalyst were dispersed on the surface of the conductive support material such as multi-walled carbon nanotubes, titanium oxide and molybdenum oxide for effective use. The preparation methods and techniques used to analyse PtRu and PtSn nano-materials are discussed. Sample preparation and other experimental parameters are also detailed.

As discussed in the literature review section, the following techniques have proven to be useful and were therefore employed in this study as techniques in the investigation of

physical-chemical properties of the supported electro-catalysts (commercial and/or synthesized).

For structural identification of the catalyst- 3 instruments were used

- X-ray diffraction microscopy (XRD)
- High-resolution transmission electron microscopy (HRTEM)
- High-resolution scanning electron microscopy (HRSEM)

For elemental analysis

- Energy dispersive spectroscopy (EDS)

For electrochemical characterization

- Rotating disk electrode (RDE)
  Cyclic voltammetry
  Linear sweep voltammetry

3.1 MATERIALS AND METHODS

3.1.1 Materials

The materials and chemicals used in this study and their suppliers are listed in Table 3.1.

MATERIALS AND CHEMICALS	SUPPLIER
20% Pt/Carbon black	Alfa Aesar
20% PtRu/C (Vulcan XC-72) (1:1) a/o	BASF
20% PtSn/C (Vulcan XC-72) (3:1) a/o	BASF
Multi-walled carbon nanotubes (MWCNTs)	Carbon Nano-material Co., LTD., Republic of Korea
Molybdenum (iv) oxide (MoO_2)	Alfa Aesar
Titanium (iv) oxide (TiO_2) anatase	Alfa Aesar
Perfluorosulfonic acid- PTFE copolymer 5% w/w solution	Alfa Aesar
Hexachloro Platinic Acid ($H_2PtCl_6.6H_2O$)	Next chimica
Ruthenium(iii) chloride, anhydrous ($RuCl_3$)	Alfa Aesar
Tin(ii) chloride dehydrate ($SnCl_2.2H_2O$)	Alfa Aesar
Potassium chloride (KCl)	Alfa Aesar
Sodium hydroxide (NaOH)	Alfa Aesar
Perchloric Acid 70%, AR ($HClO_4$)	KIMIX
2-Propanol, ACS, 99.5% min (IPA)	Alfa Aesar
Ethylene glycol (EG)	KIMIX
Nitric Acid 55% (HNO_3)	KIMIX
Sulfuric Acid 95-97% (H_2SO_4)	FLUKA
Methanol 97-99% (CH_3OH)	Alfa Aesar
0.05 AND 5.0 MICRON GAMMA AND ALPHA MICROPOLISH ALUMINA	BUEHLER, USA

Table 3.1: *Materials and Chemicals used in this study*

3.1.2. Methods of Synthesis

Electro-catalysts can be synthesized using various methods as detailed in the literature review section. Among them is the impregnation of the metal precursor salts with conventional active reducing agent, such as $NaBH_4$ and N_2H_4 *etc*... The issue with use of these strong reducing agents is that the catalyst prepared by these active reducing agents tends to form large agglomerates as reported by King-Tsai *et al* [76] and incorporate impurities such as boron oxide, resulting in poor catalytic activity. In this study, the colloidal method was employed using ethylene glycol (known as the polyol approach) as both reducing agent and solvent in the synthesis of PtRu and PtSn electro-catalysts supported on MWCNTs, TiO_2 and MoO_2 materials as detailed in the literature review section. Below are some of the reasons why ethylene glycol was chosen for this work as the method of synthesis for the preparation of PtRu and PtSn electro-catalysts decorated on different supporting materials.

The polyol method which uses ethylene glycol (EG) both as a reducing agent and a solvent has been reported in many studies as an attractive method to conventional reducing agents, since metal nanoparticles with a narrow size distribution can be attained and deposited on support material uniformly. A homogenous distribution and small particle size has been attributed to the effect of the glycol, which is denser than aqueous media [71]. The function of the EG is twofold: 1) it works as a chelating agent for the complexation and dispersion of metal ions in the reduction process leading to small sized particle; and 2) it serves as a mild reducing agent to convert the metal or alloy nanoparticles [76-78]. Moreover, it is a straight forward method.

3.1.2.1. Synthesis and deposition of electrocatalyst onto support material

PtRu and PtSn electrocatalyst were synthesized using the polyol method similar to the one used by King-Tsai *et al*. [76] and deposited on MWCNTs, TiO_2, and MoO_2 for effective use. Before the synthesis and deposition of electrocatalysts, the MWCNTs support material was modified; the metal oxide support material was used as received without any further treatment.

Purification and treatment of the commercial multi-walled carbon nanotubes

Multi-walled carbon nanotubes were obtained from the Republic of Korea having a diameter of ~ 20 nm and a length of ~ 10 µm. The as received CNTs was oxidized in a hot solution composed of a mixture of HNO_3 and H_2SO_4 (3:1) v/v; the method used is similar to the one stated by King-Tsai *et al* [76] and Yu-Chun *et al* [79]. A known amount of CNTs was placed in a 250 ml round bottom flask and was then impregnated with a mixture of nitric and sulphuric acid and refluxed for 5 hours at 120^o C under refluxing conditions with a constant flow of nitrogen gas. After the time had elapsed, the CNTs were then washed with ultra-pure water to remove all the acid until pH neutral. CNTs were then oven-dried overnight at 100^o C and after drying them the CNTs were grounded into a fine powder using a pestle and a mortar and were then labelled as acid treated CNTs and were ready to be used as the catalyst support material. Purification of CNTs was done to remove impurities on their outer walls. These impurities could be the amorphous form of carbon generally formed as a side product along

with the formation of multi-walled carbon nanotubes. Purification was also done to remove trace amounts of Fe metal which come from Fe nanoparticles used as a catalyst (and its given by the supplier that they used Fe as a catalyst) during the synthesis of MWCNTs. Purification of CNTs surfaces is important because it also prevents self-poisoning by foreign impurities. Treatment of CNTs was also done to introduce functional groups on the surface of CNTs and is usually termed functionalization or surface modification. The introduction of functional groups on the surface of MWCNTs is essential in enhancing catalyst loading and dispersion of the catalyst on the support, as these functional groups, like carboxylic (-COOH), carbonyl (-C=O) and hydroxyl (-OH), act as reactive sites for metal particles and therefore assist in anchoring these particles on the surface of MWCNTs. This, in turn, promotes the deposition of electro-catalyst on the support material and results in uniform distribution of the electro-catalyst. Furthermore, functionalized MWCNTs were found to be more active than non-functionalized MWCNTs [76-78]. Below is a detailed description of how the electro-catalyst were synthesized and deposited on the support material.

a. Synthesis and deposition of 20% PtRu on MWCNTs (1:1)a/o

A known amount of CNTs was impregnated with 60ml of EG and 10 ml of ultra-pure water was added. The above mixture was sonicated for 25 minutes and stirred for a further 40 minutes using a high speed stirrer, this was done to form a homogenous paste and to allow EG to completely cover the MWCNTs surface. In a separate beaker, 10 ml of EG was placed and dissolved to it, were known amounts of $H_2PtCl_6.6H_20$ and $RuCl_3$ used as Pt and Ru electro-catalyst precursor salts respectively. The salt/EG solution was then slowly added to MWCNT/EG paste and the pH adjusted to about 2-4 by adding drop-wise suitable amounts of 4N NaOH. The resultant mixture was subjected to high speed stirring for an hour for the complexed metal salts/ions to adhere to the surface of MWCNTs. After that, the mixture was transferred into a 250 ml round bottom flask and then refluxed for three hours at 150^o C under continuous flow of nitrogen. After the time had elapsed, it was left to cool down and then washed with ultra-pure water. The final step was the oven-drying at 60^o C overnight. The resultant supported electro-catalyst was grounded after to a fine powder using a pestle and a mortar. The catalyst was labelled and ready to be used as 20% PtRu/MWCNTs

b. Synthesis and deposition of 20% PtSn on MWCNTs (3:1) a/o

The procedure for synthesis and deposition of 20% PtSn on MWCNTs is exactly the same as that of PtRu/MWCNT, the only small change is that the pH was adjusted to about 13-14 adding 4N of NaOH instead of 2-4 as is the case in PtRu/MWCNTs preparation. The exact method was again followed for the deposition of PtRu and PtSn electro-catalyst on TiO_2 and MoO_2. Instead of MWCNTs, the metal oxide support material of interest was used.

3.1.2.2. Heat treatment of the synthesized supported electrocatalysts

After synthesis, half of all the synthesized electrocatalyst was then subjected to heat treatment, and compared to the other half of untreated electrocatalyst. Heat treatment was done to remove any undesirable impurities resulting from early stages of preparation and more importantly to allow a uniform dispersion and stable distribution of the metal on the support, thereby improving the electrocatalytic activity of the synthesized catalysts as it is detailed in the literature review section.

The heat treatment was done using a tube furnace. The quartz tube in a tube furnace was pre-purged with dry nitrogen gas flowing at 500ml/min for one hour, to suppress possible surface oxidation of Pt particles due to oxygen remaining within the tube resulting from previous heat treatment. After pre-purging the quartz tube, the tube furnace was pre-heated to 700^{o} C. After 700^{o} C was reached, an alumina boat, loaded with the synthesized supported electro-catalyst, was inserted into the centre of the quartz tube. The samples were heated at 700^{o} C for 3 hours under nitrogen gas flowing this time at a rate of 5ml/min. After the time had elapsed, the tube was allowed to cool down with nitrogen gas still flowing at the same rate. After cooling down, the samples were taken out and labelled as the heat-treated electro-catalysts.

3.2. CHARACTERIZATION OF SUPPORTED ELECTRO-CATALYST

The characterization of nanophase electro-catalysts is the next rational step after their preparation and prior to their application. The characterization of physical-chemical properties forms the starting point of the optimisation in order to achieve the desirable cost

reduction and high electrocatalytic performance of nanophase electrocatalysts. Several techniques were used to characterize the electrocatalysts, as it is further detailed below.

3.2.1 Physical Characterization of Supported Electrocatalysts

3.2.1.1 X-Ray Diffraction

X-ray diffractometry (XRD) is a powerful non-destructive technique for characterizing crystalline material. It provides information on structures, phases, preferred crystal orientation, and other structural parameters such as, crystalline or grain size, crystallinity, and crystal defects [80]. It is therefore, an indispensable tool for material characterization and thus, forms an integral part in a comprehensive characterization study of nanophase electrocatalyst. XRD in this study was utilized for the direct examination of crystalline structure, phase identification, particle size, and lattice parameter.

3.2.1.1.1 Working principle of XRD

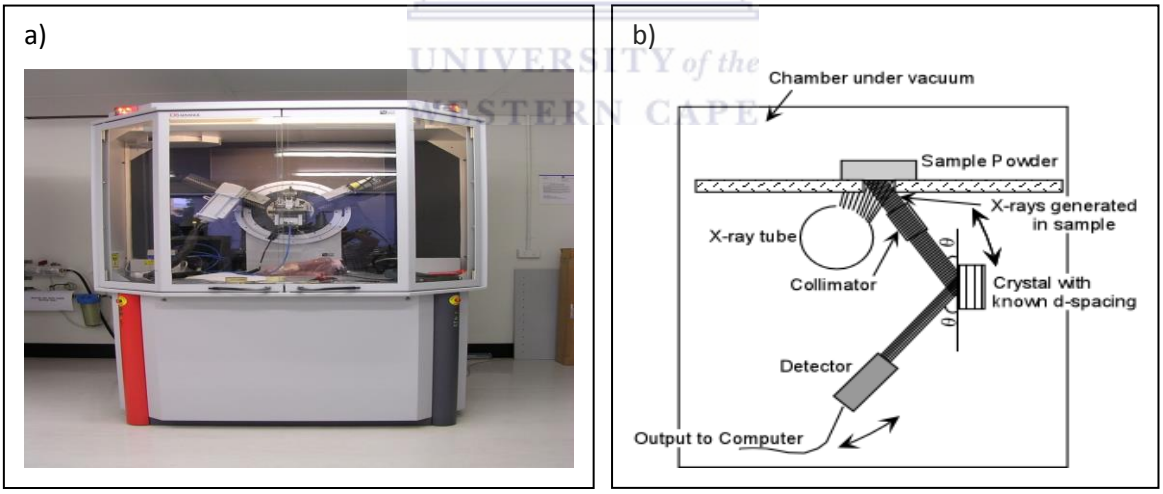

Figure 3.1: Picture of Bruker AXS D8 advance a), and b) schematic diagram of the XRD

Figure 3.1 above illustrates a picture of an XRD (a), and a schematic diagram (b) demonstrating the working principle of an XRD. In a typical XRD analysis, X-rays are generated in a cathode ray tube by heating the filament to produce electrons. The produced electrons are then accelerated toward the target material by applying voltage and bombarding the target material with electrons [80-81]. When the electrons have enough energy to dislodge the inner shell electrons of the target material, characteristic X-ray spectra are produced.

Copper is generally the most used target material for single-crystal diffraction, with a CuKα radiation of 1.5418Å. These X-rays are collimated and directed onto the sample. As the sample and detector are rotated, the intensity of the reflected X-rays is recorded. The interaction of the incident rays with the sample produces constructive interference and a peak in intensity occurs when the conditions satisfies Bragg's law (equation 3.1). A detector records and processes this X-ray signal and converts the signal to a count rate which is then output to a device such as computer or printer.

$$n\lambda = d\sin\theta \qquad (3.1)$$

By varying the angle θ, the Bragg's law conditions are satisfied by different d-spacing in polycrystalline materials. Plotting the angular positions and intensities of the resultant diffracted peaks of radiation produces a pattern, which is a representative of the sample where a mixture of different phases is present. The addition of an individual pattern then brings about a diffractogram. Now based on the principle of X-ray diffraction, a wealth of structural, physical and chemical information about the material being investigated can therefore be acquired [80-85].

XRD can be used quantitatively for the determination of average particle size as mentioned above, using the Scherrera equation given below as:

$$D = \frac{0.9\lambda}{\beta\cos\theta} \qquad (3.2)$$

Where D is the particle size, 0.9 the shape factor, λ the wavelength of the X-ray, β is the peak width at half peak height (radians), and θ being the angle of reflection [83-85].

The lattice parameter (a_o) could also be calculated using the following equation:

$$a_o = d\,(h^2 + k^2 + l^2)^{1/2} \qquad (3.3)$$

Where h, k, and l constitute the Miller indices of a crystal facet, and d is the interplanar spacing determined using Bragg's equation.

Crystalline size determination is performed by measuring the broadening of a particular peak in a diffraction pattern associated with a particular planar reflection from within the crystal

unit cell [82]. Particle size is inversely related to the half-width at half maximum of an individual peak. Typically the narrower and more intense the peak, the more crystalline the sample is. A broad peak is usually associated with small particle size and an amorphous material.

3.2.1.1.2 Sample preparation

In the XRD analysis, dry nanophase electrocatalyst samples were mounted in plastic sample holders and the surface was flattened to allow maximum X-ray exposure. Experimental parameters for XRD analysis are given as follows:

X-ray Diffractometer: Bruker AXS D8 Advance from Ithemba labs.

Tube:	Copper
Detector:	Sodium Iodide
Monochromator:	Graphite
Electron Intensity:	40 kV
X-ray Source:	CuKα (λ= 1.5418Å)
Current:	40 mA
Scan Range:	$10^o < 2\theta < 100^o$

3.2.1.2 High Resolution Transmission Electron Microscopy

High resolution transmission electron microscopy (HRTEM) is an imaging mode of the transmission electron microscope (TEM) that allows for direct imaging of the atomic structure of the sample [63-64]. HRTEM has become a powerful and is considered to be an indispensable tool for studying the properties of nanostructured materials such as nanoparticles, and sp^2 bonded carbon (e.g. carbon nanotubes and graphite) and the high resolution makes it perfect for imaging materials on the atomic scale [86-88]. HRTEM was utilized in this study to examine the metal nanoparticle size, nanoparticle size distribution,

homogeneity of dispersion, and agglomeration of the nanoparticles in supported nanophase electrocatalysts. The metal surface area (SA_{Pt}) could be calculated using HRTEM data. It is obtained using an equation presented by Prabhuram et al. [89] and is given as:

$$SA_{Pt} = \frac{6000}{d(P)} \qquad (3.4)$$

Where d is the density of Pt (21.4 $g.cm^{-3}$), and p is the particle size in nm

3.2.1.2.1 Working principle of HRTEM

The HRTEM works by using a high voltage electron beam to create an image. The electron beam is produced by an electron gun, normally fitted with a tungsten filament cathode as an electron source [86-88]. Figure 3.2 below provides an illustration of the HRTEM; a picture of the HRTEM (a) and (b) the schematic diagram showing the inside of the microscope.

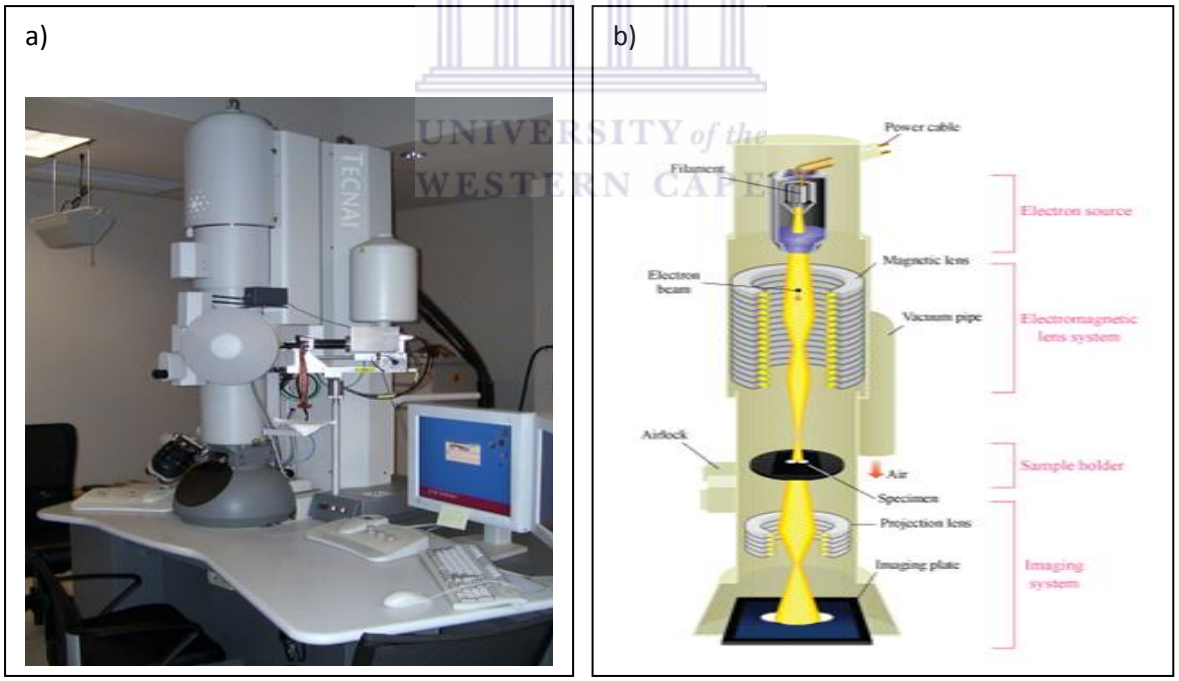

Figure 3.2: Picture of an HRTEM a) and schematic diagram of an HRTEM b)

The electron beam is accelerated by an anode typically at plus 100 KeV (40-400 KeV) with respect to the cathode, and the electron beam is focused by electro-static and electro-magnetic lenses [86-88]. The focused beam is then transmitted through the specimen that is in part transparent to the electrons and in part scatters them out of the beam. When the electron beam

emerges from the specimen it carries information about the structure of the specimen that is magnified by the objective lenses of the microscope. The image is viewed by projecting the magnified electron image onto a fluorescent viewing screen coated with a phosphor or scintillator material such as zinc sulphide [86-88]. Alternatively, the image can be photographically recorded by exposing a photographic film or plate directly to the electron beam, or use a high resolution sensor that may be coupled by means of a lens optical or fibre optic guide to the sensor of a charge-coupled-device (CCD) camera. The image detected by the CCD is then displayed on either a monitor or computer. TEMs are able to produce images with a resolution down to 0.2 nm. This resolution is smaller than the size of most atoms and thus, TEM have the ability to produce images that reveal the true structural arrangements of atoms in specimen material [86-88].

3.2.1.2.2 Sample preparation

HRTEM samples were prepared by dispersion of a spatula-tip of the supported electrocatalyst of interest in a 5 ml ethanol solution. The suspension was then sonicated for 15-20 minutes. The resultant suspension was deposited on a copper grid covered by carbon film using a 10 µl micropipette to drop the suspension onto the copper grid. The ethanol was allowed to evaporate at room temperature. One of the most essential things to note during sample preparation for HRTEM analysis is that the specimen is required to be extremely thin (less than 100 nm), in order to allow the electrons to pass through the specimen and create an image. Samples were then mounted in a sample holder, which was introduced directly to the shaft of the microscope (HRTEM-TF 20 Model) for analysis. Experimental parameters are given as follows:

Accelerating Voltage:	200 KeV
Current:	20 µA
Objective aperture:	2
Exposure time:	2.1seconds

3.2.1.3 High Resolution Scanning Electron Microscopy

High resolution scanning electron microscopy (HRSEM) is a versatile imaging technique capable of producing three-dimensional profiles of material surface [90]. HRSEM was used in this study to extract quantitative and qualitative information pertaining to particle morphology, surface appearance of supported nanophase electrocatalysts, and elemental analysis using the energy dispersive spectroscopy (EDS) detector.

3.2.1.3.1 Working principle of an HRSEM

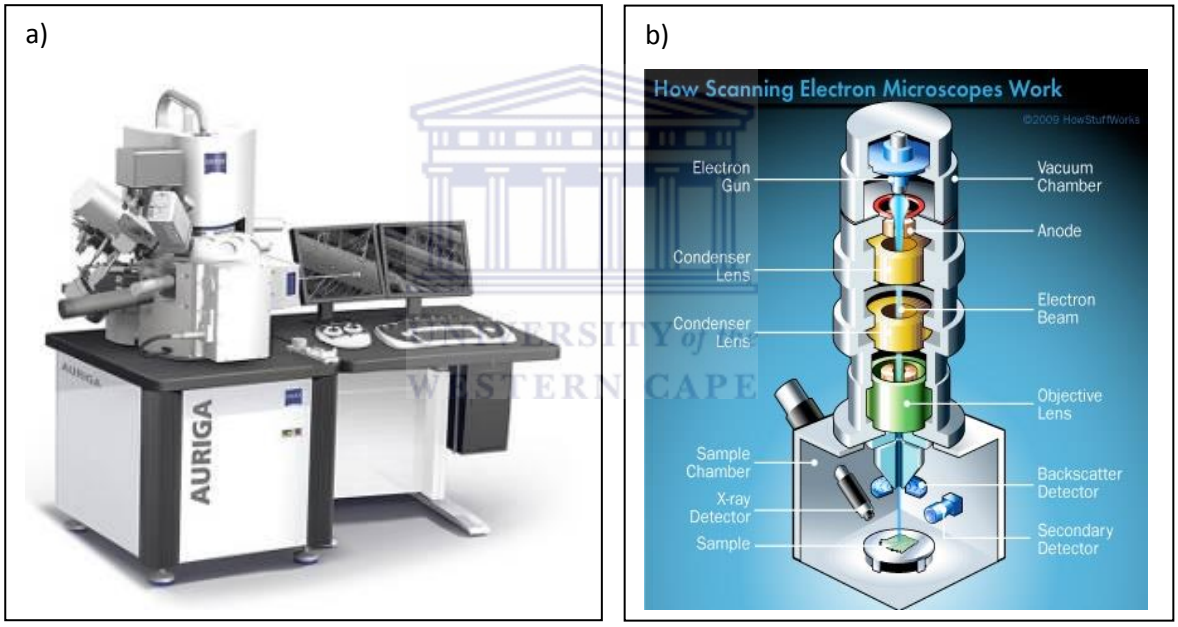

Figure3.3: Picture of HRSEM a) and a schematic diagram of an HRSEM b)

Different from HRTEM where the electron beam carries the information of the specimen, in HRSEM the electron beam does not at any time carry the complete image of the specimen, instead the HRSEM produces an image by probing the specimen with a focused electron beam that is scanned across a rectangular area of the specimen (raster scanning) [82-87]. Figure 3.3 above shows: - (a) a picture of HRSEM and (b) is the schematic diagram representing the working principle of an HRSEM. When the electron beam interacts with the specimen, it loses energy by a variety of mechanisms. The lost energy is converted into alternative forms such as, heat, emission of low-energy secondary electrons and high energy backscattered electrons, light emission (cathoduluminescence) or X-ray emission (as shown in Figure 3.3

(b) above), which provide signals carrying information about the properties of the specimen surface such as topography, morphology and composition. HRSEM is considered to be a non-destructive technique, that is, the X- rays generated by electron interaction do not lead to volume loss of the sample, and so it is possible to analyse the same materials repeatedly [86-87, 90-92].

3.3.1.3.2 Sample preparation

HRSEM samples were prepared by placing double-sided conductive carbon tape on an aluminium specimen stub. A very small amount of the sample was deposited on the specimen stub and flattened with a spatula, then gently tapped to remove the excess and loose sample. The nanoparticles supported on TiO_2 and MoO_2 were found to be less conductive because of the supporting material (metal oxides are not very conductive materials) and were therefore required to be coated with gold/palladium alloy material to make them conductive. Conductivity of specimen is a requirement for HRSEM analysis operating in conventionally high vacuum. Thus, non-conductive specimens have to be coated in order to be used in an HRSEM. This is because non-conductive specimen tends to charge when scanned by the electron beam, and especially in secondary electrons imaging mode and this charging causes scanning faults and other image artifacts. The conductive materials currently used to coat specimen include, gold/palladium alloy, gold, carbon, chromium, tungsten, osmium, and indium [90-91]. The nanoparticles supported on MWCNTs and commercial catalysts did not require any coating, as they were conductive enough to be imaged without charging. The samples were then introduced into the vacuum chamber of the microscope for analysis. In this study HRSEM Auriga was used with the experimental parameters listed below as:

Working distance: 10 nm

Accelerating Voltage: 5 KeV

Tilt Angle: 0^o

3.2.1.4. Energy Dispersive Spectroscopy

Energy dispersive spectroscopy (EDS) detector which is connected to the HRSEM was used in this study to investigate the elemental composition of the electrocatalyst both commercial and synthesized. After taking HRSEM images, the samples would then be scanned on six different areas to obtain the average wt. % of the metals.

3.2.2 Electrochemical Characterization of Supported Electrocatalyst Using Rotating Disk Electrode

Rotating disk electrode (RDE) is by far the most popular and extensively used hydrodynamic method together with the rotating ring disk electrode (RRDE). Researchers take full advantage of the stable and steady-state laminar flow conditions in line to an RDE or an RRDE to carefully collect information about the electrode reaction kinetics [93]. RDE has been widely used for evaluating/screening the electrochemical activity and durability of small quantities of novel electrocatalysts for PEMFCs [94]. RDE was used in this study to mimic the conditions of PEMFCs as Kocha *et al* [95] once wrote *"trends of activity and durability in RDE measurements can be used to predict trends of activity and durability in PEMFCs"*. Thin film rotating disk electrodes (TF-RDEs) were prepared using supported catalysts identical to those used in PEMFCs and which can provide a reasonably realistic practical assessment of the catalyst activity [94]. RDE was employed in this study to examine the electro-active surface area and durability of the electro-catalyst using cyclic voltammetry and to examine the electro-catalyst's specific and mass activity using linear sweep voltammetry. The electro-chemical surface area, Pt mass specific activity and Pt area specific activity are the accepted measures of true ORR catalyst activity. It was also employed to study the effect of methanol cross-over on oxygen reduction reaction.

3.2.2.1 Cyclic Voltammetry

Cyclic voltammetry (CV) is a type of potential-controlled electrochemical technique, which can be used to examine the electrodes surface reactions, the behaviour of the electrochemically-active species, and to investigate the quality of electrocatalysts [93]. Cyclic voltammetry provides information on the thermodynamics of redox processes and kinetics of

heterogeneous electron transfer reactions [77-78]. It plays an integral role in the comprehensive characterization of nanophase electrocatalysts.

In cyclic voltammetry the potential of the working electrode is swept linearly with time and between two potential ends. By adjusting the potential of the working electrode, electrons are transferred between the electrode and the molecules in the electrolyte, which records the current response of the working electrode when the potential is swept back and forth between two selected potentials [96-97]. Cyclic voltammetry was used in this study to examine the electro-active surface area (ECSA) and durability of nanophase supported electrocatalysts.

The experiments were conducted in a three electrode cell, connected to a Metrohm Autolab which in turn was fitted with a rotating disk electrode as shown in Figure 3.4 (a) and (b) below. The three electrodes are the GCRD electrode tip as the working electrode, Pt wire as the counter electrode and Ag/AgCl as the reference electrode. 0.1 M $HClO_4$ was used as the electrolyte of choice as perchloric acid which is known for its low anion adsorption on Pt and is also expected to simulate the perfluorosulfonic acid (PFSA) membranes more closely than sulphuric or phosphoric acid [94]. The potential was applied with an Autolab potentiostat PGSTAT 30 (name of the Autolab model) and the experiments were controlled with General Purpose Electro-chemical System (GPES) software. All experiments were carried out at room temperature (23 ± 2^{o} C). Prior to measurements, the electrolyte was purged with nitrogen gas for 45 minutes to remove dissolved oxygen, and the surface of the electrode was then conditioned by scanning the potential between -0.2 and 0.9 V for 100 cycles at 100 mV/s vs. Ag/AgCl. This conditioning of the working electrode is done to remove any impurities on the surface of the electrode as well as to attain stable voltammograms. After conditioning the working electrode, the electrolyte was purged again with nitrogen gas for 30 minutes to ensure that it was saturated with nitrogen before scanning the potential between -0.2 and 0.9 V for three cycles at 20mV/s vs. Ag/AgCl; the three cycles were then used to examine the electro-active surface area of the electrocatalysts.

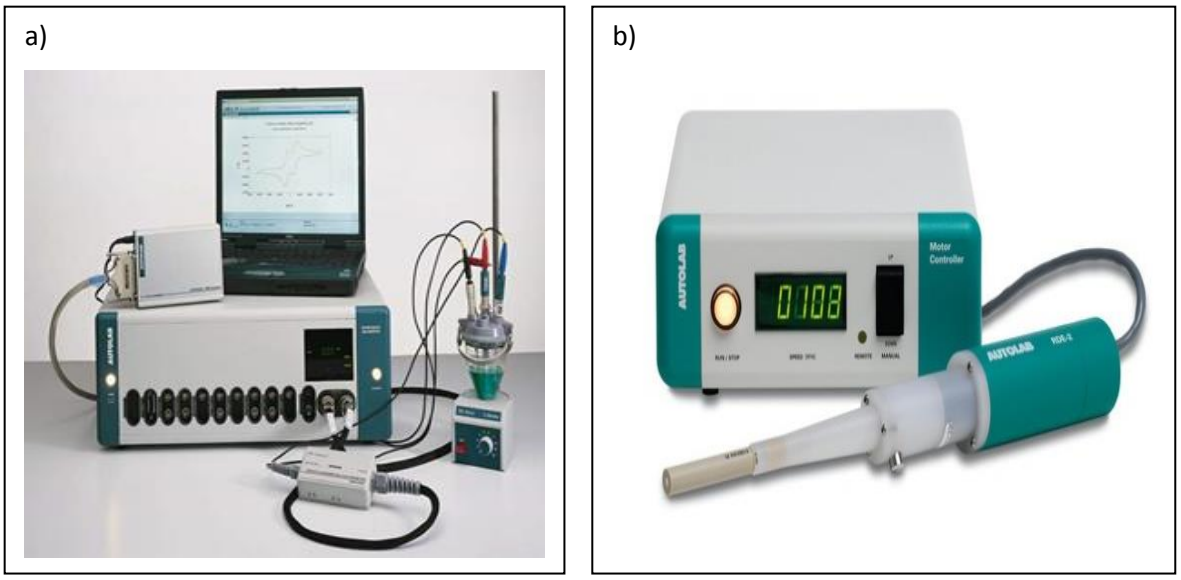

Figure 3.4: Three-electrode cell connected to an auto-lab a) and an RDE b)

To test for the durability of the electro-catalysts, the same procedure as the one stated above was followed. Instead of three cycles, 1000 cycles were scanned at 50mV/s under nitrogen gas serving as a blanket. After 1000 cycles were completed the electrode was purged for 30 minutes with nitrogen and three cycles were scanned at 20mV/s, which was then compared to the three scans before 1000 cycles scanned. All experiments were conducted under nitrogen atmosphere. The intent of durability study testing of DMFC catalyst is to assess the performance decay rate or what percentage of the initial performance is lost overtime.

3.2.2.2 Linear Sweep Voltammetry

Linear sweep voltammetry (LSV) differs from CV in that the applied potential is swept at a fixed sweep rate from an initial potential to a final potential and there is no back and forth [93]. LSV was used in this study to investigate the oxygen reduction reaction and methanol oxidation reaction.

To study ORR, the electrolyte was purged with oxygen for 45 minutes and the following rotation speed rates were used to measure the LSV current-potential curves: 3600 rpm, 2500 rpm, 1600 rpm, 900 rpm, and 400 rpm and the cycles were conducted at 20mV/s and the working electrode swept from -0.2 V to 0.9 V vs. Ag/AgCl. The electrolyte was purged for 15 minutes with oxygen in between speed rates; and during all experiments the oxygen gas was used as a blanket to cover the electrolyte. Thus, all experiments were in an oxygen atmosphere. The current potential curve at 1600 rpm was then used to examine the Pt mass

specific activity, and Pt area specific activity. The collection of speed rate was used for the Koutecky-Levich (K-L) plot. To study MOR the electrolyte-methanol solution was purged with oxygen for 45 minutes and using 1600 rpm as the speed rate the LSV curves were measured. All gases used were from Afrox Company. The experimental parameters are given below as:

Autolab connected with RDE:	Metrohm
Working electrode:	GCRDE tip coated with the catalyst of interest
Counter electrode:	Pt wire basket
Reference electrode:	Ag/AgCl
Scan rate:	20mV/s
Potential window:	-0.2-0.9 V

3.2.2.3 Electrode Preparation for RDE Analysis

The electrode ink preparation method used in this study is similar to the one stated by Yannic *et al*. [98]. The Pt loading for all electrocatalyst (commercial and home-prepared) used in this study was 20µg.cm^{-2}. The electrode ink was prepared by placing in a small glass vial 9.8 mg of the catalyst of interest, 20 µl of Nafion, 4.15 ml of ultra-high pure (UHP) water, and 0.830ml of isopropanol (IPA) to make a 5ml ink stock solution. The resultant mixture was then sonicated in an ice bath for 60 minutes to obtain a uniform suspension. After sonication 10 µl of the ink solution was dropped onto a clean shinny glassy carbon electrode tip (5 mm diameter with a geometric area of 0.196 cm^2 embedded in a Teflon cylinder) using a 10 µl micropipette. The electrode was then covered with a beaker and allowed to dry overnight, after which it was then ready to be used as the working electrode.

Cleaning of the glassy carbon rotating disk electrode (GCRDE) tip

The GCRDE tip was cleaned after every use, by polishing the electrode for 5 minutes on Microcloth ^{TM} (Buehler) using 5.0 and 0.05 micron alumina slurries in sequence. The polished electrodes were rinsed well with UHP water, and then sonicated for 5 minutes in UHP water to remove any residual alumina. The electrodes were then dried for not less than an hour at room temperature before use.

Cleaning of glassware

Successful and reproducible electrochemical experiments require all components of the system to be thoroughly cleaned of impurities that could affect the catalyst. Particularly, halide anions (F^-, Cl^-, and Br^-), organics and sulphurous compounds have detrimental effect on the rate of ORR on Pt catalysts. A jacket glass electro-chemical cell was cleaned by soaking it in concentrated nitric acid for several hours. The cell was then rinsed thoroughly and boiled for 1 hour in UHP water. This rigorous cleaning was done bi-weekly.

CHAPTER 4

CHARACTERIZATION OF SUPPORTED CATALYSTS

4.1 STRUCTURAL CHARACTERIZATION OF MWCNTs

Prior to deposition of the electrocatalyst on MWCNTs, the surface of the MWCNTs was modified using acid treatment to improve dispersion of the metal particles on the support material as detailed in chapter 3. This section therefore presents the structural characterization and interpretation of results for commercial MWCNTs. The results start off with the characterization of surface morphology of the functionalized MWCNTs using HRTEM and HRSEM techniques followed by direct characterization of crystallinity and graphitization using XRD. The as received commercial MWCNTs was also characterized and used as reference for comparison purposes.

4.1.1 HRTEM Characterization of MWCNTs

HRTEM was used to directly examine the structural changes of the commercial MWCNTs before and after functionalization. Figure 4.1 below shows HRTEM images of a) as received and b) acid treated commercial MWCNTs.

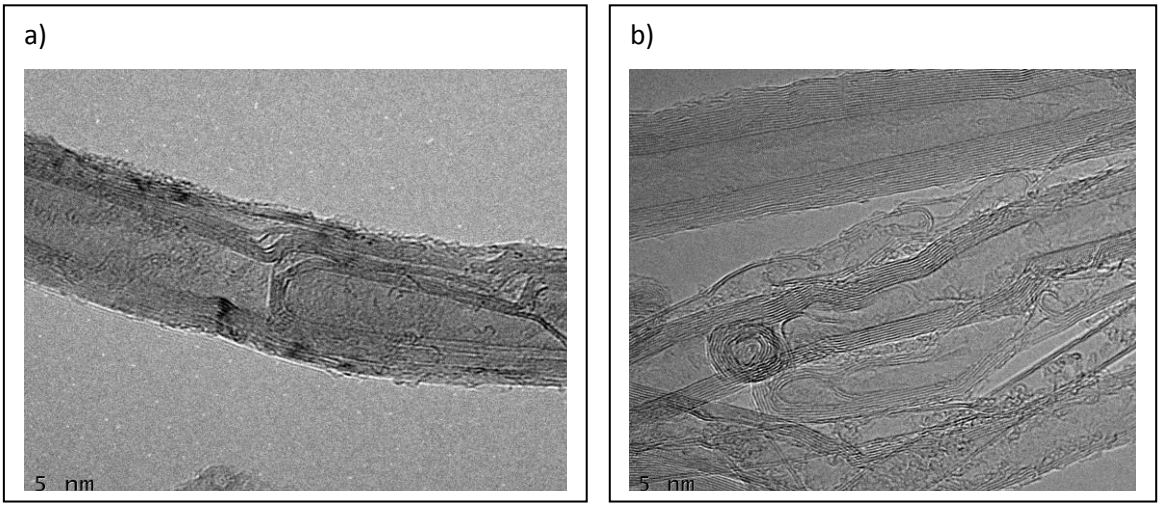

Figure 4.1: HRTEM images of commercial MWCNTs a) as received and b) functionalized MWCNTs

Figure 4.1 a) and b) above illustrates the high resolution TEM images of the samples which provided insight into the structure of MWCNTs. The tubular structure of the carbon nanotubes was observed in both samples. It was observed that the surface of the as received MWCNTs was smooth with amorphous carbon layers adhering to the nanotube walls and the Fe metal particles trapped inside the tube walls and at the tip of the walls. After acid treatment, the tube walls were distinctly visible, something that is linked to the removal of the amorphous carbon layers adhering to the nanotube walls and the catalyst particles trapped inside the walls before acid treatment. Nitric acid is known to be efficient in removing amorphous carbon and solving metal particles and was used for the treatment of MWCNTs [99]. Functionalized MWCNTs image shows the open end of MWCNTs, revealing that the cap is etched off and the wall of the graphite structure is not significantly damaged and this also was confirmed by XRD analysis as the d-spacing for the MWCNT which was found to be 0.336 nm and 0.339 nm for the as received and functionalized MWCNTs respectively, indicating that the acid was strong enough to remove amorphous carbon, most of metal particles and generate surface functional groups without causing any significant damage to the structure of the MWCNTs. The rough surface with some debris observed on the functionalized MWCNTs is an indication that some active carbon layers on the surface were reacted [104-105].

4.1.2 HRSEM Characterization of MWCNTs

The HRSEM was utilized for structural and morphological study of the MWCNTs. Figure 4.2 below demonstrates the effect on the surface of the nanotubes before and after functionalization. Figure 4.2 a) shows an HRSEM image of the as received and b) of the acid treated commercial multi-walled carbon nanotubes.

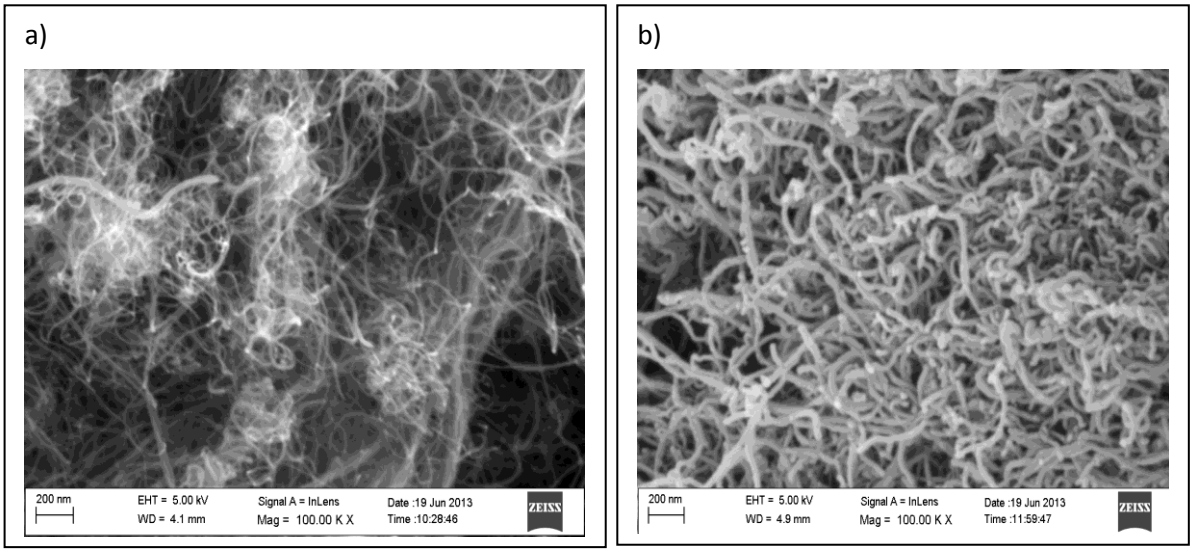

Figure 4.2: HRTEM images of the commercial MWCNTs a) as received and b) functionalized MWCNTs

Figure 4.2 above shows HRSEM images of the a) as received and b) functionalized commercial MWCNTs there is a distinct change on the nanotube structure affected by the acid functionalization process. The smooth surface with amorphous carbon adhering on the carbon nanotubes Figure 4.2 a) has been altered to appear as groovy surface after the functionalization process Figure 4.2 b), with the amorphous carbon removed, the groovy surface that can be linked to the chemical functional groups attached on the nanotubes surface. The transparency of the nanotubes also has been decreased after functionalization as compared to the as received MWCNTs which possible connects also to the introduction of functional groups [104-105].

4.1.3 XRD Characterisation of MWCNTs

XRD was employed to examine the crystallinity and structural alterations in the acid treated MWCNTs compared with the commercial MWCNTs. Figure 4.3 below displays the XRD patterns of the as received and acid treated commercial MWCNTs.

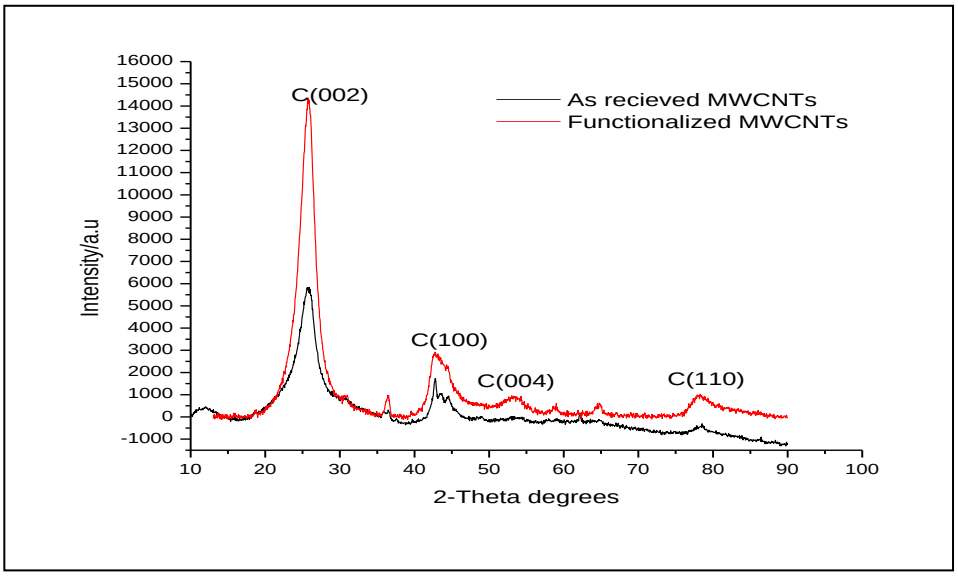

Figure 4.3: XRD patterns of the as received and functionalized commercial MWCNTs

The XRD patterns of the MWCNTs sample are presented in Figure 4.3 above. The strongest and sharpest diffraction peak for both samples at around $2\theta = 25.6^{o}$ could be indexed as (002) reflection of the graphite, and the other characteristic diffraction peaks of graphite at 2θ of about 42.6^{o}, 51.8^{o}, 76.8^{o} corresponded to (100), (004), and (110), respectively. All diffraction peaks were observed at the same 2θ values for both samples. Distinctly, the intensity of the diffraction peak at (002) in functionalized MWCNTs was more intense in comparison with the as received MWCNTs. This is an indication of the loosely of the MWCNTs floss after the acid treatment and form more ordered MWCNTs floss in the functionalized MWCNTs. The functionalized MWCNTs are more crystalline in comparison to the as received MWCNTs, and thus, are expected to possess higher electronic conductivity than the as received MWCNTs. The interplanar d-spacing was calculated using Bragg's law and found to be 0.336 nm and 0.339 nm for as received and acid treated MWCNT respectively and the small difference is an indication that the structure of the MWCNTs was not significantly damaged as was observed with HRTEM but that the surface functional groups were generated using the acid treatment. The calculated d-spacing of the samples was found to be in the same range to that of an ideal graphite crystal which is 0.335 nm. Furthermore, the XRD pattern for the functionalized sample was observed to be similar to that of the as received sample indicating that the structure of MWCNTs was protected after acid treatment (HNO_3/H_2SO_4 mixture) [104-107].

4.1.4 Summary

Multi-walled carbon nanotubes were successfully treated using an acid mixture of HNO_3 and H_2SO_4 to remove metal particles and generate surface functional groups and were characterized using powerful techniques such as HRTEM, HRSEM and XRD. HRTEM revealed that the metal particles trapped inside the walls and amorphous carbon adhering on the surface of the walls was removed and the rough surface of the acid treated carbon nanotubes observed revealing that some active carbon layers on the surface of the tubes were reacted. HRSEM showed the smooth surface of the untreated MWCNT which was also observed in HRTEM images to be altered after acid treatment as a result of surface functional groups generated by the acid treatment. The graphitic structure of the carbon nanotubes was retained even after acid treatment as shown by the XRD, which also showed higher crystallinity of the functionalized MWCNTs after acid treatment. All three techniques proved that the MWCNT was successfully treated using an acid mixture of HNO_3 and H_2SO_4 without any major damage to the structure of the MWCNTs. Therefore, acid treated MWCNT was ready to be used as the support material for PtRu and PtSn electro-catalyst.

CHARACTERIZATION OF SUPPORTED PtRu CATALYST

This section reports on physical and electrochemical characterization of PtRu supported on MWCNTs, TiO_2, and MoO_2 support material. The commercial Pt/C and PtRu/C were also characterized and used as the baseline for comparison purposes. Physical characterization forms the first point of study as it influences the electro-chemical behaviour of the resultant electrocatalyst. PtRu was then physically and electrochemically characterized to investigate if it can possibly be employed as a cathode electrode in DMFC applications. Physical characterization was directly followed by electrochemical characterization.

4.2 STRUCTURAL CHARACTERIZATION OF PtRu CATALYST

Structural characterization of the synthesized PtRu was done using a variety of powerful techniques such as XRD, HRTEM, HRSEM, and EDS as detailed in chapter 3.

4.2.1 Particle Size and Crystallinity of the Supported PtRu Catalyst

The particle size and crystallinity of supported PtRu electrocatalyst employed in this study was investigated using XRD. The powder X-ray diffraction of the synthesized and commercial electro-catalysts recorded at 2θ range of 10^o to 100^o is presented in Figure 4.4 and 4.5 below for the PtRu supported on MWCNTs and metal oxides respectively. The average particle size and lattice parameter values are presented in Table 4.1 and 4.2 for PtRu supported on MWCNTs and metal oxides respectively.

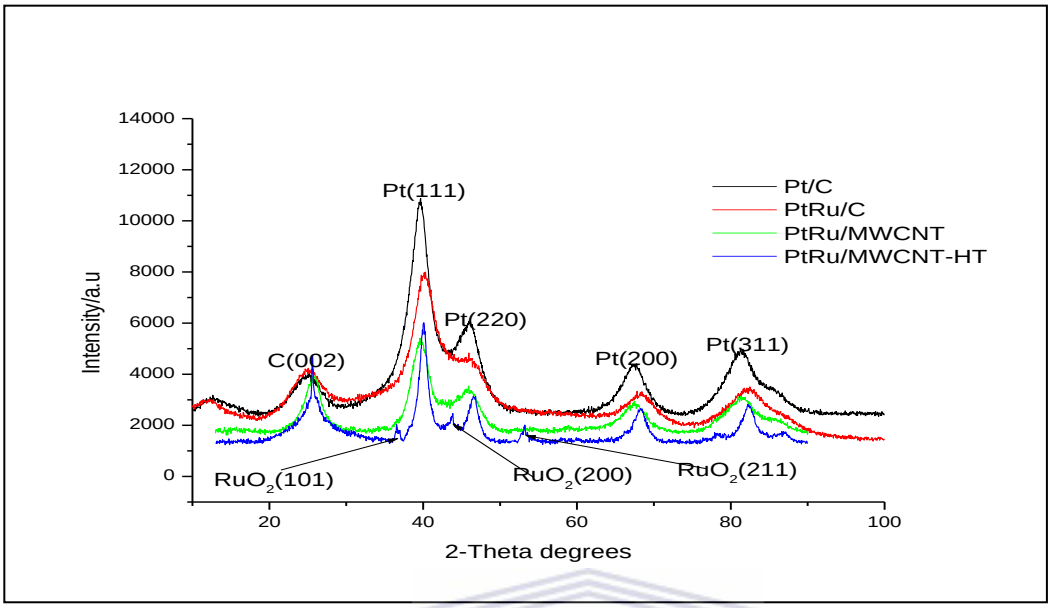

Figure 4.4: XRD patterns of the home-prepared PtRu/MWCNT and compared with Pt/C and PtRu/C commercial electrocatalysts

Figure 4.4 above displays the XRD patterns of the as prepared PtRu/MWCNT and heat treated (HT) PtRu/MWCNT compared with Pt/C and PtRu/C commercial electro-catalysts. The diffraction pattern at low 2θ values about 25^{o} observed in all XRD pattern is attributed to the diffraction (002) plane of the hexagonal structure of the carbon support. The binary PtRu electro-catalyst both as prepared and commercial display characteristic patterns similar to that of the standard Pt/C electro-catalyst, an indication that all catalysts have prevailed the Pt face-centred-cubic (fcc) crystal structure. These diffraction peaks in all samples corresponded to (111), (200), (220) and (311) of the Pt- rich fcc crystalline structure. However, the 2θ values of the binary catalyst shifted slightly to higher values, an indication of a decrease in lattice constant of Pt due to the incorporation of the Ru atom [108-116], revealing that single phase PtRu was formed on the carbon support material. The home-prepared PtRu/MWCNT and PtRu/MWCNT-HT resultant characteristic peaks showed broader peaks in comparison with the commercial PtRu/C, indicating a somewhat amorphous structure for the as prepared samples. It was also observed that the diffraction peaks for PtRu/MWCNT did not shift to higher values, in itself an indication that not all of Ru formed alloy with Pt. PtRu/C and PtRu/MWCNT showed no apparent peaks corresponding to the hexagonal-close-pack (hcp) phase of the Ru element. This phenomenon is commonly found in carbon supported PtRu

electro-catalyst, except those of highly Ru-rich particles. The absence of Ru peaks can be attributed to the coincidence that the signal peaks of both Pt and Ru elements appear at almost the same positions. The Pt element being a much larger size atom it therefore exhibits a more pronounced signal pattern than that of the small size Ru atom counterpart. It can also be as a result of the incorporation of the relative small size of the Ru atom into the fcc structure of Pt indicating an alloy formation between Pt and Ru. These results are consistent with the findings of Hsieh *et al.* [110] who reported that PtRu alloys would take the fcc structure of Pt, if Ru content is below 60%. Even though pure Ru and/or their oxides were not detected using XRD, their presence, however, cannot be discarded because they might be present in smaller amounts or even in an amorphous form. An EDS analysis result of the supported PtRu has shown Ru content. In the heat-treated PtRu/MWCNT, the diffraction peaks corresponding to RuO_2 (101), (200) and (211) were observed as shown by the arrows in Figure 4.4. This is due to the formation of different crystalline structure as a result of heat treatment which also promotes the formation of ruthenium oxides and improves alloying [108-116]. However, it should be emphasized that the intensity of RuO_2 is considerably weak, in itself an indication that RuO_2 is present only in small quantities.

The XRD was commonly employed to calculate the mean particle size of the electrocatalyst nanoparticles supported on carbon material using Scherrer's equation explained in chapter 3, and using the platinum diffraction peak (220).

$$D = \frac{0.9\lambda}{\beta(2\theta)Cos\theta max} \qquad (4.1)$$

The calculated values of the average particle size and lattice parameter are presented in Table 4.1. All catalyst showed relatively small particle size which is known to enhance the electrochemical surface area of the catalyst. PtRu/MWCNT showed a particle size growth after heat treatment owing to the fact that heat treatment promotes size growth of nanoparticle and also improves alloying of the electrocatalyst. Lattice parameter was calculated using the following equation:

$$a_{fcc} = \frac{\sqrt{2}\lambda}{sin\theta} \qquad (4.2)$$

Catalyst	Particle size/nm	Lattice parameter (a_{fcc})/nm
Pt/C	2.28	0.393
PtRu/C	3.02	0.388
PtRu/MWCNT	3.22	0.393
PtRu/MWCNT-HT	6.62	0.388

Table 4.1: *Summary of average particle size and lattice parameter of PtRu/MWCNT compared with Pt/C and PtRu/C commercial electrocatalyst obtained from XRD measurements*

The a_{fcc} values were collected and presented in Table 4.1 above. The a_{fcc} value for pure platinum on carbon support has been reported in literature [112] to be 0.39155 nm and 0.39244 nm, whereas in the present study the obtained value of a_{fcc} is 0.393 nm. The a_{fcc} value for PtRu/C and PtRu/MWCNT-HT is the same and smaller compared to Pt/C, the decrease in the lattice constant of Pt as explained above is due to the incorporation of the Ru atom, indicating a high degree of alloying and that the single phase PtRu was actually formed on the carbon support. These results are consistent with the results reported by Prabhuram *et.al* [114] and Antolini *et.al* [121] who reported that the introduction of a second transition metal causes a decrease in the lattice parameter of Pt. The decrease in the lattice parameter indicates a contraction of the Pt-Pt distance due to the high degree of alloying as a second metal is expected to shorten the Pt-Pt distance thereby improving the activity of the resultant electro-catalyst. It was observed, however, that the lattice parameter value for the untreated PtRu/MWCNT was higher compared to the heat-treated sample. It was also observed that the diffraction peaks for the untreated PtRu/MWCNT did not shift to higher values, an indication that there was no contraction of the Pt-Pt distance, and hence, the high value in lattice parameter. This indicates poor alloying of Ru with Pt which clearly improved after heat treatment as expected from literature.

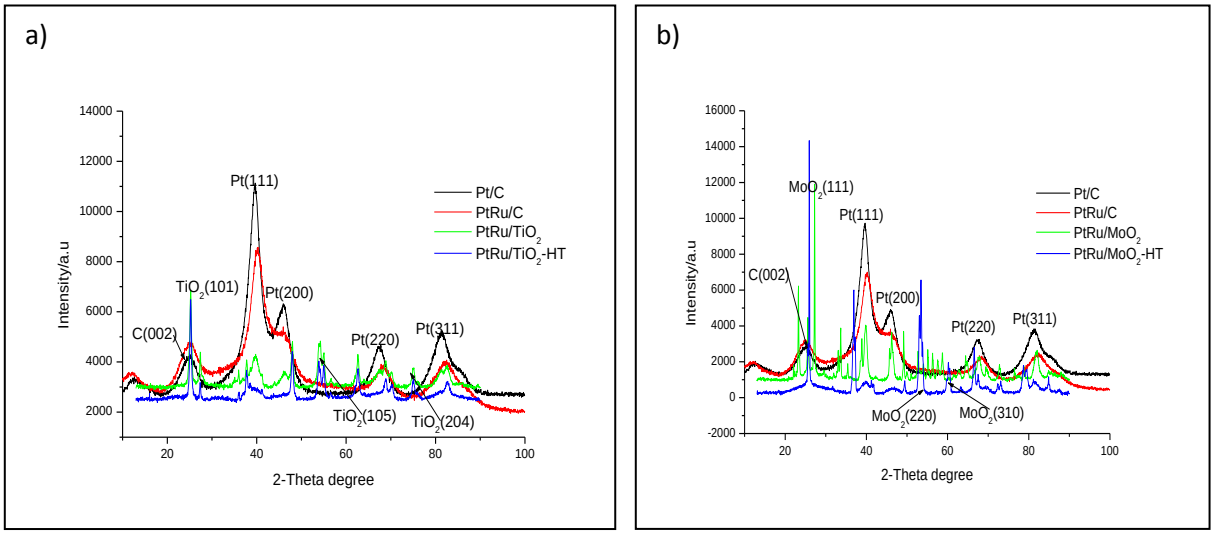

Figure 4.5: XRD pattern of home-prepared a) PtRu/TiO_2 and b) PtRu/MoO_2 compared with Pt/C and PtRu/C commercial electrocatalysts

Figure 4.5 above shows the XRD pattern of the as prepared a) PtRu/TiO_2 PtRu/TiO_2-HT and b) PtRu/MoO_2 and PtRu/MoO_2-HT as compared to the commercial Pt/C and PtRu/C electro-catalysts. All samples display diffraction peaks of Pt (111), Pt (200), Pt (220) and Pt (311) of the fcc crystalline structure of platinum at their corresponding diffraction positions. However, the XRD pattern for the as prepared electro-catalysts is extremely broadened and the intensity is weak in comparison to the commercial electro-catalysts and this could be attributed to the amorphous structure of the prepared catalyst. The peak at 25^o is attributed to the diffraction at the (002), (101) and (111) plane of the carbon, titanium oxide and molybdenum oxide support respectively as they appear almost at the same position. The other diffraction peaks were attributed to the TiO_2 (105), (204) and MoO_2 (220), (310) phase as indicated by the arrows in their respective figures [61, 130].

Catalyst	Particle size/nm	Lattice parameter (a_{fcc})/nm
Pt/C	2.28	0.393
PtRu/C	3.02	0.388
PtRu/TiO_2	12.85	0.419
PtRu/TiO_2-HT	14.47	0.385
PtRu/MoO_2	13.96	0.391
PtRu/MoO_2-HT	19.65	0.397

Table 4.2: *Summary of average particle size and lattice parameter of PtRu supported on metal oxides compared with Pt/C and PtRu/C commercial electrocatalysts obtained from XRD measurements*

The average particle size and lattice parameter were collected and presented in Table 4.2 above. All average particle size for the prepared catalyst show an increase after heat treatment as expected from literature. The average particle size for the metal oxide supported electro-catalyst varies significantly with the results obtained using the HRTEM technique. However, for the carbon supported electro-catalyst, the results seem to be in agreement and within error of course. The lattice parameter for the untreated $PtRu/TiO_2$ was higher than the commercial Pt/C, an indication that not all of the Ru formed alloy with Pt. However, after heat treatment, the a_{fcc} value decreased from 0.419 nm to 0.385 nm as presented in Table 4.2, which is lower than that of the commercial PtRu/C and Pt/C electro-catalysts, an indication that alloying of Pt with Ru improved upon heat treating the sample as expected from literature. For $PtRu/MoO_2$ the lattice parameter value for the untreated $PtRu/MoO_2$ showed a decrease compared to the Pt/C, implying that Ru has alloyed with platinum. After heat treatment, the lattice parameter increased, indicating that heat treatment has an influence in the structure of $PtRu/MoO_2$. It is interesting to observe that heat treatment affects the same electro-catalyst differently according to the support material in which it is dispersed in. This could be as a result of the interaction between the catalyst and the support material and the characteristics of the support material [61, 70, and 130].

4.2.2 Particle Size and Size Distribution

Since the particle size and particle morphology greatly influences the electro-chemical activity of the catalyst owing to the relationship between catalytic activity and surface structure, HRTEM analysis of the supported electro-catalyst was therefore carried out before the comparison of their catalytic activity. Figure 4.6 and 4.7 shows HRTEM images of PtRu electro-catalyst supported on MWCNT and metal oxide respectively. Their respective average particle size values were collected and presented in Table 4.3 and 4.4.

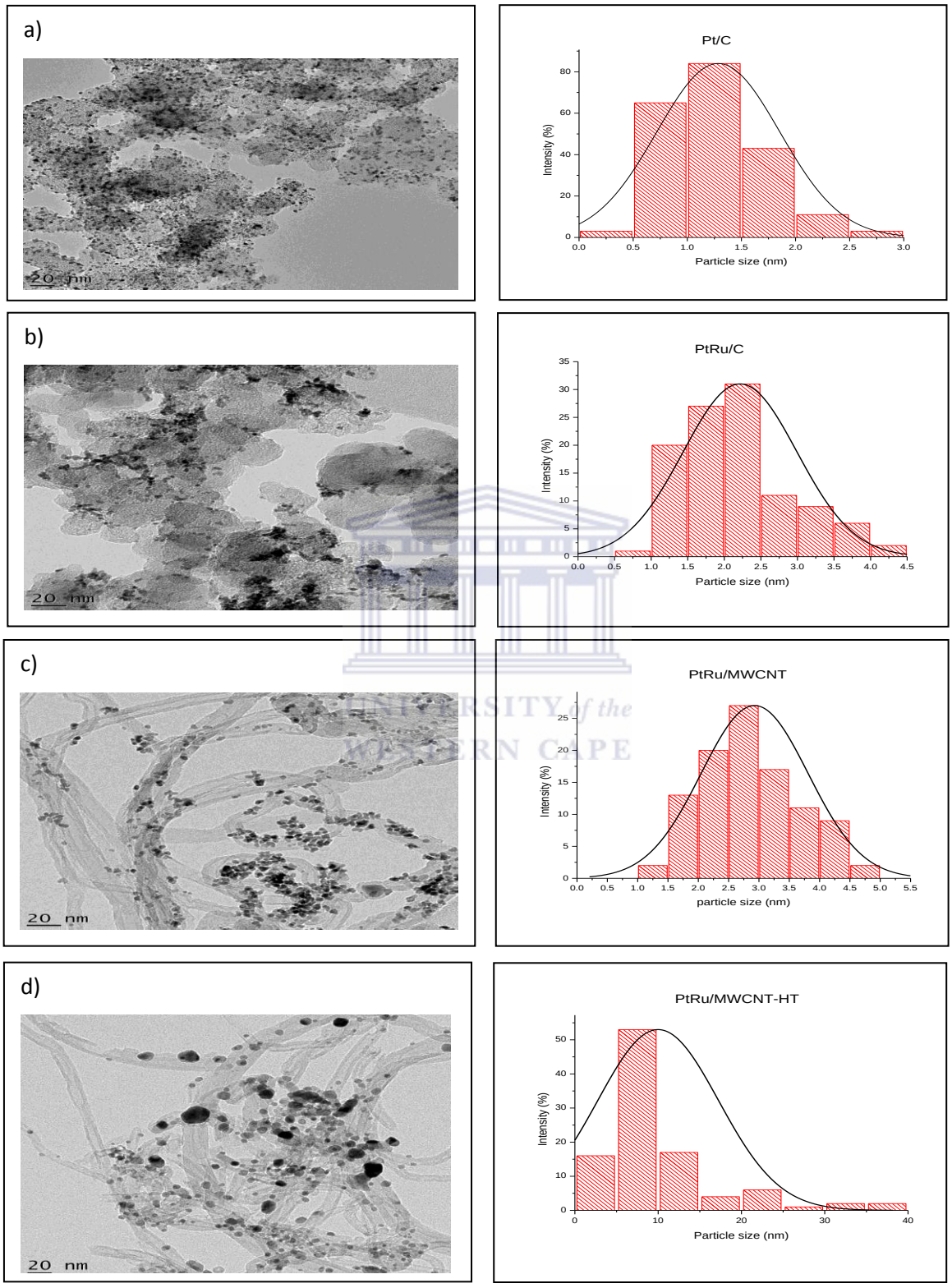

Figure 4.6: HRTEM images with their respective histograms for a) Pt/C, PtRu/C, c) PtRu/MWCNT and d) PtRu/MWCNT-HT

Catalyst	Particle size/nm
Pt/C	1.28
PtRu/C	2.21
PtRu/MWCNT	2.93
PtRu/MWCNT-HT	9.99

Table 1.3: *HRTEM average particle size estimated from 100 particles in random regions of PtRu/MWCNT compared with Pt/C and PtRu/C commercial electrocatalysts*

Figure 4.6 above presents typical HRTEM images of the commercial Pt/C and PtRu/C and the as prepared PtRu/MWCNT and PtRu/MWCNT-HT electro-catalyst with their respective histograms estimated from 100 particles selected from random regions. The average particle size was collected and presented in Table 4.3 above. It was observed that the spherical metal nanoparticles are uniformly dispersed on the carbon support with few agglomerates on some parts of the sample for the commercial Pt/C. The uniformity of the catalyst particle distribution is known to be important factor for electro-catalytic activity. PtRu/C showed poor size distribution with agglomerates on some parts of the sample. The average particle size for Pt/C and PtRu/C range from 1.3 and 2.2 nm respectively, while the relative particle size distribution was between 1.3-5.1 nm for Pt/C and 2.2 and 5 nm for PtRu/C. For the home-prepared PtRu/MWCNT and PtRu/MWCNT-HT, the HRTEM images show that the platinum nanoparticles clusters agglomerate to some extent and disperse on the surface of multi-walled carbon nanotubes non-homogenously, even though the presence of individual particles could still be observed in magnified images. The size increase was observed as was expected for the PtRu/MWCNT sample after heat-treatment. The wide particle size distribution was between 2.9-5.7 nm for PtRu/MWCNT and 9.9 to 37.8 nm for the heat-treated PtRu/MWCNT as is shown in their respective histograms [117-124].

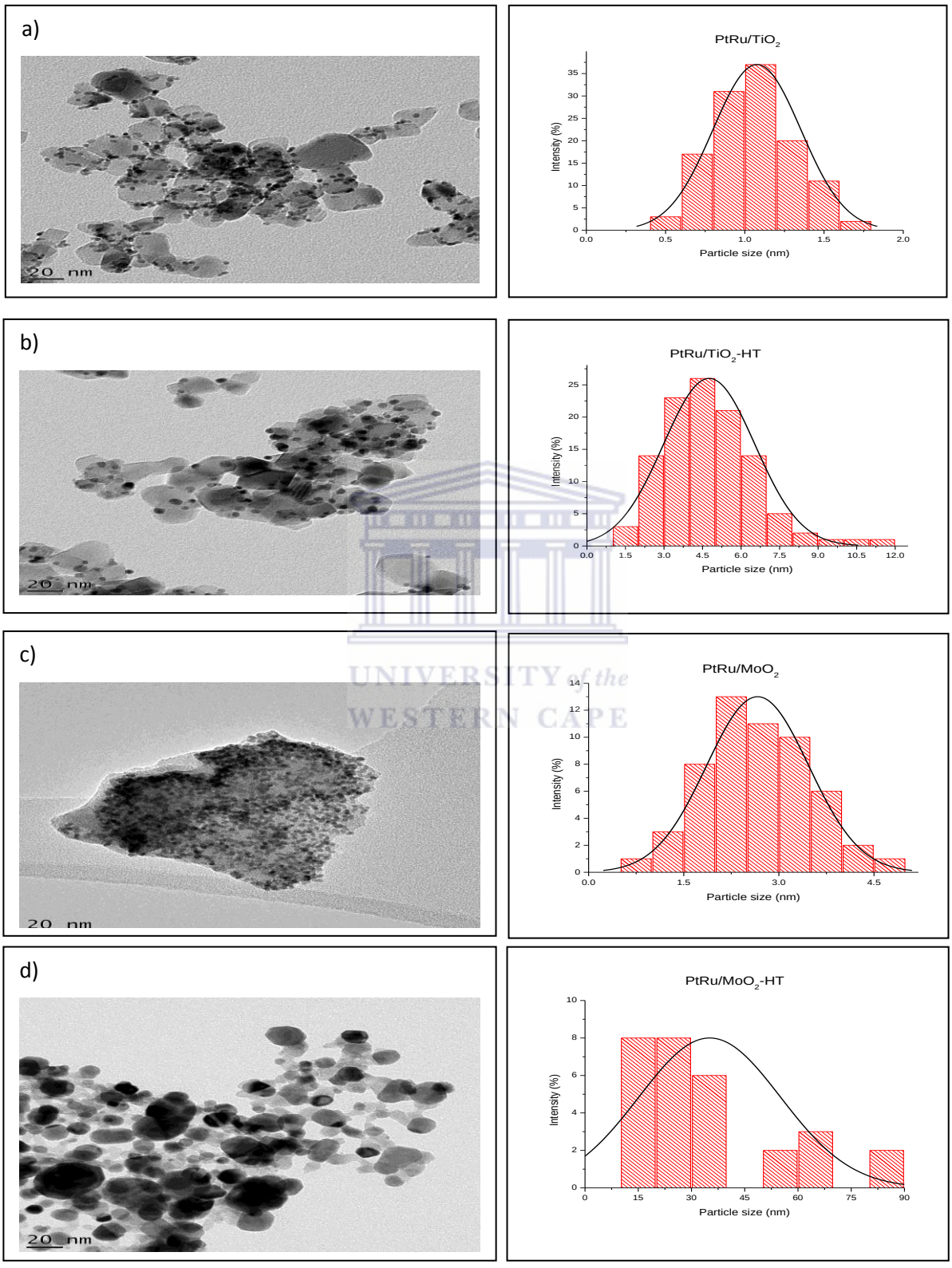

Figure 4.7: HRTEM images of a) PtRu/TiO_2, b) PtRu/MoO_2 and d) PtRu/MoO2-HT with their respective histograms

Catalyst	Particle size/nm
$PtRu/TiO_2$	1.08
$PtRu/TiO_2$-HT	4.76
$PtRu/MoO_2$	2.66
$PtRu/MoO_2$-HT	15.9

Table 24.4: *HRTEM average particle size estimated from 100 particles in random regions of PtRu electrocatalyst supported on metal oxides*

The morphologies and particle size distribution for $PtRu/TiO_2$, $PtRu/TiO_2$-HT, $PtRu/MoO_2$ and $PtRu/MoO_2$-HT are shown in Figure 4.7 above. The metal particles are dispersed on the metal oxide support. Agglomerates were also observed in certain areas of the samples, with large agglomeration of platinum nanoparticles particularly distinct in the heat-treated $PtRu/MoO_2$ sample that had uneven particle size distribution. Based on the measurements of 100 particles selected from random regions the distribution of the Pt particle sizes are portrayed in the histograms above and the average particle size values are presented in Table 4.4 above. They show particle size distribution between 1.1 and 2.0 nm and 4.0 and 11.0 nm for $PtRu/TiO_2$ and $PtRu/TiO_2$-HT respectively. The average particle size shows that by heat-treating the supported electro-catalyst, the mean particle size increases as expected from literature. For $PtRu/MoO_2$ the average particle size was 2.7nm and after heat treatment the particle size increased to 16 nm. The wide particle size distribution was observed to be between 2.7 and 4.8 nm for $PtRu/MoO_2$ and 15.9 and 35 nm for the heat-treated $PtRu/MoO_2$ [61, 70, and 130].

4.2.3 Morphology and Elemental Analysis of Supported Electrocatalyst

Morphology and elemental analysis of the supported home-prepared and commercial electro-catalysts was conducted by HRSEM and EDS following procedure outlined in section 3.2.1.1. The elemental loading/composition study of commercial PtRu/C electrocatalyst was conducted and used as a reference for comparison purposes. The elemental composition study for the heat treated sample was conducted to examine any alterations in the loading of the sample as a result of heat treatment. For it has been revealed in literature that heat treatment affects the loading of the resultant electrocatalyst. The results were collected and presented in Table 4.5 and 4.6 for the PtRu electrocatalyst supported on MWCNTs and metal oxides

respectively. Figure 4.8 and 4.9 below display the HRSEM images of the PtRu electrocatalyst supported on MWCNTs and metal oxides respectively.

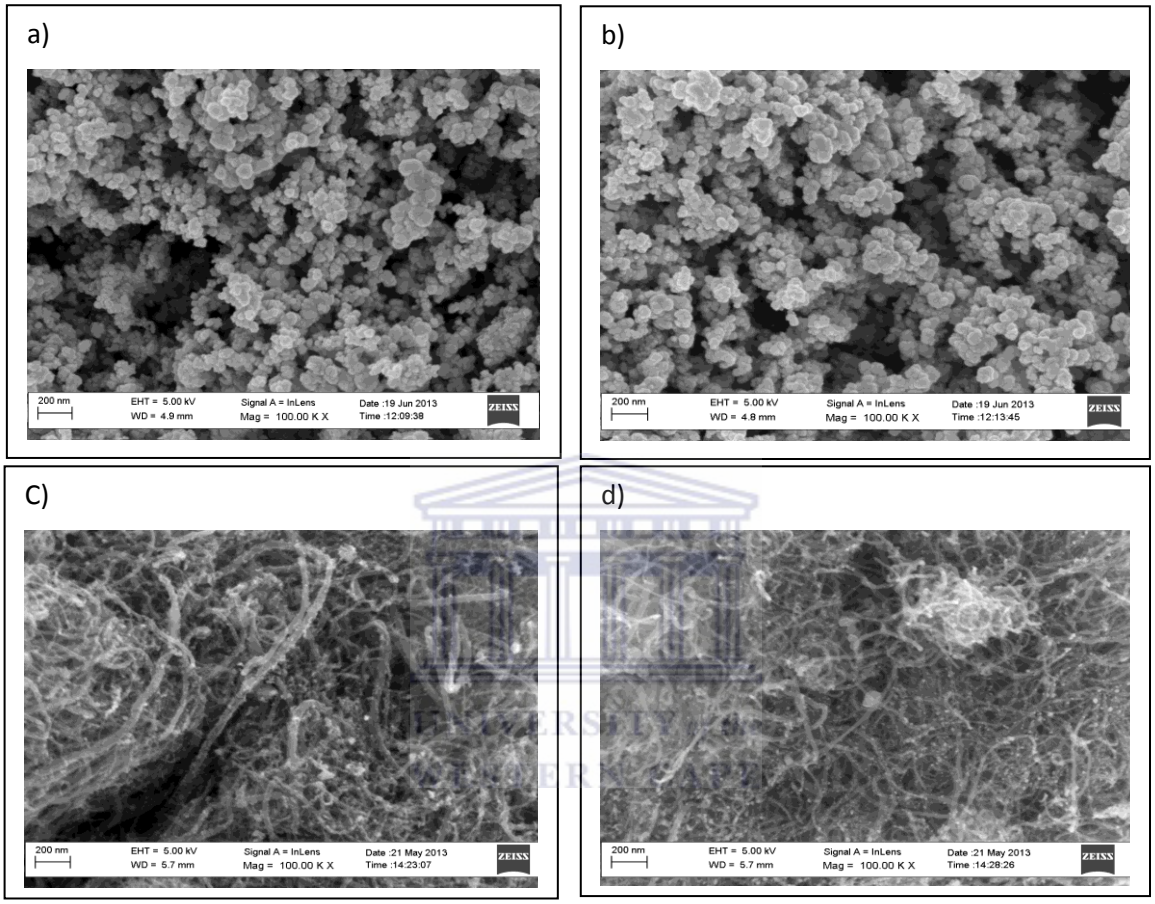

Figure 4.8: Figure 4.8: *HRSEM images of a) Pt/C, b) PtRu/C, c) PtRu/MWCNT and d) PtRu/MWCNT-HT*

Catalyst	**EDS wt.%**	
	Pt	**Ru**
PtRu/C	9.05	5.41
PtRu/MWCNT	10.79	5.84
PtRu/MWCNT-HT	9.44	3.58

Table 4.5: *EDS elemental analysis results for PtRu/MWCNT compared to PtRu/C commercial electrocatalyst*

Figure 4.8 above presents the HRSEM micrographs of commercial Pt/C and PtRu/C, together with the home-prepared PtRu/MWCNT and PtRu/MWCNT-HT electro-catalyst. The HRSEM micrographs for the commercial catalyst shows spherical grains with nanoparticles on them aggregated and loosely stacked in a porous state, which provides high specific area. The metal particles were observed decorated on the carbon nanotubes support material. Agglomerates on some part of the sample were also observed in the prepared sample as was also observed in the HRTEM results. A change in the heat-treated sample was observed as it displayed more well-dispersed metal particles on the support [117-124].

The loading of the catalyst presented in Table 4.5 above revealed that the prepared catalyst metal loading was close to the metal loading of the commercial PtRu/C catalyst. A decrease in the loading was observed after heat treatment for the as prepared electro-catalyst, an indication that the heat treatment decreases the loading of the resultant electro-catalyst, though it improves alloying, stability and dispersion of metal particles on the support [117-124].

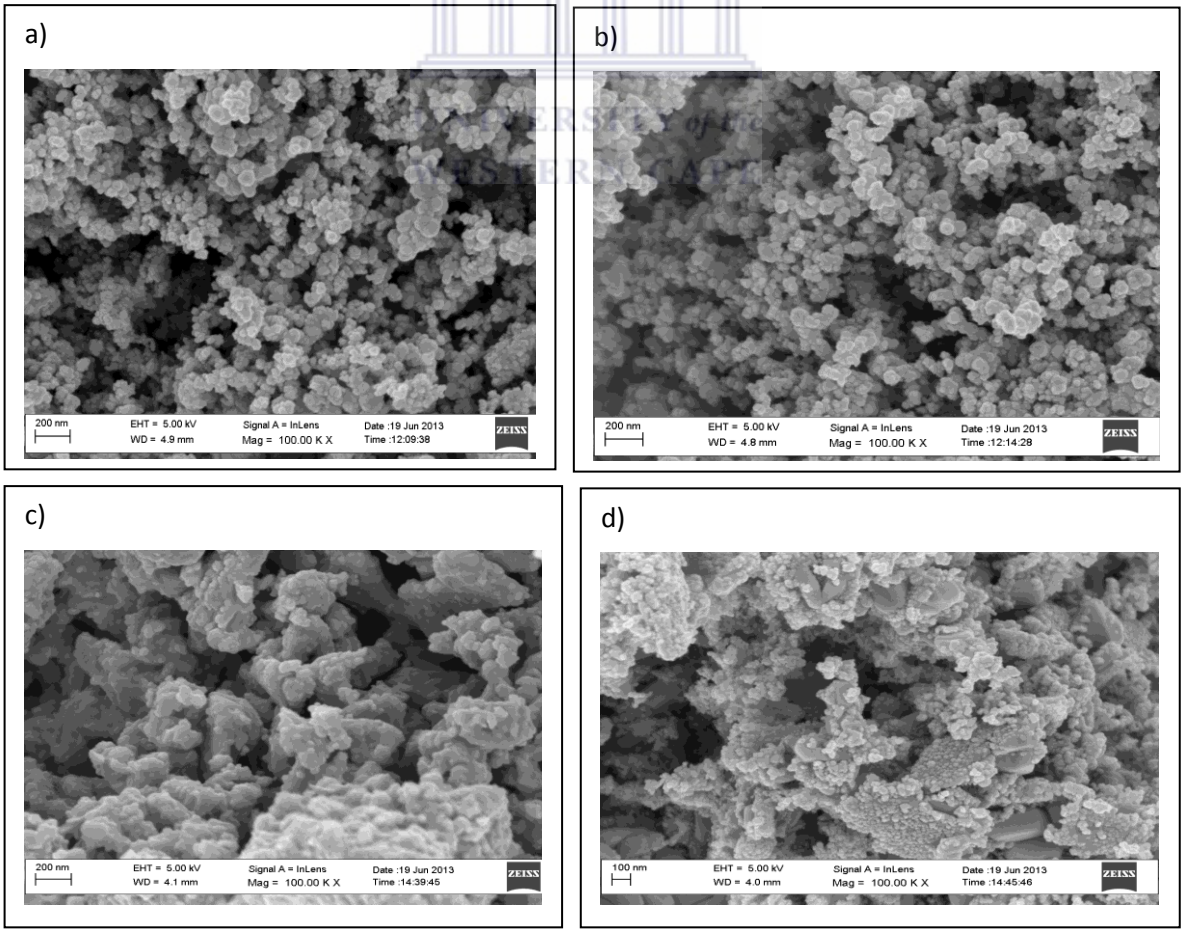

Figure 4.9: HRSEM images of a) PtRu/TiO_2, b) PtRu/TiO_2-HT, c) PtRu/MoO_2 and d) PtRu/MoO_2-HT

Catalyst	EDS wt.%	
	Pt	Ru
PtRu/C	9.05	5.41
PtRu/TiO_2	11.2	4.9
PtRu/TiO_2-HT	8.1	3.4
PtRu/MoO_2	12.5	2.3
PtRu/MoO_2-HT	14.2	6.4

Table 4.6: *EDS elemental analyses results of PtRu supported on metal oxides and compared with PtRu/C commercial electrocatalyst*

The HRSEM images of PtRu supported on metal oxides are shown in Figure 4.9 above. The dispersion of metal particles was observed in all samples. For the PtRu supported on MoO_2, it was observed that all metal particles had decorated the metal oxide with large agglomeration on other portion of the sample, as was also observed with HRTEM results. After heat treatment, the sample showed great increase in size with severe agglomeration. The metal loading was collected from EDS analysis results and presented in Table 4.6 above and shows relatively high content of Pt, more than the commercial catalyst and, interestingly, the loading increased with heat treatment for PtRu supported on MoO_2 unlike with PtRu supported on MWCNTs and TiO_2 where the loading decreased with heat treatment. The metal loading for the titanium oxide supported catalyst was very close to the metal loading of PtRu/C commercial catalyst and decreased with heat treatment as was observed with the PtRu/MWCNT catalyst. This shows that catalyst behaves differently as the catalysts are influenced by the support material used [61, 70, and 130].

4.3 ELECTROCHEMICAL CHARACTERIZATION OF PtRu USING RDE

It is generally accepted that the ECSA, mass activity (MA) and specific activity (SA) are the true measures of the catalyst catalytic activity. This section is dedicated to presenting results obtained from RDE measurements for the supported PtRu electro-catalyst. The results start off with the cyclic voltammograms (CVs) to examine the electro-active surface area and durability of the catalysts, followed directly by the examination of their mass-area and specific-area activity for ORR and MOR using LSV polarization curves.

4.3.1 Examination of ECSA Before and After Durability Studies Using CV

It is generally believed that the electro-chemical surface area of platinum is one of the most indispensable parameters for characterizing a fuel cell electrode. A large electro-chemical surface area indicates a better electrode, as more catalyst sites are available for electro-chemical reactions. It is reported that the performance degradation of DMFC is largely owed to the electro-chemical surface area loss of the electrodes [33]. The decrease in the electro-active surface area mainly results from the growth of platinum alloy nanoparticles size, the dissolution of platinum and/or other platinum alloy nanoparticles from the carbon support material. This results in poor durability of the fuel cell catalyst and, accordingly, the fuel cell system [33].

Figure 4.10 a) and b) and 4.11 a) and b) presents cyclic voltammograms of the home-prepared PtRu electro-catalyst supported on MWCNTs and metal oxides respectively. The numerical ECSA and the percentage loss for the supported PtRu electro-catalyst on MWCNTs and metal oxides electro-catalyst are detailed in Table 4.7 and 4.8 respectively. Commercial Pt/C and PtRu/C electro-catalysts were also characterized and used as standards for comparison purposes.

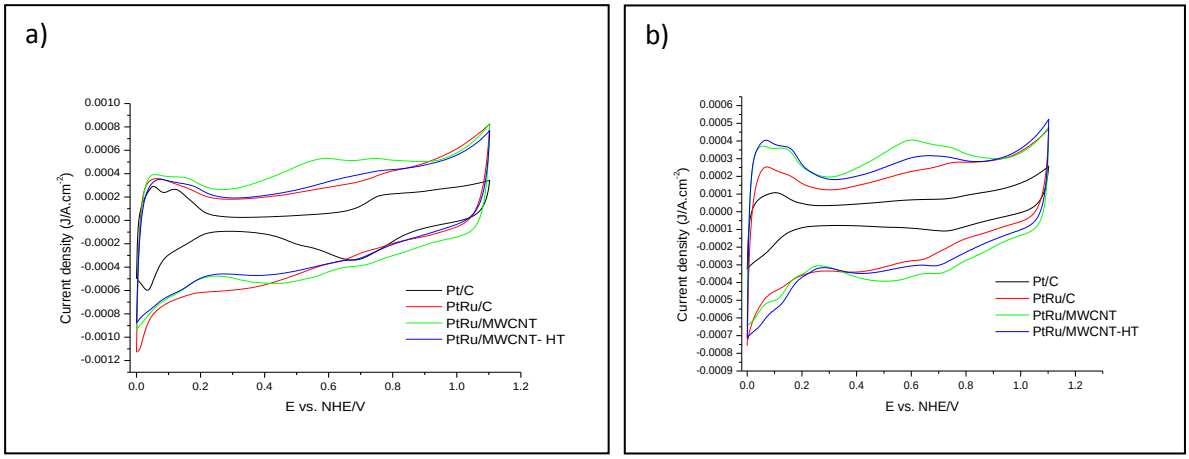

Figure 4.10: RDE cyclic voltammogram of the home-prepared PtRu/MWCNT compared with Pt/C and PtRu/C commercial electrocatalysts in N_2-saturated 0.1M $HClO_4$ @ 20mV/s a) pre-durability and b) post-durability studies

The catalysts were characterized electrochemically using CV and presented in Figure 4.10 a) and b). These CVs were obtained in nitrogen saturated 0.1M $HClO_4$ using RDE. The CV sweep rate was set at 20mV/s and the potential range was within -0.2 and 0.9 V vs. Ag/AgCl and all potentials were converted to the normal hydrogen electrode (NHE) scale and shown as such throughout this work unless otherwise noted. All CVs exhibited three regions: 1) adsorption-desorption of hydrogen (0-0.2 V vs. NHE); 2) double layer formation (0.2-0.4 V vs. NHE); and 3) oxidation-reduction of Pt (0.4-0.8 V vs. NHE). The CVs show PtRu samples display much bigger double-layer current than Pt/C does. The big capacitive charging current has been usually accredited to the activation of H_2O on Ru sites in PtRu samples. These findings are consistent with the results by Li *et al* [117]. As discussed in the literature review section, H_2O could be easily activated and dissociated on Ru surface with $Ru\text{-}(OH)_{ads}$ species at lower potentials (0.25 V vs. NHE). The resulted $Ru\text{-}(OH)_{ads}$ species could then facilitate the removal of CO_{ads}-like poisoning species during the methanol oxidation at lower potentials and, accordingly, improve the methanol oxidation activity. Figure 4.10 b) shows cyclic voltammograms obtained after durability studies. A decrease in the current layer in all regions for all samples is observed after durability studies and the decrease is even more prominent for the Pt/C commercial catalyst.

The effective surface area of the catalyst was calculated from the area of the hydrogen-desorption peak after subtracting contribution from the double-layer charging. This area was then converted into the effective active surface area by using the factor 210 $\mu C.cm^{-2}$ for the monoloyer of hydrogen adsorbed on polycrystalline platinum. It is assumed that the hydrogen

could only adsorb on free Pt surface. The results were collected and presented in Table 4.7 below. All ECSA calculations for this study were done following equation 4.3 given below as [111]:

$$\text{ECSA } (m^2.g^{-1}_{Pt}) = \left[\frac{\text{QH}-\text{adsorption (C)}}{210\mu C cm^{-2} LPt(mgPt.cm^{-2})Ag\ (cm^2)}\right] 10^5 \quad (4.3)$$

Q_H = 210µC.cm^{-2} is the charge of full coverage for clean polycrystalline Pt and is used as the conversion factor; L_{Pt} is the working electrode Pt loading (mg.cm^{-2}); and Ag is the geometric surface area of the glassy carbon electrode (i.e. 0.196 cm^2). The values for ECSA are reported in $m^2.g^{-1}_{Pt}$.

Catalyst	**Particle size/ nm**		**ECSA pre-DT/$m^2.g^{-1}$**	**ECSA post- DT/ $m^2.g^{-1}$**	**% ECSA loss**
	XRD	**HRTEM**			
Pt/C	2.28	1.28	45.7	16.6	64
PtRu/C	3.02	2.21	28.0	19.01	32
PtRu/MWCNT	3.22	2.93	31.96	23.99	25
PtRu/MWCNT-HT	6.62	9.99	26.66	24.17	9

Table 4.7: *Summary of catalyst particle size and their ECSA values of pre-durability and post-durability results of PtRu/MWCNT compared with Pt/C and PtRu/C commercial electrocatalysts (DT-durability test)*

Table 4.7 above presents the ECSA values of the supported electro-catalyst. From the ECSA results it is clear that Pt/C has a higher ECSA than the binary electro-catalyst, which could be attributed to the small Pt particle size and uniform distribution known to enhance the electro-chemical surface area of the catalyst. However, after durability studies, the commercial Pt/C lost a high percentage (64%) of its ECSA and this could be credited again to the small particle size known from literature to show a strong tendency to agglomerate due to their high specific surface energy. When Pt particles agglomerate to bigger ones, the electro-chemical surface area of Pt decreases, and, consequently, the performance of DMFC. This reveals that after long cycles the small Pt nanoparticles agglomerated and resulted in the high loss of the

ECSA for the Pt/C catalyst as shown in Figure 4.10 b). The binary electro-catalyst, however, displayed more stability than mono-metallic Pt, indicating that alloying platinum with a second metal does improve the durability of the resultant catalyst. It was observed that the PtRu supported on MWCNT retained higher ECSA than the commercial PtRu/C (which lost 32% of its ECSA) with the heat-treated PtRu/MWCNT losing just 9% of its activity after 1000 cycles, an indication again that heat treatment improves dispersion of the nanoparticles on the support and consequently the stability of the resultant electro-catalyst as shown in Figure 4.10 b) can also be credited to the support material since electro-catalyst supported on MWCNT displayed more stability than the commercial electro-catalyst supported on carbon black, an indication that carbon black gets oxidized faster than MWCNT. Thus, MWCNTs are more resistant to corrosion than carbon black and, accordingly, electro-catalyst supported on MWCNT showed higher stability than the commercial catalyst. These findings are consistent with the literature on this issue. The ECSA values of the binary PtRu electro-catalyst showed very little difference for both the home-prepared and commercial PtRu/C electro-catalyst, following the trend: PtRu/MWCNT>PtRu/C>PtRu/MWCNT-HT. The high ECSA for the home-prepared PtRu/MWCNT could be attributed to the metal loading since PtRu/MWCNT had slightly higher metal loading (Table 4.6) than the two samples. The electro-chemical behaviour of PtRu/MWCNT-HT was more or less the same as the commercial PtRu/C catalyst as shown in Table 4.8 and Figure 4.10 a) and the EDS results Table 4.6 showed the platinum content for both these samples to be on the same level. The lower ECSA in the heat-treated sample, compared to the untreated sample, could be credited to the increase in particle size for the heat-treated sample. Available literature says that small particle size enhances the ECSA of the electro-catalyst [108-124].

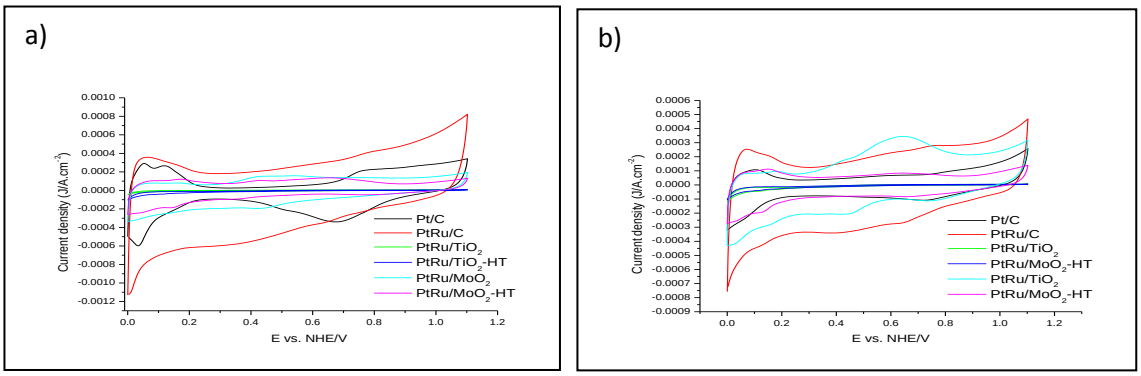

Figure 4.11: RDE cyclic voltammogram of the home-prepared PtRu supported on metal oxides compared with Pt/C and PtRu/C commercial catalysts a) pre-durability and b) post-durability studies

Catalyst	**Particle size/ nm**		**ECSA pre-DT/m^2.g^{-1}**	**ECSA post-DT/m^2.g^{-1}**	**% ECSA loss**
	XRD	**HRTEM**			
Pt/C	2.28	1.28	45.7	16.6	64
PtRu/C	3.02	2.21	28.0	19.01	32
PtRu/TiO_2	12.85	1.08	1.83	1.29	29
PtRu/TiO_2-HT	14.47	4.76	1.87	1.51	19
PtRu/MoO_2	13.96	2.66	5.95	2.15	64
PtRu/MoO_2-HT	19.65	35.12	6.1	3.3	46

Table 4.8: *Summary of PtRu supported on metal oxides particle size and their ECSA values of pre-durability and post-durability studies compared with Pt/C and PtRu/C commercial electrocatalysts*

Figure 4.11 a) and b) above presents the cyclic voltammograms of the home-prepared PtRu supported on metal oxides compared with commercial Pt/C and PtRu/C electro-catalyst before and after durability studies respectively. Table 4.8 presents their ECSA values calculated following the equation 4.3. From Table 4.8, it is clear that the catalyst supported

on metal oxide possess a low ECSA. Thus, the CVs for the electro-catalyst supported on these metal oxides in Figure 4.11 a) are suppressed by the more active commercial electro-catalysts. As discussed in chapter 2, the objective of employing the metal oxide was not to enhance the catalytic activity of the catalyst, but rather, to enhance their durability. PtRu supported on titanium oxide showed less electro-catalytic activity compared to PtRu electro-catalyst supported on molybdenum oxide. However, the anatase titania supported electro-catalyst proved to be more stable than the molybdenum supported electro-catalyst losing 19% of its ECSA compared to 64% lost by the molybdenum supported catalyst. The % loss of ECSA for the prepared PtRu supported on molybdenum oxide is the same as that of Pt/C commercial catalyst, indicating that the electro-catalyst supported on these materials lose their activity at higher percentages as a result of the instability of the support material which is not desirable for their projected life-times for fuel cell applications. The stability shown by the anatase titania is consistent with the finding by Huang *et.al* [118] who reported that Pt supported on anatase titania showed improved stability than the commercial Pt/C electro-catalyst. Thus, catalyst supported on anatase titania proved to be more stable than catalyst supported on molybdenum oxide. However, catalyst supported on molybdenum oxide showed better activity than catalyst supported on anatase titania.

4.3.2 Studying the Activity of Catalysts in ORR and MOR Using RDE-LSV

The electro-chemical activity of catalysts towards ORR was studied in pure oxygen saturated 0.1M $HClO_4$ solution and in the presence of 1M CH_3OH in order to investigate the tolerance of the catalyst towards methanol. In the cathode of a DMFC, both reactions (ORR and MOR) take place simultaneously at separate places at the electrode surface as shown in equation 4.4 and 4.5 below. Thus, for DMFC, the cathode catalyst is required not only to be highly active in ORR but must also be methanol tolerant in order for it to be considered for practicality purposes in DMFC applications. The methanol that crosses over gives rise to various processes on the Pt surface of a DMFC cathode, as follows [119]:

1) On separate places at the electrode surface, oxidation of methanol and reduction of oxygen occur simultaneously:

$$CH_3OH + H_2O \rightarrow CO_2 + 6H^+ + 6e^- \quad (4.4)$$

$$O_2 + 4H^+ + 4e^- \rightarrow H_2O \quad (4.5)$$

The above reactions then give rise to a mixed potential at the cathode

2) A heterogeneous chemical reaction between methanol and oxygen occurs

$$CH_3OH + {}^3/_2O_2 \rightarrow CO_2 + 2H_2O \quad (4.6)$$

3) Methanol adsorption can cause blocking of the surface due to the formation of adsorbed carbon monoxide-like species, producing an additional shift of potential

$$CH_3OH + Pt \rightarrow COads + 6H^+ + 6e^- \quad (4.7)$$

The electrocatalytic activity of the catalyst is best compared by their mass-and area-specific activities using the mass transport correction for thin-film RDE according to the following equation:

$$\text{Jk (A)} = \frac{J\,(A) \times J(Lim)}{J(Lim) - J\,(A)} \quad (4.8)$$

J (A) is the value of the curve at E = 0.90 V and J_{lim} is that at E = 0.4 V vs. NHE

The Pt mass specific activity (MA) is estimated via calculation of kinetic current (Jk) and normalization to the Pt loading of the disk electrode according to the following equation:

$$\text{MA (mA.mg}^{-1}) = \frac{Jk\,(A)}{Pt\ loading(\ mg)} \quad (4.9)$$

The Pt area specific activity is estimated via the calculation of mass specific activity and normalization to the Pt electrochemical surface area (obtained using equation 4.3) according to the following equation:

$$\text{SA (mA.cm}^{-2}) = \frac{MA\ (mA.mg^{-1})}{ECSA\ (cm^{-2}mg^{-1})} \quad (4.10)$$

The numerical values of the Pt mass-specific activity (MA) and area-specific activity (SA) at E = 0.9 V vs. NHE derived from both the ORR and MOR polarization curves shown in Figure 4.12 and Figure 4.13 are detailed in Table 4.9 and Table 4.10

Figure 4.12 and 4.13 presents the RDE-ORR and MOR polarization curves of PtRu supported on MWCNT and metal oxide respectively. Table 4.9 and 4.10 presents the MA and SA for the ORR and MOR of PtRu supported on MWCNT and metal oxide respectively. The home-prepared supported catalysts were compared to the standard commercial Pt/C and PtRu/C electrocatalysts.

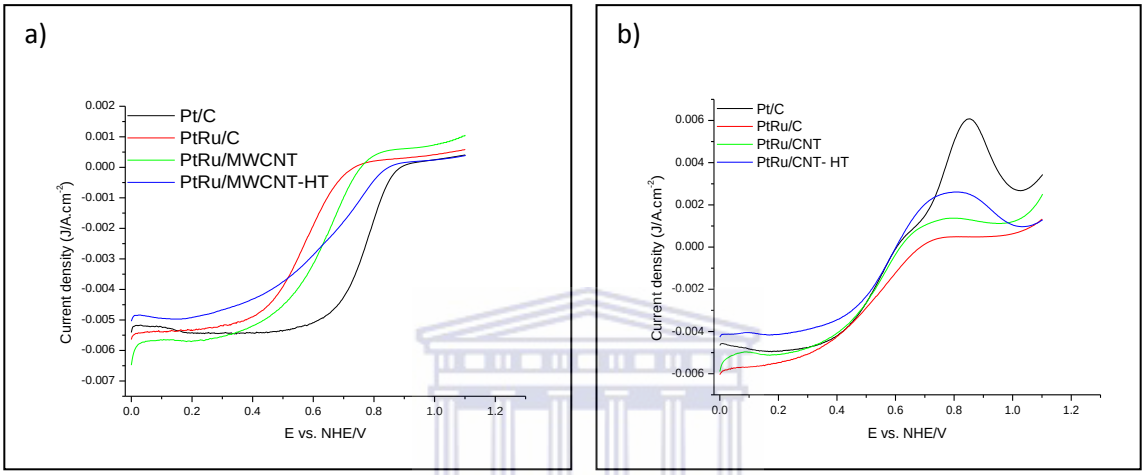

Figure 34.12: a) ORR polarization curves and b) MOR polarization curves of PtRu/MWCNT compared with Pt/C and PtRu/C commercial catalysts in O_2-saturated 0.1M $HClO_4$ @ 20mV/s for MOR 1M CH_3OH was added to 0.1M $HClO_4$ the reaction was set @ 1600rpm

		ORR catalytic activity @ 0.9 V		MOR catalytic activity @ 0.9 V	
Catalyst	**ECSA/$m^2.g^{-1}$**	**MA/ mA.mg-^{1}**	**SA/ mA.cm-^{2}**	**MA/ mA.mg-^{1}**	**SA/ mA.cm^{-2}**
Pt/C	45.7	85.85	0.188	-122.6	-268
PtRu/C	28.0	463	1.66	2.83×10^3	10.10
PtRu/MWCNT	31.96	35.6×10^3	111	8.67×10^3	27.12
PtRu/MWCNT-HT	26.66	2.72×10^3	0.029	28.85×10^3	108

Table 4.9: *Studying the activity of PtRu/MWCNT electrocatalyst towards ORR and the tolerance of the catalyst to methanol and comparing it to the Pt/C and PtRu/C commercial catalysts*

The ORR polarization curves were obtained in an O_2-saturated 0.1M $HClO_4$ while the ORR curves in the presence of CH_3OH (from henceforth will be referred to as MOR) were obtained in an O_2-saturated 0.1M $HClO_4$ +1M CH_3OH solution using RDE. The LSV sweep rate was set at 20mV/s using the anodic direction and the potential range was within -0.2 and 0.9 V vs. Ag/AgCl and the rotation speed rate was set at 1600 rpm. Mass activity, that is the current per unit amount of catalyst, and specific activity, which is for unit surface area of catalyst are normally two approaches used to express the catalytic activity. The mass activity has practical implications in fuel cells because the cost of the electrode depends on the amount of platinum used, and the specific activity provides a measure of the electrocatalytic activity of platinum atoms in the particle surface. Specific activity is particularly meaningful for structure-sensitive reactions [111, 115].

All curves for ORR {Figure 4.12 a)} display the typical polarization behaviour for the electro-chemical reduction of molecular oxygen. The ORR is under mixed kinetic-diffusion control in the potential range between 0.9 and 0.6 V, followed by a region where diffusion limiting current can be observed. Figure 4.10 a) shows the ORR polarization curves and it can be seen that the commercial Pt/C is more active in pure oxygen-containing electrolytes. However, in the presence of methanol {Figure 4.12 b)}, the commercial Pt/C is the least active, owing to CO_{ads}- like species which blocks the active site of the catalyst resulting in lower activity of the catalyst, as also shown in Table 4.9, so that in the presence of methanol the commercial Pt/C, it shows lower mass and specific activities, indicating that the mono-metallic catalyst is not methanol tolerant as was also expected from literature. From the table above, it was also noted that mass and specific activities were higher for binary electro-catalyst, with an exception in SA of the as prepared heat-treated catalyst, owing to an increase in nanoparticle size. The increase in MA and SA is an indication that alloying Pt with a second metal improves mass and specific activity. The commercial PtRu and home-prepared PtRu/MWCNT-HT showed better MA and SA activity in the presence of methanol, an indication that they are methanol tolerant oxygen reduction catalysts. The enhanced activity in methanol containing electrolytes has been explained in literature [115-118] to be as a result of the removal of CO or COH from the platinum during the cross-over of methanol oxidation by alloy formation with Ru and/or second metal. Thus, this increased the number of available sites for oxygen reduction. It was also observed, however, that the home-prepared PtRu/MWCNT showed a high mass and specific activity for ORR in pure oxygen

electrolytes. But, in the presence of methanol, the catalyst's mass and specific activities decreased and this could be a result of poor alloying which was observed in XRD results, and has, therefore, resulted in the poor performance of the electro-catalyst in the presence of methanol [108-125].

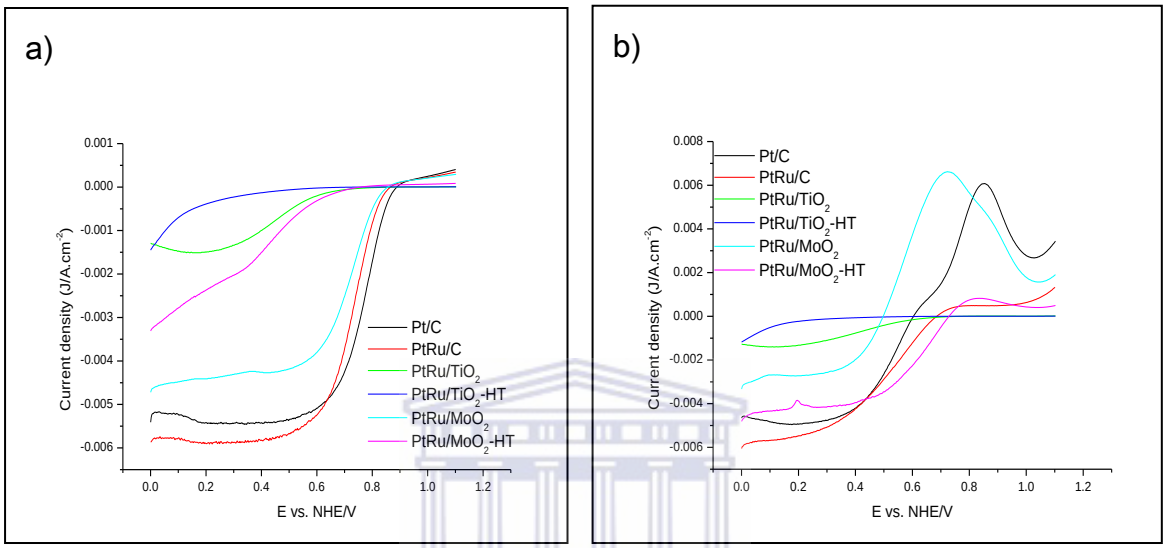

Figure 4.13: *a) ORR polarization curves in O_2-saturated 0.1M HCLO4 and b) MOR polarization curves in O_2-saturated 0.1M $HCLO_4$+1M CH_3OH solution with a scan rate of 20mV/s @ 1600rpm for PtRu supported on metal oxides compared with Pt/C and PtRu/C commercial electrocatalysts*

Figure 4.13 above presents the a) ORR polarization curves of PtRu supported on the metal oxide obtained in an O_2-saturated 0.1M $HClO_4$ and b) MOR curves obtained in an O_2-saturated 0.1M $HClO_4$ +1M CH_3OH solution using RDE. The LSV sweep rate was set at 20mV/s and the potential range was within -0.2 and 0.9 V vs. Ag/AgCl and the scans were taken at 1600 rpm using the anodic sweep. The polarization curves of the as prepared samples were compared with commercial Pt/C and PtRu/C catalysts. The commercial catalyst clearly showed higher activity than the as prepared metal oxide supported PtRu, followed by the $PtRu/MoO_2$ which showed better activity than the rest of the metal oxide supported PtRu in ORR as shown in 4.13 a) above. Table 4.10 below presents the ORR and MOR mass and specific activities for the supported electro-catalysts. From this Table, it is observed that $PtRu/TiO_2$ showed better activity in the presence of methanol than in pure oxygen containing electrolytes, an indication that that catalyst supported on titanium oxide are methanol tolerant catalyst. However, their activity towards ORR in pure oxygen electrolytes needs major improvement if they are to be considered for practicality purposes in DMFC applications. For $PtRu/MoO_2$, the untreated sample showed better MA and SA in methanol free electrolytes

than in the presence of methanol, whereas in the heat-treated sample, it showed better MA and SA in the presence of methanol than in pure oxygen electrolytes. PtRu supported on anatase showed poor activity both in ORR and MOR. This could be attributed to the low ESCA of the catalysts. It was also observed that as the surface area decreases, the specific activity generally increases. This indicates that oxygen reduction on platinum surface is indeed a structure-sensitive reaction. The observed effect, depending on the particle size, can be explained in terms of the variation of the different Pt crystal facets [61, 70, 124, 125, and 130].

		ORR catalytic activity @ 0.9V		**MOR catalytic activity @ 0.9 V**	
Catalyst	**ECSA/$m^2.g^{-1}$**	**MA/ $mA.mg^{-1}$**	**SA/$mA.cm^{-2}$**	**MA/ $mA.mg^{-1}$**	**SA/$mA.cm^{-2}$**
Pt/C	45.7	85.85	0.188	-122.6	-268
PtRu/C	28.0	463	1.66	2.83×10^3	10.10
PtRu/TiO_2	1.83	18.94	1.04	71.8	3.93
PtRu/TiO_2-HT	1.87	-5000	-2.6×10^3	20.37	1.09
PtRu/MoO_2	5.95	997	17.82	-21.29	-380
PtRu/MoO_2-HT	6.1	418.5	6.86	3.88×10^3	63.6

Table 4.10: *Studying the activity of PtRu supported on TiO_2 and MoO_2 towards ORR and the tolerance of the catalyst to methanol and comparing it to Pt/C and PtRu/C commercial electrocatalysts*

Commenting generally on Figure 4.14 and 4.15 which presents the ORR polarization curves taken at various rotation rate (left), Koutecky-Levich (K-L) plot obtained for different rotation speed at potential range between 0.60 and 0.62 V versus NHE (centre), Tafel plots taken from the 1600 rpm rotation rate (right) for PtRu supported on MWCNT compared with Pt/C and PtRu/C commercial electrocatalyst and PtRu electrocatalyst supported on metal oxides respectively. Various rotation rates were used to collect data for the K-L plot analysis

as presented in the following figures below. Linear relationships with constant slopes for the as prepared PtRu supported on MWCNT and MoO_2 were observed and it was similar to the commercial Pt/C and PtRu/C commercial electro-catalyst, confirming that oxygen reduction reaction follows the first order kinetics with respect to molecular oxygen. As for the prepared PtRu supported on anatase titania, the K-L plot reveals that the reaction did not follow the first order kinetics with respect to molecular oxygen, further indicating that the reaction took the two electron transfer of producing hydrogen peroxide which is undesired in fuel cell reaction as it a slow reaction. The Tafel slope for the electro-catalyst were calculated and presented in Table 4.11 below. The PtRu supported on MWCNT and MoO_2, their Tafel slope values were close to those of the commercial Pt/C and PtRu/C, suggesting that the ORR mechanism is similar to that of Pt/C. For the PtRu supported on anatase titanium, the values were slightly higher, taking the 120 mV/dec, which is still an acceptable value for ORR on platinum electrode [124, 125, and 130].

Catalyst	**Tafel slope b/mV.dec^{-1}**
Pt/C	-62.2
PtRu/C	-58.6
PtRu/MWCNT	-59.1
PtRu/MWCNT-HT	-58.0
PtRu/TiO_2	-119.8
PtRu/TiO_2-HT	-104
PtRu/MoO_2	-53.1
PtRu/MoO_2-HT	-50.3

Table 4.11: *Tafel slopes values for the home-prepared PtRu supported on MWCNT, TiO_2 and MoO_2 compared with Pt/C and PtRu/C commercial electrocatalysts*

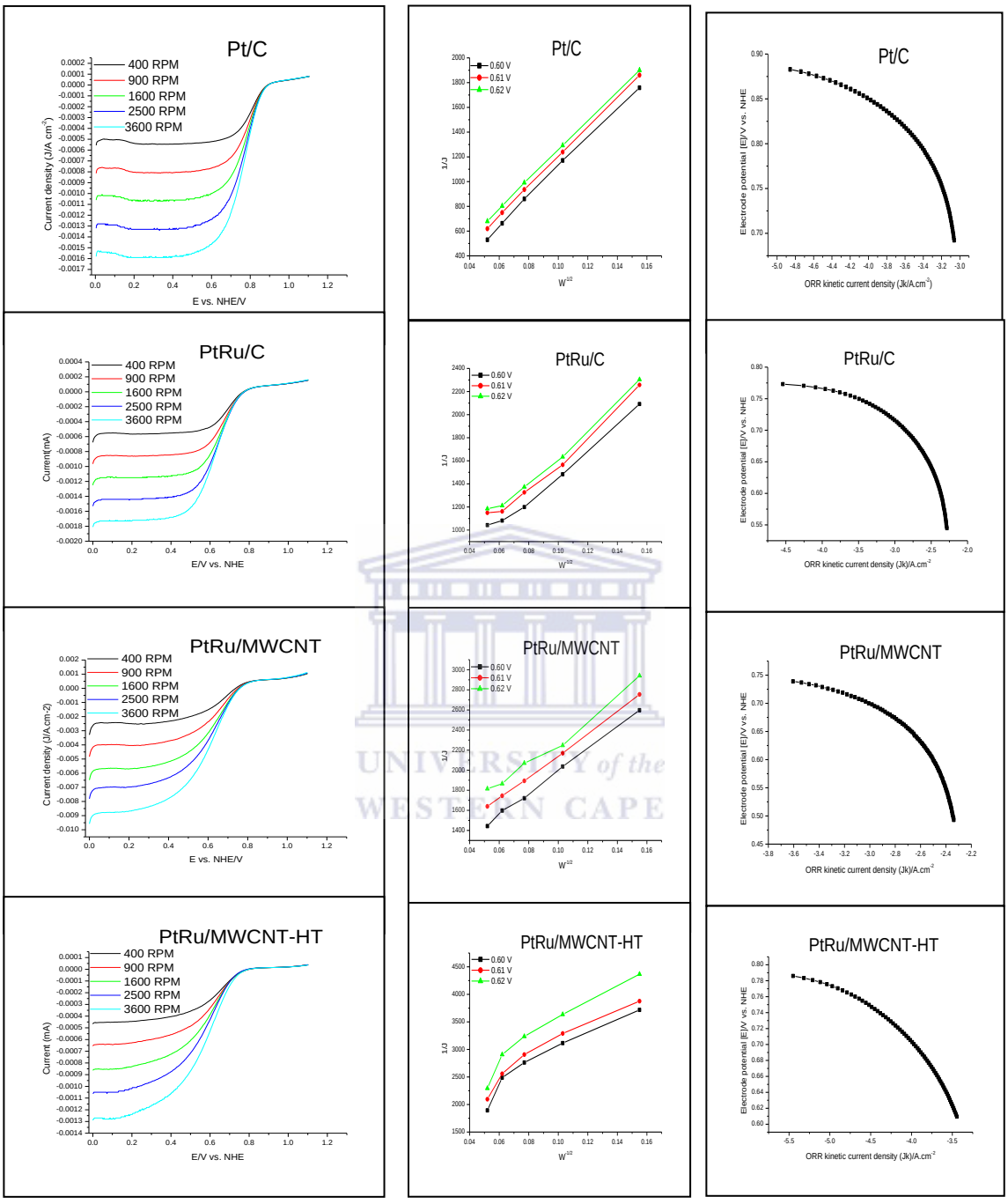

Figure 4.14: (left) RDE data for commercial Pt/C and PtRu/C and home-prepared PtRu/MWCNT at various rotation rates; (centre) Koutecky-Levich plots; (right) Tafel plots for electrocatalyst under test in O_2-saturated 0.1M $HCLO_4$

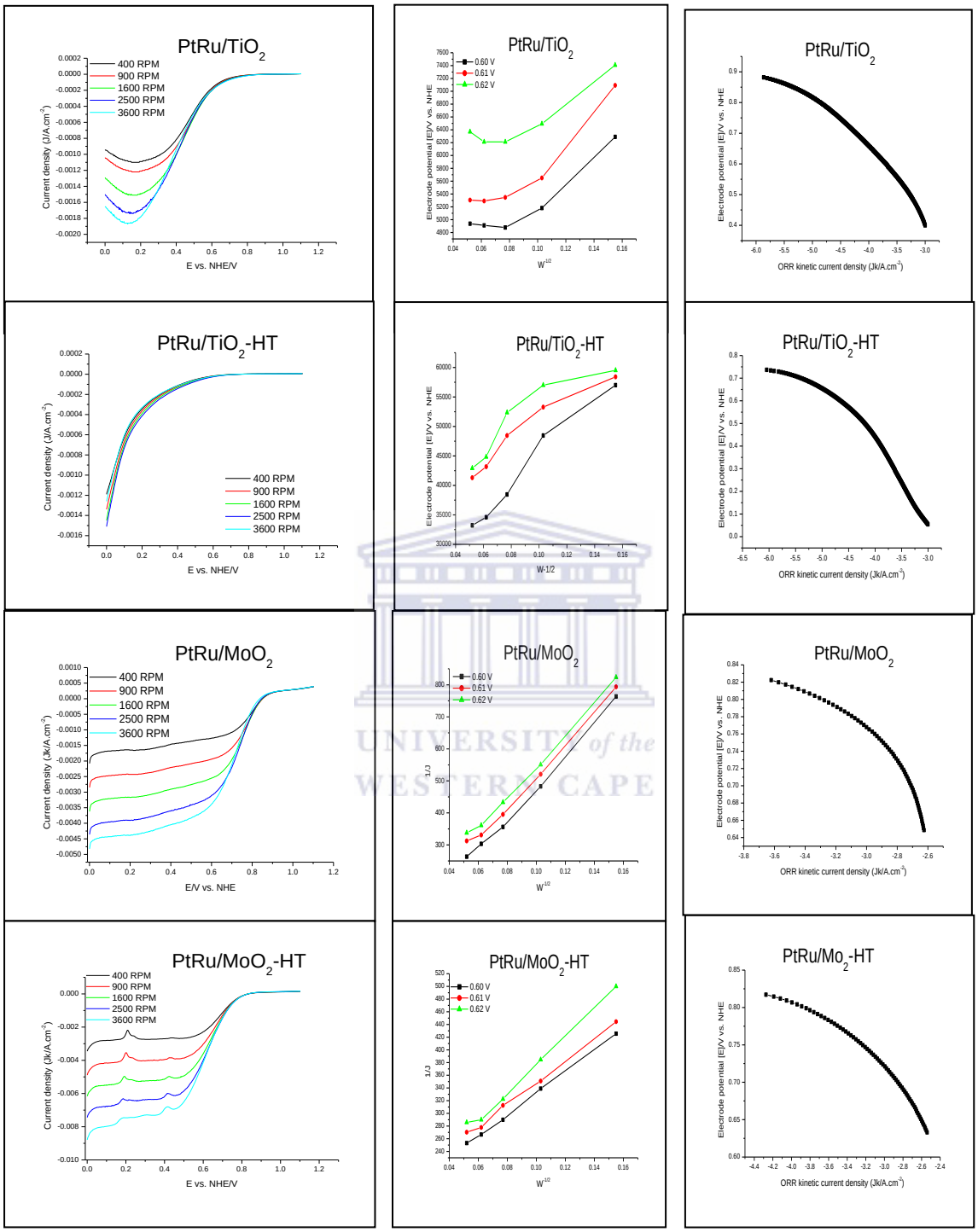

Figure 4.15: *(left) RDE data for the home-prepared PtRu supported on metal oxides at various rotation rates; (centre) Koutecky-Levich plots; (right) Tafel plot for each electrocatalyst under test in O_2-saturated 0.1M $HClO_4$*

4.3.3 Summary

PtRu was synthesized using the polyol approach and supported on multi-walled carbon nanotubes, titanium oxide and molybdenum oxide. Part of the supported electro-catalyst was then heat-treated to improve alloying, stable distribution and uniform dispersion of the metal nanoparticles on the support material. The supported electro-catalyst was then physically and chemically characterized to investigate its applicability in the cathode of a direct methanol fuel cell and the results compared to Pt/C and PtRu/C commercial electro-catalysts. Different techniques were used in the characterization; for structural identification XRD, HRTEM, HRSEM and EDS were used. For electro-chemical characterization RDE-CV and RDE-LSV were employed.

Catalyst supported on MWCNTs showed high activity both in pure oxygen containing electrolytes and in the presence of methanol than catalyst supported on metal oxides, an indication that they are methanol tolerant oxygen reduction electro-catalyst. Pt/C showed a high ECSA and it was credited to the small particle size and uniform distribution known to enhance the electro-chemical surface area. The binary electro-catalyst supported on carbon black and MWCNTs s showed similar electro-chemical behaviour. After durability studies, the Pt/C lost a high percentage of its active surface area compared to the binary catalysts, an indication that the binary electro-catalyst are more stable than the mono-metallic platinum. It was also observed that the catalysts supported on MWCNTs are more stable than catalyst supported on carbon black. The catalyst supported on metal oxide showed low activity. However, the catalyst supported on titanium oxide proved to be more stable and catalyst supported on molybdenum oxide showed less stability, but their activity in ORR was impressive, particularly the untreated PtRu/MoO_2 catalyst.

5. CHARACTERIZATION OF PtSn ELECTROCATALYST

This section presents physical and chemical characterization of PtSn electrocatalyst supported on MWCNT and metal oxides and the results are compared to commercial Pt/C and PtSn/C electrocatalysts. The results start off with physical characterization which is followed directly by electrochemical characterization.

5.1 PHYSICAL CHARACTERIZATION OF PtSn CATALYST

Physical characterization of the supported PtSn binary electrocatalyst was done using powerful techniques such as XRD, HRTEM, HRSEM and EDS as detailed in chapter three.

5.1.1 Particle Size and Crystallinity Study of the Supported PtSn Catalyst

The crystallinity, particle size, degree of alloying and lattice spacing of the Pt based electro-catalyst was determined using XRD, following the procedure given in section 3.2.1.1. Figure 5.1 and 5.2 shows the XRD patterns of PtSn electrocatalyst supported on MWCNTs and metal oxides respectively. The average particle size values are presented in Table 5.1 and 5.2 for PtSn electrocatalyst supported on MWCNTs and metal oxides respectively. Commercial Pt/C and PtSn/C were also characterized and used as baseline for comparison purposes.

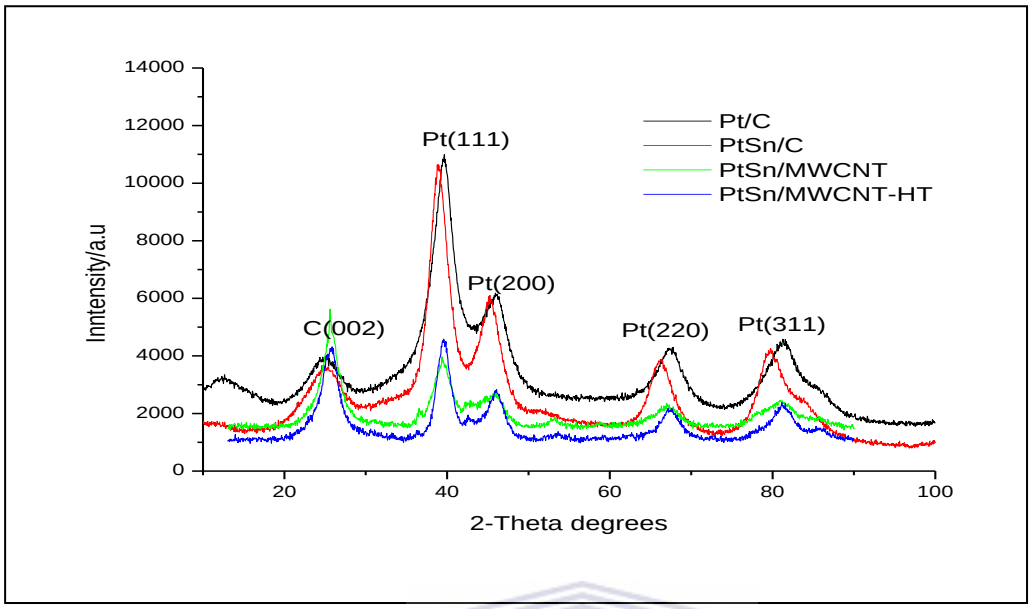

Figure 5.1: *XRD patterns of Pt/C, PtSn/C, PtSn/MWCNT and PtSn/MWCNT-HT*

Catalyst	Particle size/nm	Lattice parameter (a_{fcc}) /nm
Pt/C	2.28	0.393
PtSn/C	3.25	0.399
PtSn/MWCNT	3.59	0.395
PtSn/MWCNT-HT	5.66	0.393

Table 5.1: *Summary of average particle size and lattice parameter for PtSn/MWCNT compared with Pt/C and PtSn/C commercial catalysts*

XRD patterns were conducted to observe the crystalline structure and to calculate the average particle size and lattice parameter of PtSn/C, PtSn/MWCNT and PtSn/MWCNT-HT. Figure 5.1 presents the XRD patterns of the carbon supported electrocatalyst. The peak at 2θ around 25^{o} in all samples is attributed to the hexagonal structure of the carbon support. All samples display four diffraction peaks of Pt (111), Pt (200), Pt (220) and Pt (311) at the corresponding diffraction positions, indicating that the catalysts have prevailed the fcc structure of crystalline Pt. The diffraction peaks of the as prepared samples were quite broadened indicating a somewhat amorphous structure for the samples. It should be noted that these peaks corresponding to the fcc structure of platinum for the binary electro-catalyst were slightly shifted to lower 2θ values revealing the formation of an alloy caused by incorporation of Sn into the fcc lattice of platinum. These results are similar with the findings by Han *et.al* [124] and Zhu *et.al* [123] who reported that the presence of Sn into the platinum shifts the 2θ

values to lower angles. No peaks corresponding to the SnO_2 phase were detected in all binary catalysts. Nevertheless, their presence cannot be discarded as they may be present in very small amounts or in an amorphous form. EDS analysis results has shown the content of Sn in all binary electro-catalyst however, the amount of Sn is very small, hence it was not detected by XRD.

The average particle size and lattice parameter were calculated following equation 4.1 and 4.2 given in chapter 4 and were collected and presented in Table 5.1 above. The average particle size value for the commercial PtSn/C and the as prepared PtSn/MWCNT was close, and upon heating the particle size increased as expected from literature, that heat treatment increases particle size and improves alloying. The lattice parameters for commercial PtSn/C and as prepared PtSn/MWCNT electrocatalysts are slightly higher than the Pt/C commercial catalyst. This shows that the addition of Sn increases the lattice parameter, indicating a Pt and Sn alloy to some extent. These findings are consistent with the report by Jehabharathi *et al*. and [23] Neto *et al*. [123]. It can be expected therefore, that as the lattice parameter increases the Pt-Pt distance also increases. This is different to the Pt-M system (M= first transition elements), where the lattice parameter is reported decreasing. Being a p block element, Sn atom is expected to be more compared to the transition metals and, hence, increase the Pt-Pt distance [23, 85]. It was observed that for the PtSn/MWCNT-HT the lattice parameter decreased and the value was the same as that obtained for the bulk Pt/C catalyst. It was also observed that after heat treatment the diffraction peaks shifted slightly to higher 2θ values for PtSn/MWCNT-HT and this may be as a result of a decrease in the Sn metal loading, resulting from the heat treatment effect. This was confirmed by EDS analysis, that after heat treatment the Sn content was smaller than before heat treatment, hence, the contraction thereof in the lattice parameter [23, 85, 126-128].

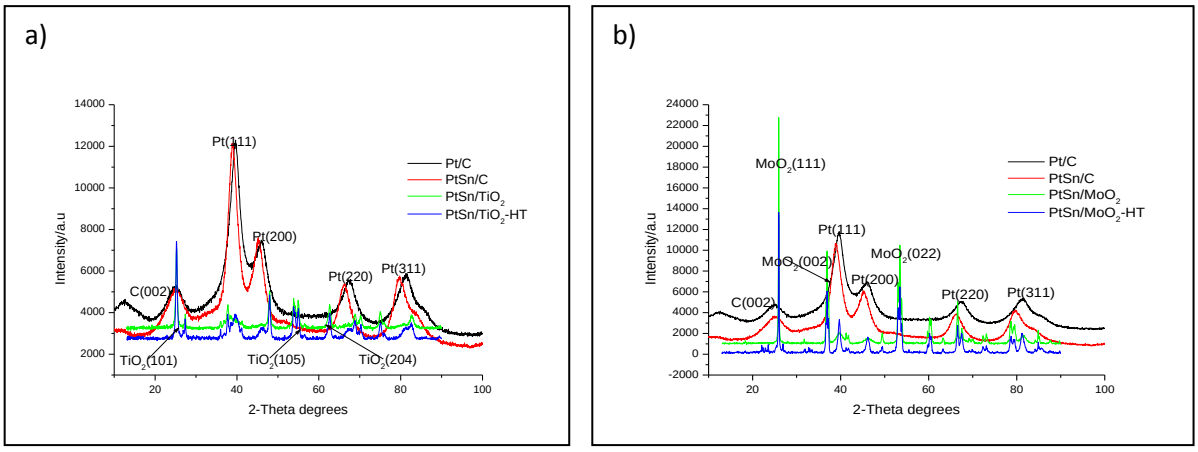

Figure 5.2: *XRD patterns of a) PtSn/TiO_2 and PtSn/TiO_2-HT and b) PtSn/MoO_2 and PtSn/MoO_2-HT*

Catalyst	Particle size/nm	Lattice parameter (a_{fcc})/nm
Pt/C	2.28	0.393
PtSn/C	3.25	0.399
PtSn/TiO_2	15.53	0.419
PtSn/TiO_2-HT	17.18	0.385
PtSn/MoO_2	19.35	0.397
PtSn/MoO_2-HT	24.98	0.397

Table 5.2: *Summary of average particle size and lattice parameter of the home-prepared PtSn supported on metal oxides compared with Pt/C and PtSn/C commercial catalyst obtained from XRD measurements*

Figure 5.2 above show XRD patterns of a) PtSn/TiO_2 and PtSn/TiO_2-HT and b) PtSn/MoO_2 and PtSn/MoO_2-HT as well as commercial Pt/C and PtSn/C electro-catalyst in both figures for reference purposes. The peaks at around 25^o in both figures is attributed to the diffraction at the (002), (010) and (111) plane of the carbon, titanium oxide and molybdenum oxide support respectively as they appear in the same position. All the reflections of the as prepared PtSn/TiO_2, PtSn/TiO_2-HT, PtSn/MoO_2 and PtSn/MoO_2-HT show the fcc structure of crystalline Pt. However, they are very much broad and the intensity is much weaker in comparison with the commercial catalyst revealing that they are more amorphous than the crystalline Pt/C and PtSn/C commercial catalyst. These diffraction peaks observed in all samples corresponded to the (111), (200), (220) and (311) of the fcc crystalline structure of platinum. The other peaks were assigned to the TiO_2 and MoO_2 phase of the oxide support and are indicated by the arrows in their respective figures. The particle size and lattice parameter was calculated and presented in Table 5.2 above. The average particle size for the

prepared PtRu supported on metal oxides was distinctly much bigger than the average particle size of the commercial catalysts. The carbon support material, being a high surface area material, allows for dispersion of small particle size to be possible, while the anatase titania and molybdenum oxide are not high surface area oxides, especially the molybdenum oxide, which could be attributed to the bigger particle size of the catalyst supported on these materials. This is because there is not enough room for nanoparticles to be well-dispersed on the support material, and as a result, they tend to cluster together, resulting in bigger particle sizes. The increase in the average particle size was observed as was expected for all home-prepared catalyst after heat treatment, because heat treatment results in particle size growth and this is also confirmed from literature. The a_{fcc} value for the as prepared $PtSn/TiO_2$ was notably much higher than that of the commercial PtSn/C (Table 5.2), indicating more alloying of Sn with Pt, since the addition of Sn into the platinum lattice is known to increase the lattice parameter, pointing to an increase in the Pt-Pt distance thereof. After heat treatment the lattice parameter decreased to a lower value, lower than the commercial Pt/C. This observation was also observed in the heat treated sample of PtSn/MWCNT, indicating that heat treatment has an effect on the Sn element. However, it should be stressed that the EDS analysis results revealed Sn content even after heat treatment. Nevertheless, it was in much smaller amounts. For $PtSn/MoO_2$ samples, the lattice parameter for the prepared catalyst interestingly did not decrease after heat treatment as was the case for the heat-treated PtSn/MWCNT and $PtSn/TiO_2$ samples. The lattice parameter was found to be 0.397 nm as shown in Table 5.2, indicating the formation of an alloy catalyst even after heat treatment, and the fact that heat treatment had no effect on the lattice spacing for the electro-catalysts supported on molybdenum oxide [121,124,130].

5.1.2 Particle Size and Size Distribution

Metal particle size and size distribution do play important roles in catalytic efficiency due to the relationship between catalytic activity and surface structure. These properties are best studied using fundamental characterization tools such as HRTEM. The average particle size is presented in Table 5.3 and 5.4 for the PtSn supported on MWCNTs and metal oxides respectively. Figure 5.3 and 5.4 show HRTEM images of the PtSn electrocatalyst supported on MWCNT and metal oxides respectively.

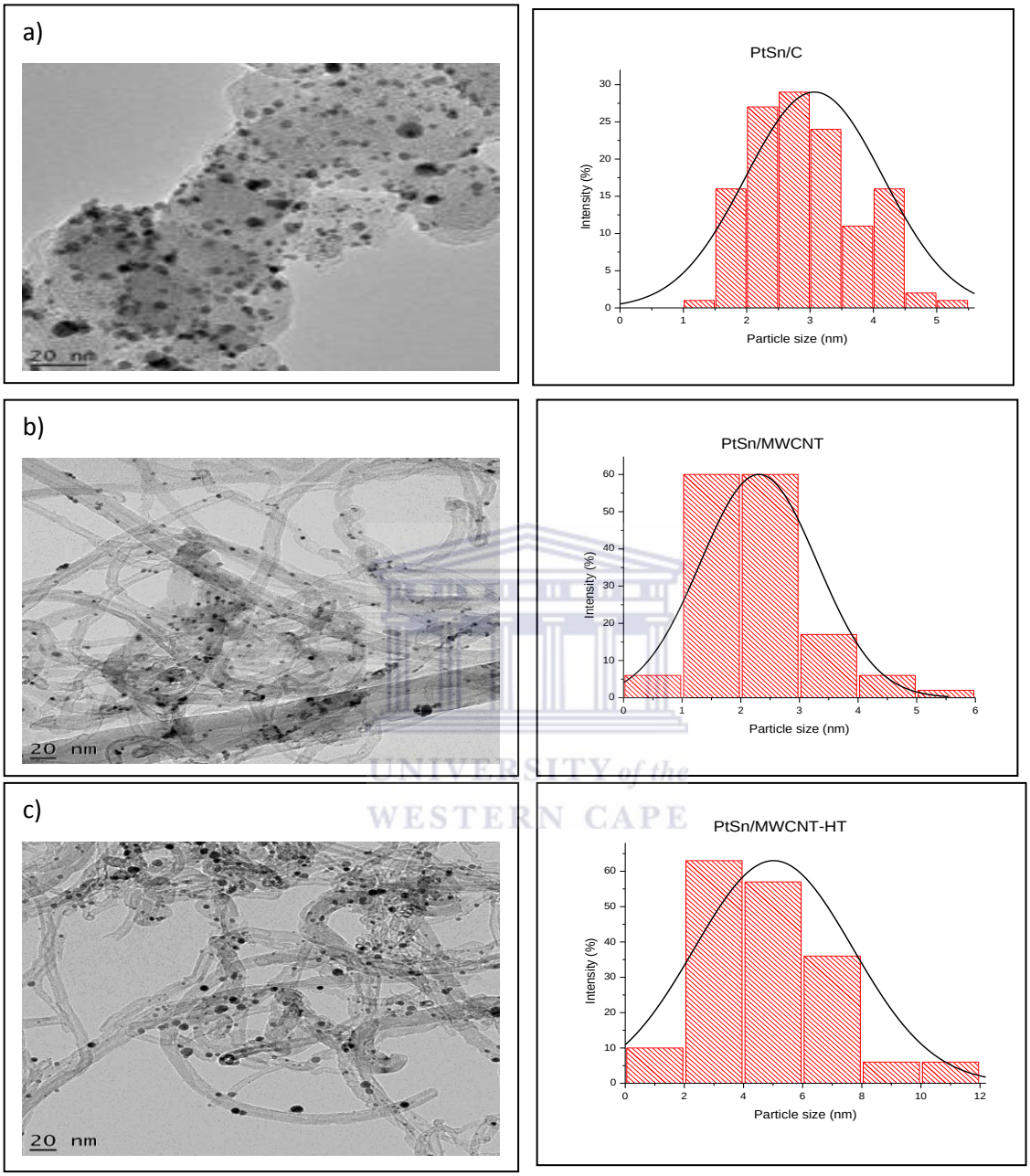

Figure 5.3: *HRTEM images of a) PtSn/C, b) PtSn/MWCNT and c) PtSn/MWCNT-HT with their respective histograms*

Catalyst	Particle size/nm
PtSn/C	3.07
PtSn/MWCNT	2.31
PtSn/MWCNT-HT	5.02

Table 5.3: *HRTEM average particle size of PtSn/MWCNT and PtSn/C estimated from 100 particles in random regions*

Figure 5.3 above presents the HRTEM micrographs of the commercial PtSn/C and the home-prepared PtSn/MWCNT and PtSn/MWCNT-HT samples with their respective histograms. Metal nanoparticles were observed to be uniformly dispersed on the carbon support for the PtSn/C commercial catalyst. For the prepared PtSn/MWCNT and PtSn/MWCNT-HT the TEM images show metal particles with very small diameter dispersed on the MWCNTs support. A little aggregation and non-uniformity was observed in the as prepared samples. The particle size estimated from 100 particles selected randomly is presented in Table 5.3 above [23, 85, 126-128].

For the commercial PtSn/C catalyst the average particle size of 3.07 nm which is very close to the average particle size obtained from XRD measurements was accompanied by the particle size distribution between 3.07 and 7.3 nm as shown in the histogram above. The average particle size shows an increase on the heat treated catalyst for PtSn/MWCNT as expected for heat treated samples to show particle size growth. The relative wide particle size distribution shown in their respective histograms (Figure 5.3 above) shows size distribution between 2.3 and 7.1 nm and 5.0 and 17.5 nm for PtSn/MWCNT and PtSn/MWCNT-HT electrocatalysts respectively.

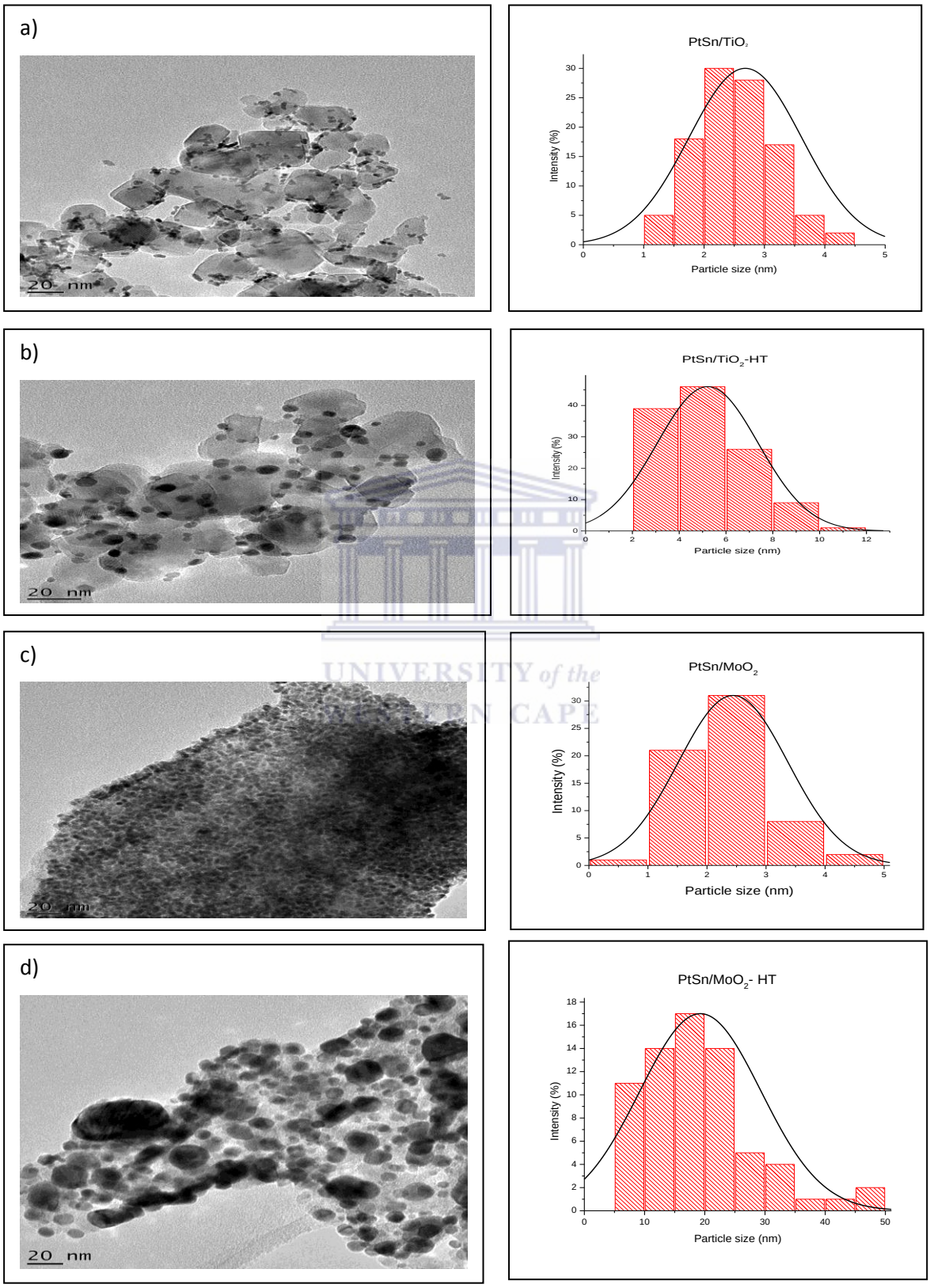

Figure 5.4: *HRTEM images of a) PtSn/TiO_2, b) PtSn/TiO_2-HT, c) PtSn/MoO_2 and PtSn/MoO_2-HT with their respective histograms*

Figure 5.4 presents HRTEM micrographs of the as prepared PtSn electrocatalysts supported on metal oxides with their respective histograms. The metal particles are dispersed on the surface of titanium oxide support non-homogeneously with small agglomerates on some parts of the sample and poor size distribution. It was observed that after heat treatment the dispersion of the metal particles on the titanium oxide support improved and an increase in size of the particles was also observed as was expected, owing to the effect of heat treatment. For $PtSn/MoO_2$ HRTEM images, it was observed that almost all nanoparticles deposited uniformly with small diameter on the molybdenum oxide and almost all molybdenum oxide was decorated with nanoparticles with little aggregation observed on some parts of the sample. However, a structure change was observed for the heat-treated $PtSn/MoO_2$, with a huge particle size growth, an indication that heat treatment at higher temperatures has an effect on the molybdenum oxide support and that, accordingly, the electro-catalyst supported on this material. The average particle size obtained from 100 particles is presented in Table 5.4 and the particle size distribution is shown in their respective histograms in Figure 5.4

Catalyst	**Particle size/nm**
$PtSn/TiO_2$	2.68
$PtSn/TiO_2$-HT	5.22
$PtSn/MoO_2$	2.44
$PtSn/MoO_2$-HT	19.28

Table 5.4: *HRTEM average particle size estimated from 100 particles in random regions of PtSn/metal oxides*

All prepared supported electro-catalyst experienced a particle size growth after heat treatment, the growth was more pronounced for the heat-treated $PtSn/MoO_2$ electro-catalyst as was also observed in the HRTEM micrographs. It should be noted that the average particle size for the prepared electro-catalyst was distinctly smaller compared to the average particle size obtained from XRD measurements. The techniques seem to give extremely different results for the electro-catalyst supported on metal oxides, but for the MWCNT one could say they are in good agreement within margin of error of course. The relatively wide particle size distribution was between 2.68 and 6.07 nm for the $PtSn/TiO_2$ and nm and 5.02 and 16.09 nm for the $PtSn/TiO_2$-HT. The histograms shown above for $PtSn/MoO_2$ and $PtSn/MoO_2$-HT show relative wide particle size distribution between 2.44 and 6.55 nm and 19.2 and 55 nm for $PtSn/MoO_2$ and $PtSn/MoO_2$-HT respectively [121, 124, and 130].

5.1.3 Surface Morphology and Elemental Analysis of PtSn Catalyst

Morphology and elemental analysis of PtSn electro-catalyst supported on MWCNTs and metal oxides was conducted using HRSEM and EDS, following the procedure outlined in chapter 3 Section 3.2.3.1. Figure 5.5 and 5.6 presents HRSEM micrographs while Table 5.5 and 5.6 presents the elemental analysis of PtSn electro-catalyst supported on MWCNTs and metal oxides respectively.

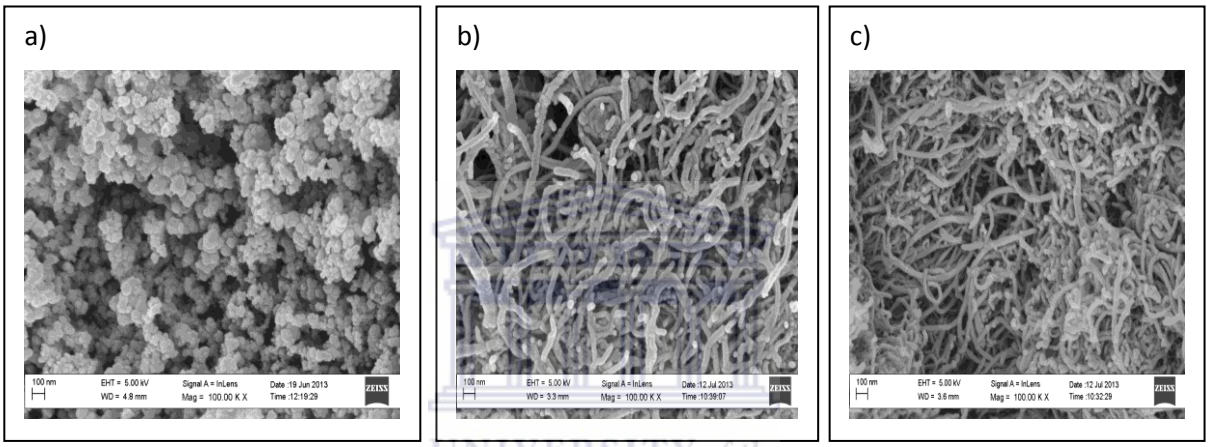

Figure 5.5*: HRSEM images of a) PtSn/C, b) PtSn/MWCNT and c) PtSn/MWCNT-HT*

Catalyst	**EDS wt.%**	
	Pt	**Sn**
PtSn/C	14.2	1.5
PtSn/MWCNT	14.09	1.18
PtSn/MWCNT-HT	13.89	0.9

Table 5.5*: EDS elemental analysis results of PtSn/MWCNT compared with PtSn/C commercial catalyst*

The HRSEM images of the PtSn electrocatalyst supported on MWCNT are presented in Figure 5.5 above together with PtSn/C commercial catalyst and all images show metal particles dispersed on the support material. The metal loading for the supported binary

catalyst was conducted using EDS and presented in Table 5.5. The loading for the as prepared catalyst was close to the commercial PtSn/C catalyst. It was observed that after heat treatment the loading decreased especially the Sn content and the effect of the decrease in metal loading was seen in the XRD results [23, 85, 126-128].

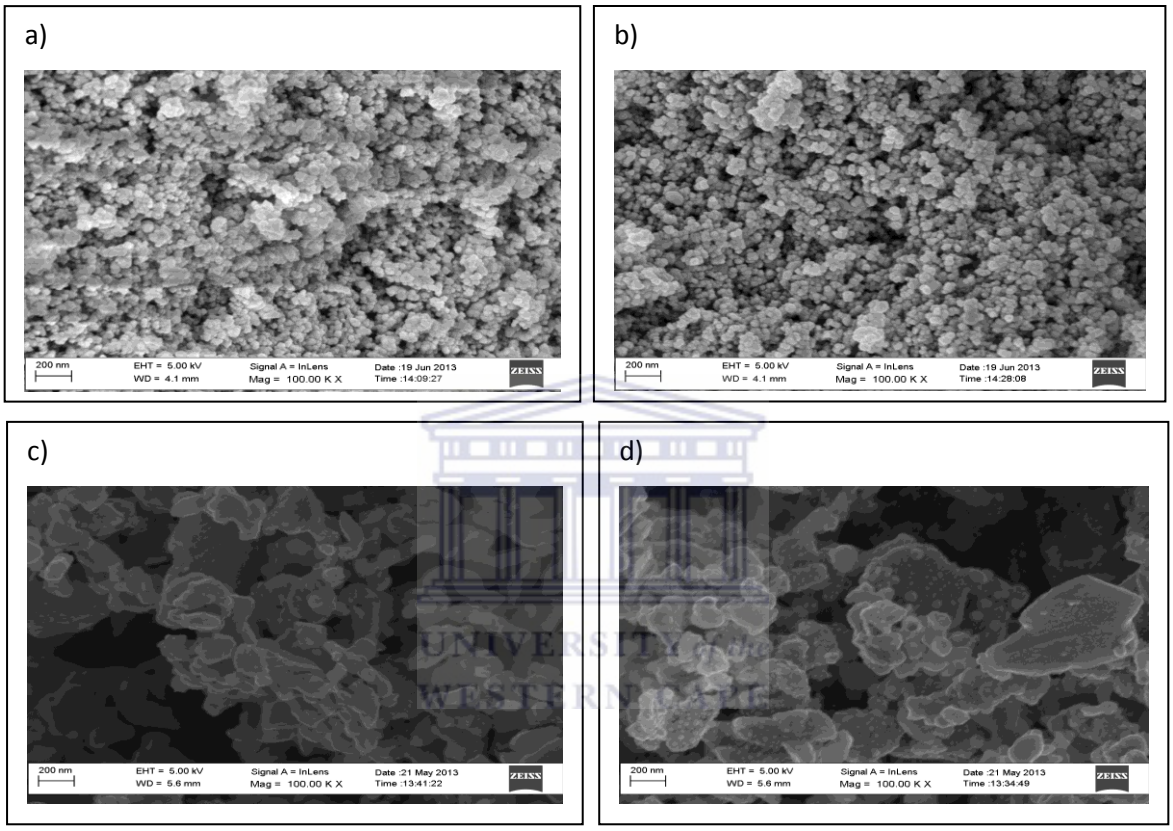

***Figure 5.6**: HRSEM images of a) PtSn/TiO_2, b) PtSn/TiO_2-HT, c) PtSn/MoO_2 and PtSn/MoO_2-HT*

Figure 5.6 display HRSEM images of the home-prepared PtSn electrocatalyst supported on metal oxides. All samples show metal particles dispersed on the support. The metal loading for the supported electrocatalyst is presented in Table 5.6. The metal loading for PtRu/TiO_2 decreased after heat treatment, as was the case with PtSn/MWCNT. Both supported catalyst experienced a major decrease in the Sn content. It was different, however, for the PtSn electro-catalyst supported on molybdenum oxide, as the metal loading increased after heat treatment as was also observed for the PtRu supported on MoO_2. Heat treatment seems to have a different effect on electro-catalyst supported on the molybdenum oxide and this is credited to the characteristics of the molybdenum oxide support [121, 124, and 130].

Catalyst	EDS wt.%	
	Pt	**Sn**
PtSn/C	14.2	1.5
PtSn/TiO_2	14.0	1.56
PtSn/TiO_2-HT	11.93	1.2
PtSn/MoO_2	15.02	2.2
PtSn/MoO_2-HT	16.25	3.07

Table 5.6: *EDS elemental analysis of PtSn/metal oxides compared with PtSn/C electrocatalyst*

5.2 ELECTROCHEMICAL CHARACTERIZATION OF SUPPORTED PtSn ELECTROCATALYST

It is generally accepted that the ECSA, mass activity (MA), and specific activity (SA) are the true measures of the catalyst catalytic activity [111]. This section is dedicated on presenting results obtained from RDE measurements for the supported PtSn electrocatalyst. The results start off with the cyclic voltammograms (CVs) to examine the electro-active surface area and durability of the catalysts, followed directly by the examination of their mass-area and specific-area activity for ORR and MOR using LSV polarization curves.

5.2.1 Examination of ECSA Before and After Durability Studies

Figure 5.7 and 5.8 presents RDE cyclic voltammograms of the as prepared PtSn electro-catalyst supported on MWCNTs and metal oxides respectively, with their ECSA numerical values presented in Table 5.7 and 5.8 respectively.

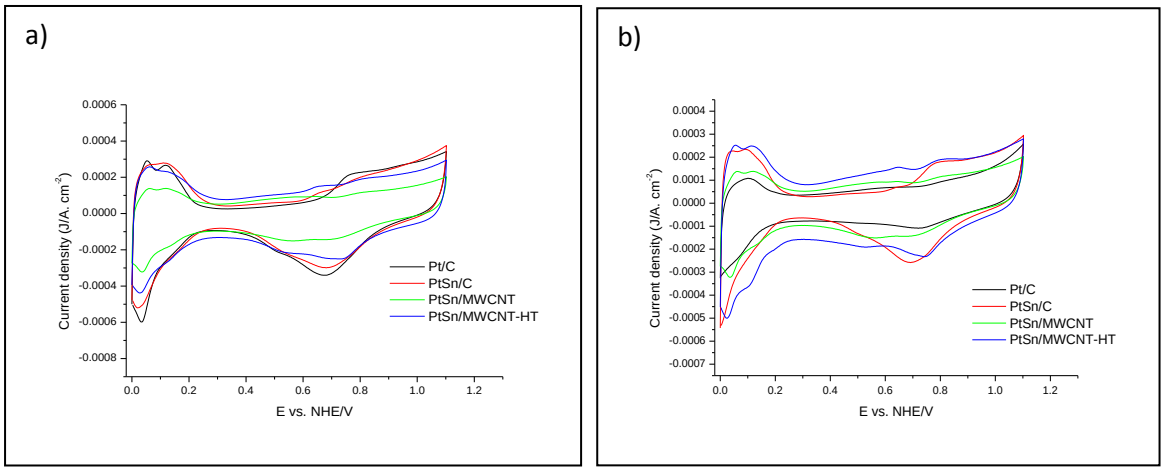

Figure 5.7: *RDE-CV of home-prepared PtSn/MWCNT compared with Pt/C and PtSn/C commercial catalysts in N_2-saturated 0.1M $HClO_4$ @ 20mV/s a) pre-durability and b) post-durability studies.*

Catalyst	Particle size/nm		ECSA pre-DT/$m^2.g^{-1}$ Pt	ECSA post-DT/$m^2.g^{-1}$ Pt	% ECSA loss
	XRD	HRTEM			
Pt/C	2.28	1.28	45.7	16.6	64
PtSn/C	3.25	3.03	50.0	33.96	32
PtSn/MWCNT	3.59	2.31	17.6	17.01	3
PtSn/MWCNT-HT	5.66	5.02	34.8	34.69	0.3

Table 5.7: *Summary of catalyst particle size and ECSA pre-durability and post-durability studies for PtSn/MWCNT compared with Pt/C and PtSn/C commercial electrocatalysts*

Electrochemical activities of PtSn supported on MWCNT compared with the commercial Pt/C and PtSn/C electrocatalyst in an N_2-saturated 0.1M $HClO_4$ by cyclic voltammetry are presented in Figure 5.7 a) before and b) after durability studies. The CV sweep rate was set at 20mV/s and the potential range was within -0.2 and 0.9 V vs. Ag/AgCl and all potentials were converted to the normal hydrogen electrode (NHE) scale and presented as such throughout this study unless otherwise stated. All CVs displayed three regions: 1) adsorption-desorption of hydrogen (0-0.2 V vs. NHE); 2) double layer formation (0.2-0.4 V vs. NHE);

and 3) oxidation-reduction of Pt (0.4-0.8 V vs. NHE). The addition of secondary metal Sn in the PtSn electrocatalyst showed very little or no effect on the CV response both for the home-prepared and commercial PtSn catalysts which is different compared to the PtRu samples. Figure 5.6 b) shows CVs obtained after durability studies. It is observed that the voltammograms exhibited the typical behaviour of Pt in acid solution in the hydrogen, double layer, and oxide regions. A decrease in the current in all regions for all samples is observed after durability studies [23, 126-128].

The electrochemical surface area of the catalyst which is an important measure of the number of electrochemically active sites per gram of catalyst was calculated following equation 4.3 for the catalysts before and after durability studies and the numerical values are detailed in Table 5.7 above. From the ECSA values it is clear that the commercial catalysts are more active than the home-prepared catalyst with PtSn/C being the most active catalyst. However, after durability studies both commercial catalysts lost high percentage of their ECSA and this is credited to an increase in Pt nanoparticle size and to the instability of the carbon black support under fuel cell conditions, as the carbon support undergoes oxidation, resulting in the dissolution of Pt nanoparticles from the support. All these factors cause a decline in the activity of the electro-catalyst. It is worth noting that when Pt is alloyed in the PtSn/C, the ECSA loss is 32% (which is about 50% less) compared to the mono-metallic Pt which lost 64 %, indicating that alloying Pt with a secondary metal forming binary catalysts not only improves activity of the catalyst but it also improves the stability of the catalyst. It was observed that the home-prepared catalyst showed higher stability than the commercial catalyst and is credited to the MWCNT support material as it is more stable than carbon black, thus, electro-catalyst supported on MWCNT showed more stability. It was also noted that, upon heat treatment, the activity of the catalyst improved greatly and this is credited with the high degree of alloying, uniform dispersion and stable distribution of the metal on the support resulting from heat treatment and this accordingly improves the electro-catalytic activity of the synthesized catalyst. Not only did heat treatment improve the activity of the catalyst but it also improved the stability as well, as it can be seen from Table 5.7 and Figure 5.7. Even though the as prepared catalysts were less active than the commercial catalyst, they showed higher stability specifically the heat treated sample which is favourable for fuel cell applications as their ability to retain their activity even after long cycles would result in long life-time for the fuel cell catalyst and accordingly the fuel cell system [23, 85, 126-128].

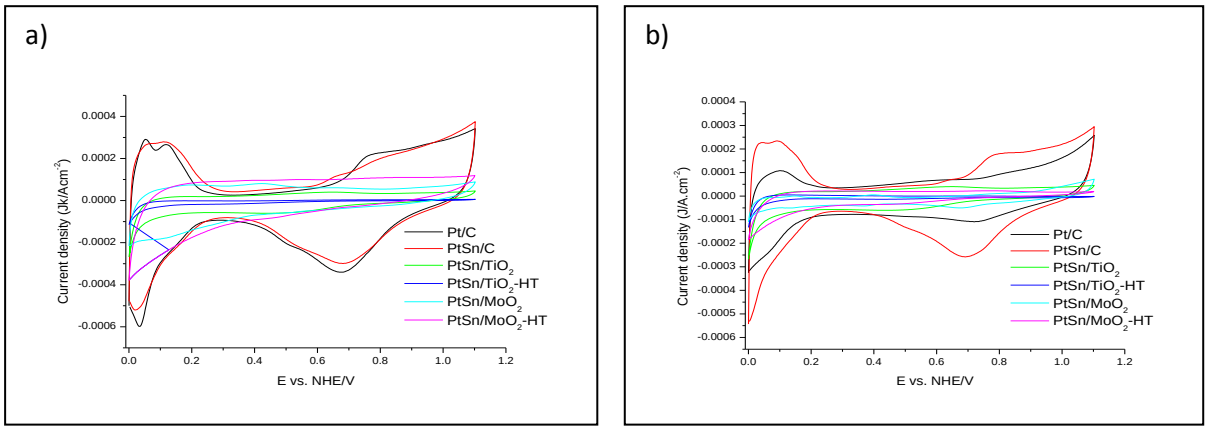

Figure 5.8: *RDE-CV of the home-prepared PtSn supported on metal oxides compared with Pt/C and PtSn/C commercial catalysts in N2-saturated 0.1M HClO4 @ 20mv/s a) pre-durability and b) post-durability studies.*

Catalyst	**Particle size/nm**		**ECSA pre-DT/$m^2.g^{-1}$**	**ECSA post-DT/ $m^2.g^{-1}$**	**% ECSA loss**
	XRD	**HRTEM**			
Pt/C	2.28	1.28	45.7	16.6	64
PtSn/C	3.25	3.03	50.0	33.96	32
$PtSn/TiO_2$	15.53	2.68	1.85	1.48	19
$PtSn/TiO_2$-HT	17.18	5.22	1.47	0.94	36
$PtSn/MoO_2$	19.35	2.44	11.9	7.91	33
$PtSn/MoO_2$-HT	24.98	19.28	6.4	2.09	67

Table 5.8*: Summary of average particle size for PtSn supported on TiO_2 and MoO_2 and their ECSA values of pre-durability and post-durability studies compared with Pt/C and PtSn/C commercial catalysts*

Figure 5.8 shows cyclic voltammograms of PtSn supported on metal oxide and compared to the commercial Pt/C and PtSn/C before and after durability studies in N_2-saturated 0.1M $HClO_4$. The CV sweep rate was set at 20mV/s and the potential range was within -0.2 and 0.9 V vs. Ag/AgCl. The PtSn supported on metal oxide CVs is suppressed by the commercial

catalysts as they are more active than the home-prepared PtSn supported on metal oxide. The ECSA was calculated and results are detailed in Table 5.8 above. PtSn supported on anatase titania shows less activity in comparison with the PtSn supported on molybdenum oxide. This was also observed for the PtRu supported on the same material, an indication that anatase titanium is not suitable to be employed as a support material for electro-catalyst as it shows low surface area and low electron conductivity to facilitate in the electron transfer during the reaction, and therefore, results in low activity on electro-catalyst supported on the material. Molybdenum oxide shows to be a promising support material, because of its relative high electron conductivity, even though it's a low surface area oxide. The heat-treated PtSn/MoO_2 shows less stability as it lost a high percentage of its ECSA, even higher than the % lost by Pt/C catalyst. The high loss can be attributed to the bigger particle size of the heat treated catalyst which resulted in the electro-catalyst falling off from the support material and consequently leading to a decline in the ECSA of the catalyst [130].

5.2.2 Studying the Activity of Catalyst in ORR and MOR

Figure 5.9 and 5.10 presents the ORR and MOR polarization curves of PtSn supported on MWCNT and metal oxide respectively compared with commercial Pt/C and PtRu/C. Table 5.9 and 5.10 presents the MA and SA for the ORR and MOR of PtRu supported on MWCNT and metal oxide respectively.

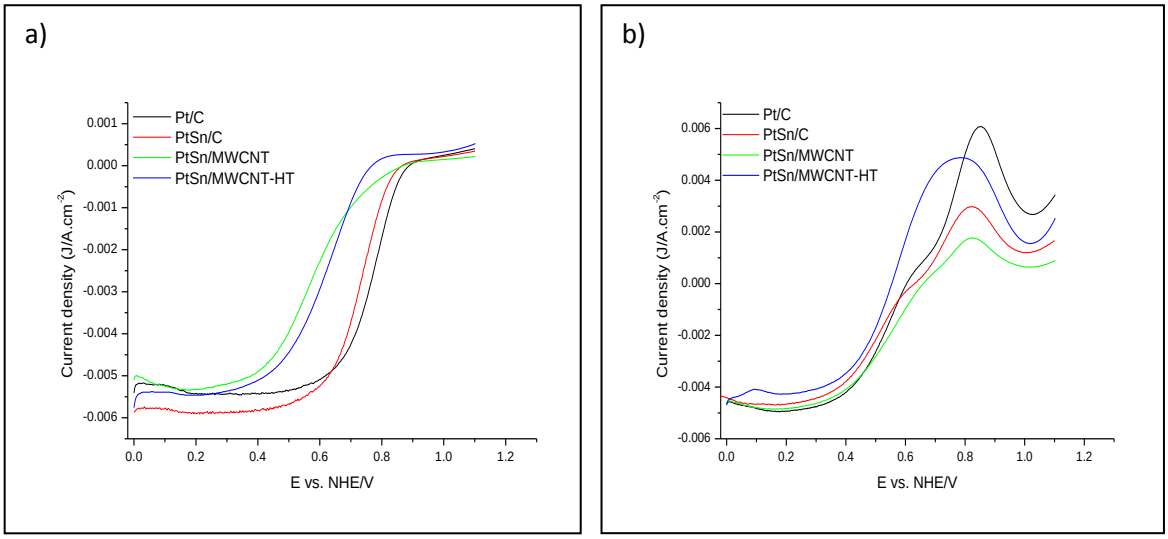

***Figure 5.9**: a) ORR polarization curves in O_2-saturated 0.1M $HClO_4$ and b) MOR polarization curves in 0.1M $HClO_4$+1M CH_3OH of PtSn/MWCNT compared with Pt/C and PtSn/C commercial catalysts @ 1600rpm at a scan rate of 20mV/s*

		ORR catalytic activity @ 0.9 V		MOR catalytic activity @ 0.9 V	
Catalyst	**ECSA/$m^2.g^{-1}$**	**MA/ $mA.mg^{-1}$**	**SA/ $mA.cm^{-2}$**	**MA/$mA.mg^{-1}$**	**SA/ $mA.cm^{-2}$**
Pt/C	45.7	85.85	0.188	-122.6	-268
PtSn/C	50.0	442.6	0.886	24.0×10^3	48.12
PtSn/MWCNT	17.6	2.7×10^3	15.40	8.1×10^3	69.1
PtSn/MWCNT-HT	34.77	1.4×10^3	4.12	-6.5×105	-1.9×10^3

***Table 5.9:** Studying the activity of PtSn/MWCNT towards ORR and the tolerance to methanol (MOR) and compared with commercial Pt/C and PtSn/C catalysts*

The ORR polarization curves were obtained in an O_2-saturated 0.1M $HClO_4$ while the MOR curves were obtained in an O_2-saturated 0.1M $HClO_4$ +1M CH_3OH solution using RDE. The LSV sweep rate was set at 20mV/s using the anodic sweep and the potential range was within -0.2 and 0.9 V vs. Ag/AgCl and the scans were taken at a rotation rate of 1600 rpm. All curves for ORR {Figure 5.9 a)} display the typical polarization behaviour for the electrochemical reduction of molecular oxygen. The ORR is under mixed kinetic-diffusion control in the potential range between 0.9 and 0.6 V, followed by a region where diffusion limiting current can be observed. The ORR and MOR mass and specific activities were calculated following equation 4.8-4.10 and are presented in Table 5.9 above. It is clear from the above Table that alloying Pt with a second metal improves both mass and specific activity. The as prepared catalyst for ORR showed a higher mass and specific activity. The decrease in MA and SA after heat treatment could be attributed to the increase in size of the alloyed nanoparticles. Thus, they follow the expected trend of increasing mass activity with decreasing particle size and as the surface area decreases the SA generally increases. Therefore, the effect of particle size in mass activity was observed for the as prepared catalyst for ORR. The commercial PtSn/C and the as prepared PtSn/MWCNT both showed a higher mass and specific activity in the presence of methanol indicating that they are methanol tolerant oxygen reduction catalysts. For the commercial Pt/C and PtSn/MWCNT-HT catalysts, the mass and specific activity in the presence of methanol decreased to negative values. This could be a result of the intolerance of the catalyst to COads-like species which poisons the catalyst by blocking the active site of the catalyst resulting in poor performance, and hence, a decrease in mass and specific activity of the catalyst. This was also shown in the EDS analysis results that the Sn content was low for the heat-treated PtSn/MWCNT. The loss of Sn during heat-treatment may be a result of the low activity of the catalyst in methanol containing electrolytes, since Sn would assist in promoting the poisonous intermediates and thus increase the number of available sites for oxygen reduction. The low loading of Sn in the heat-treated sample also resulted in the similar electro-chemical behaviour to the commercial Pt/C. The performance of PtSn/C and PtSn/MWCNT towards ORR in pure oxygen electrolytes and in the presence of methanol is very promising, an indication that they are methanol tolerant oxygen reduction catalysts. These findings are consistent with the findings by Jeyabharathi *et.al* [23] who reported that PtSn/C showed high methanol tolerance than Pt/C catalyst in the cathode of a direct methanol fuel cell.

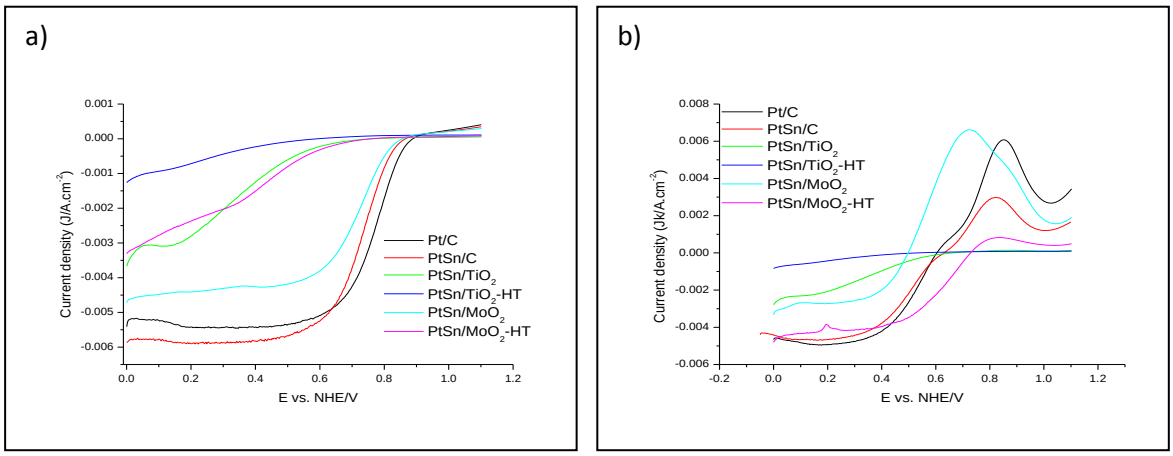

***Figure 5.10**: a) ORR polarization curves in O_2-saturated 0.1M $HClO_4$ and b) MOR polarization curves in 0.1M $HClO_4$+1M CH_3OH of PtSn supported on metal oxides compared with commercial Pt/C and PtSn/C commercial catalysts taken @ 1600rpm at a scan rate of 20mV/s*

		ORR catalytic activity @ 0.9 V		MOR catalytic activity @ 0.9 V	
Catalyst	**ECSA/$m^2.g^{-1}$**	**MA/mA.mg^{-1}**	**SA/mA.cm^{-2}**	**MA/mA.mg^{-1}**	**SA/mA.cm^{-2}**
Pt/C	45.7	85.85	0.188	-122.6	-268
PtSn/C	50.0	442.6	0.886	24×10^3	48.12
PtSn/TiO_2	1.85	182	9.84	745.6	40
PtSn/TiO_2-HT	1.47	895	60.88	5000	3.4×10^5
PtSn/MoO_2	11.9	465	4.16	11×10^3	101
PtSn/MoO_2-HT	6.4	211.7	3.31	834	13.0

***Table 5.10:** Studying the activity of PtSn/metal oxides towards ORR and tolerance of the catalyst to methanol and comparing with Pt/C and PtSn/C commercial electrocatalysts*

The ORR polarization curves were obtained in an O_2-saturated 0.1M $HClO_4$ while the MOR curves were obtained in an O_2-saturated 0.1M $HClO_4$ +1M CH_3OH solution using RDE. The LSV sweep rate was set at 20mV/s and the potential range was within -0.2 and 0.9 V vs.

Ag/AgCl and the scans were taken at a rotation rate of 1600 rpm using the anodic sweep. The mass and specific activities calculated using equation 4.8-4.10 is presented in Table 5.10 above. Figure 5.10 a) shows that the PtSn/MoO_2 displayed better activity towards ORR than the rest of PtSn supported on metal oxide. It could be argued that it had a higher electro-active surface area compared to the other home-prepared PtSn supported on metal oxide. But, for MOR in Figure 5.10 b), the catalyst showed less activity while the heat-treated PtSn/MoO_2 showed higher activity of ORR in the presence of methanol, indicating that it is a methanol tolerant electro-catalyst. From Table 5.10, it is clear that all binary catalysts showed higher mass and specific activities in the presence of methanol, an indication that they are methanol tolerant and oxygen reduction catalysts [130].

General comments on Figure 5.11 and 5.12, which presents the ORR polarization curves taken at various rotation rate (left), Koutecky-Levich (K-L) plot obtained for different rotation speed at potential range between 0.60 and 0.62 V versus NHE (centre) and Tafel plots taken from the 1600 rpm rotation rate (right) for PtSn supported on MWCNT compared well with Pt/C and PtSn/C commercial electro-catalyst and PtSn electro-catalyst supported on metal oxides respectively. Various rotation rates were used to collect data for the K-L plot analysis as presented in the following figures below. Linear relationships with constant slopes for the as prepared PtSn supported on MWCNT and PtSn/MoO_2 was observed and it was similar to the commercial Pt/C and PtRu/C commercial electro-catalyst, confirming that oxygen reduction reaction follow the first order kinetics with respect to molecular oxygen. As for the heat-treated PtSn supported molybdenum oxide and on anatase titania the K-L plot, it is non-linear and non-parallel, revealing that the reaction did not follow the first order kinetics with respect to molecular oxygen. This is a clear indication that the reaction took the two electron transfer of producing hydrogen peroxide which is undesired in fuel cell reaction, as it a slow reaction and the produced H_2O_2 is also poisonous to the catalyst. The Tafel slope values for the electro-catalyst were calculated and presented in Table 5.11 below. The PtRu supported on MWCNT and MoO_2 the Tafel slope values were close to those of the commercial Pt/C and PtSn/C, suggesting that the ORR mechanism is similar to that of Pt/C [23, 85, 117-128].

Catalyst	Tafel slope/mV.dec^{-1}
Pt/C	-62.2
PtSn/C	-61.5
PtSn/MWCNT	-63.9
PtSn/MWCNT-HT	-60.5
PtSn/TiO_2	-62.4
PtSn/TiO_2-HT	-58.5
PtSn/MoO_2	-55
PtSn/MoO_2-HT	-57.3

Table 5.11: *Tafel slope values for the home-prepared PtSn electrocatalyst supported on MWCNT, TiO_2 and MoO_2 and compared with Pt/C and PtSn/C commercial electrocatalysts*

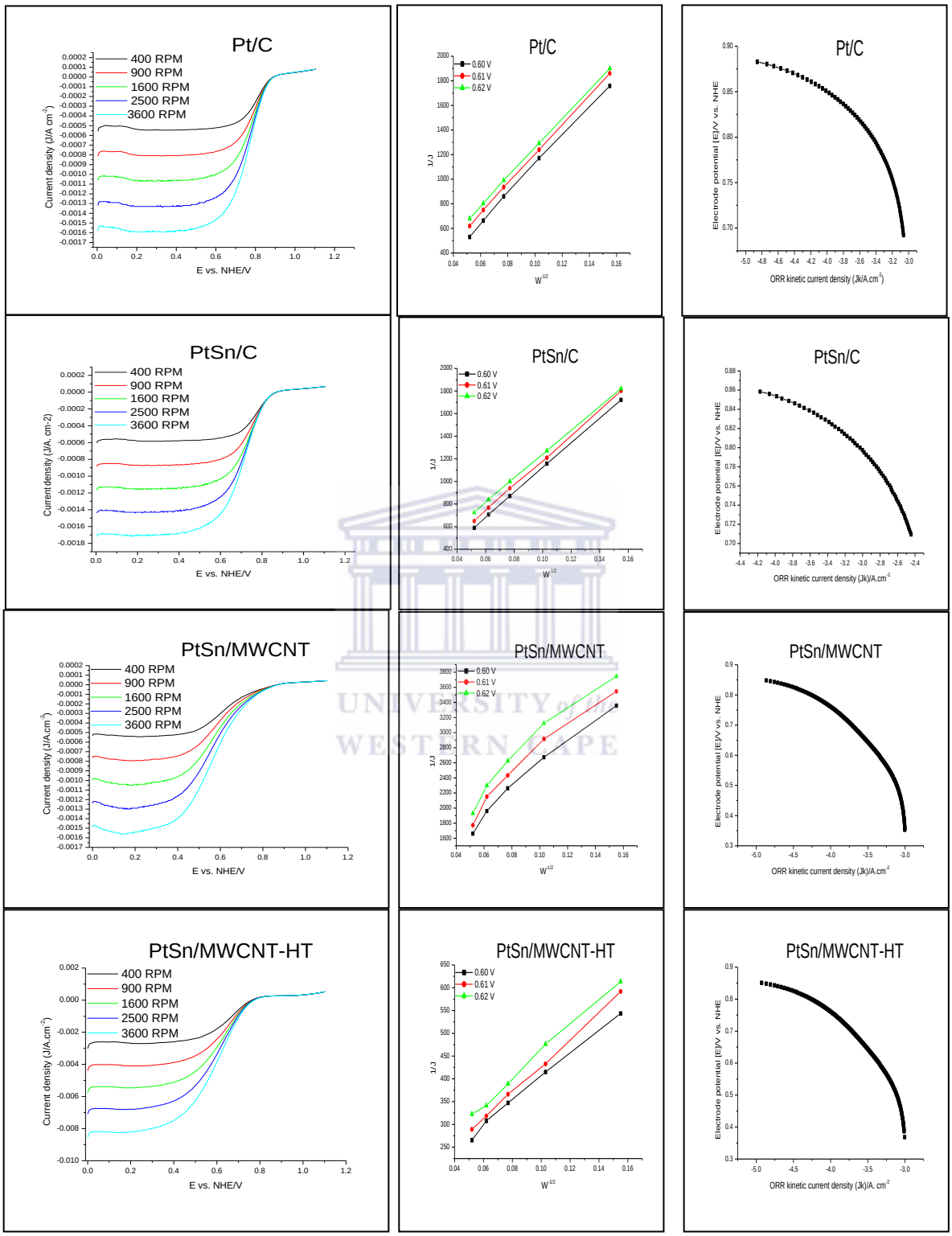

Figure 5.11: *(left) RDE data for Pt/C, PtSn/C, PtSn/MWCNT and PtSn/MWCNT-HT at various rotation rates in an O_2-saturated 0.1M $HClO_4$ at 20mV/s; (centre) Koutecky-Levich plots; (right) Tafel plots for each catalyst*

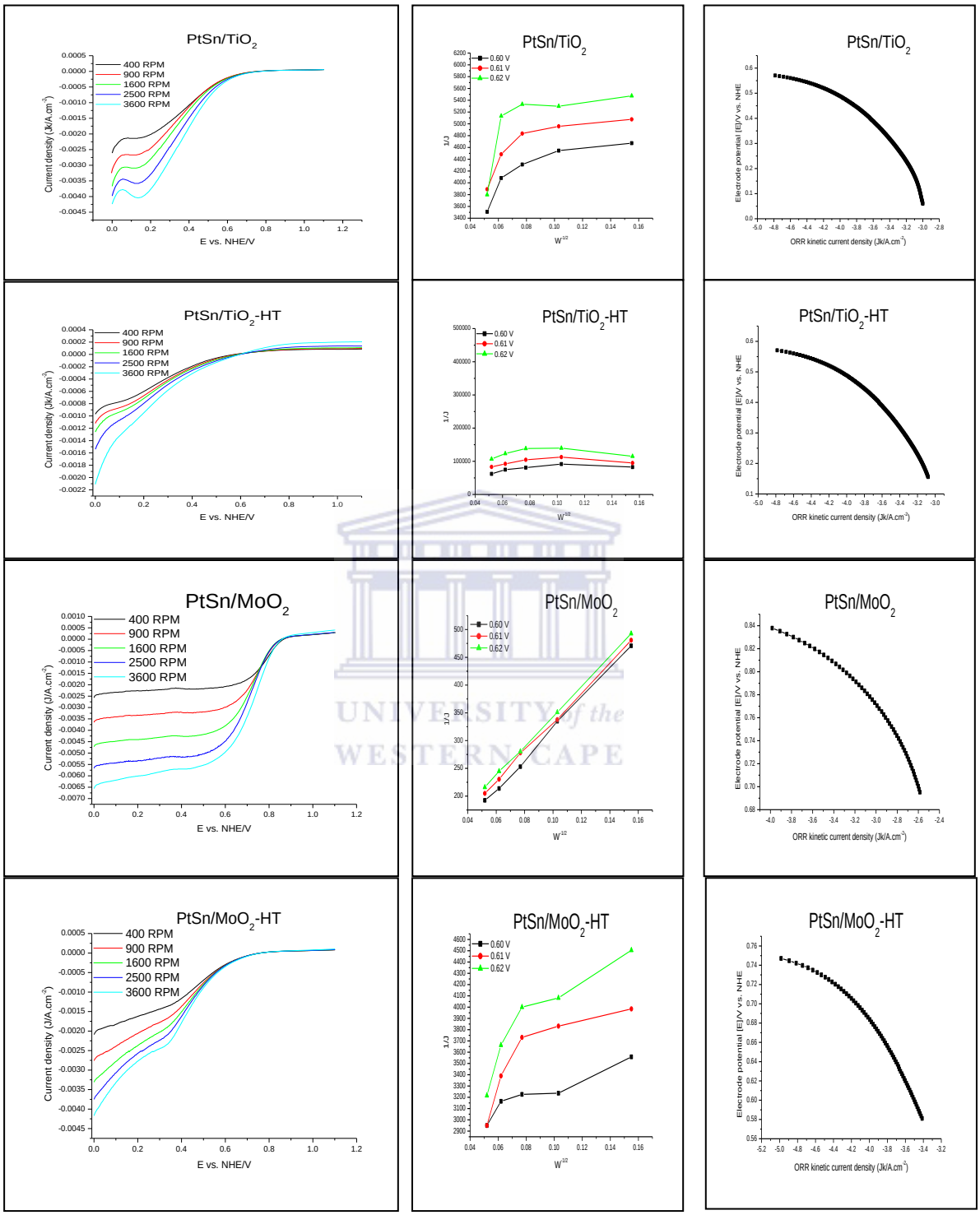

Figure 5.12: (*left) RDE data for PtSn supported on metal oxides at various rotation rates in an O_2-saturated 0.1M $HClO_4$ at a scan rate of 20mv/s; (centre) Koutecky-Levich plots; (right) Tafel plots for each electrocatalyst*

5.2.3 Summary

PtSn electro-catalyst was synthesized following the polyol method outlined in chapter 3 and supported on multi-walled carbon nanotubes, titanium oxide and molybdenum oxide. Part of the synthesized supported electro-catalyst was then subjected to heat treatment so as to improve alloying, stable distribution and uniform dispersion of the metal nanoparticles on the support material, with the overall result of improving the electro-chemical surface area of the resultant electro-catalyst. The supported electro-catalysts, both commercial and home-prepared, were then evaluated for their electro-catalytic properties. Physical characterization was done using powerful techniques such as XRD, HRTEM, HRSEM and EDS. For electro-chemical characterization RDE-CV and RDE-LSV was employed. Commercial catalysts used as baseline standards were Pt/C and PtSn/C.

It was observed that the performance of the electro-catalyst largely depends on structural properties of the catalyst metal, support material and the morphology of the electro-catalysts. PtSn/MWCNT-HT possesses higher performance in most areas than the rest of the home-prepared supported electro-catalyst and this could be certainly attributed to heat treatment because before heat treatment, the catalyst showed low electro-active surface area. However, the commercial PtSn/C was the most active electro-catalyst in all areas. Electro-catalyst supported on molybdenum oxide showed higher activity than catalyst supported on titanium oxide and this could be attributed to the fact that molybdenum oxide is more electron conductive than anatase titania. All home-prepared electro-catalyst generally showed to be more stable than the commercial catalyst supported on carbon black. This shows that carbon black is thermo-dynamically unstable, resulting in the degradation of catalyst supported on this material and accordingly in poor durability of the fuel cell system.

CHAPTER 6

CONCLUSION AND RECOMMENDATIONS

The objective of this study was to investigate the influence of the support material on the electro-catalyst whilst simultaneously determining the support material that will enhance the activity and durability of the binary PtRu and PtSn electro-catalyst to be used as cathode catalysts for direct methanol fuel cell applications. It is confirmed from literature that supported electro-catalyst gives better performance than bulk unsupported catalyst, and hence, the focus on support material. The support material is required to possess certain properties that will make it a suitable material to be employed as support material for the metal catalyst. Up to now, carbon has been seen as the ideal material for supporting nanosized metallic particles in the electrode for low-temperature fuel cells, such as PEMFC and DMFC. No other materials except carbon material have the essential properties of electronic conductivity, high surface area and the low cost required for the commercialization of fuel cells. Multi-walled carbon nanotubes were, thus, chosen for this study as they possess special properties such as good electronic, physical and mechanical properties which have made them to be proposed as replacement for the traditional carbon black as alternate support for fuel cell catalysts. In addition, literature has revealed that electro-catalyst supported on these materials show improved activity and stability. However, it is well-known that all carbon support materials suffer from corrosion under the operating conditions of the fuel cell, which in due time, leads to performance decrease due to accelerated loss of active surface area of the catalyst. In order to account for the instability of carbon materials, this study chose to investigate the possibility of conductive metal oxides, such as titanium oxide and molybdenum oxide, as support materials for fuel cell electro-catalyst with the main objective of enhancing the durability of the electro-catalyst, as conductive oxides are known to be extremely resistant to corrosion. PtRu and PtSn were chosen as electro-catalysts to examine if they could be methanol tolerant oxygen reduction electro-catalysts for DMFC. Alloying Pt with a second metal, Ru and Sn in the case of this study, was used as it was expected from literature to be able to remove the CO poisoning of the platinum catalyst and, thus, increase

the number of available sites for oxygen reduction, hence the focus on binary electro-catalysts. PtRu and PtSn electro-catalysts were synthesized using the polyol approach as detailed in chapter 3 and supported on MWCNT, TiO_2 and MoO_2 materials followed by heat treating part of the synthesized supported electro-catalysts. Heat treatment was done to improve alloying and to allow for uniform dispersion and stable distribution of the metal on the support and, accordingly, to enhance the electro-catalytic activity and durability of the synthesized catalysts. The MWCNTs were purified and functionalized before using them as support materials and metal oxides were used as received without any further treatment. In addressing the overall objectives, structural attributes of the commercial and home-prepared supported electro-catalysts were evaluated using XRD, HRTEM, HRSEM and EDS for elemental analysis. This was followed by an evaluation of the electro-chemical activities of the supported electro-catalysts using RDE-CV and RDE-LSV. The commercial electro-catalysts used for comparison were Pt/C, PtRu/C and PtSn/C.

A comparison of the commercial acid treated MWCNT was done with the as received commercial MWCNT using XRD, HRTEM and HRSEM. Purity was confirmed, although small amounts of catalysts particles were observed by HRTEM after acid treatment.

XRD revealed that all home-prepared electro-catalysts possessed the face-centred-cubic structure of the poly-crystalline Pt that is similar to that of the commercial electro-catalysts. Peak shifts to higher values and contraction in the lattice parameter for the supported PtRu electro-catalyst were observed, confirming alloying of Ru into the Pt structure, whilst for the supported PtSn electro-catalyst peaks shifted to lower values and the increase in the lattice parameter observed was an indication that Sn formed alloy with Pt. XRD and HRTEM average particle size showed an increase in the particle size after heat treatment for the home-prepared electro-catalyst.

Electro-chemical characterization showed that, in terms of active surface area PtSn/C and Pt/C, commercial catalyst possessed the highest ECSA credited to uniform dispersion and small average particle size. The electro-active surface area of the supported catalyst followed the trend: PtSn/C> Pt/C> PtSn/MWCNT-HT> PtRu/C> PtRu/MWCNT> PtRu/MWCNT-HT> PtSn/MWCNT> PtSn/MoO_2> PtSn/MoO_2-HT> PtRu/MoO_2-HT> PtRu/MoO_2> PtSn/TiO_2-HT> PtSn/TiO_2> PtRu/TiO_2-HT> PtRu/TiO_2. PtSn, therefore, proved to be the most active catalyst of all the supported electro-catalyst. The home-prepared catalysts

supported on multi-walled carbon nanotubes proved to be the most active and this is credited to the support material as MWCNTs are known to possess high surface area and are more electronic conductive than the metal oxide, an indication that the activity of the catalyst is governed by the support material it is dispersed on. Durability studies conducted to examine the stability/longetivity of the fuel cell catalyst, as one of the challenges currently faced with commercialization of DMFC is the durability of the fuel cell catalyst and accordingly the fuel cell system. Commercial catalyst supported on carbon black proved to be the least durable catalysts and this was attributed to the oxidation of the carbon support after long cycles, resulting in the loss of active surface area. It was also observed that the binary catalysts are more stable than the mono-metallic platinum, proving that alloying platinum with the second metal improves the stability of the catalyst. Catalyst supported on multi-walled carbon nanotubes and titanium oxide proved to be more durable, an indication of the stability of the support materials. The extent of CO poisoning was shown in mass and specific activities of Pt/C, PtSn/MWCNT-HT and PtRu/MoO_2 electro-catalyst. All other supported electro-catalyst showed higher mass and specific activities in the presence of methanol, as a result of the presence of the second metal promoting CO and therefore creating more active sites for oxygen reduction. This showed that the catalysts are methanol tolerant as well as being active in catalyzing the oxygen reduction reaction.

This study has observed that the same catalyst prepared using the same method, will behave differently in same chemical environment as it is influenced by the support material it is dispersed on. Therefore, support materials have been observed, in this study, to play a huge role since they influence the activity and durability of the catalyst. The final conclusion drawn from this study is that MWCNT proved to be the best support material since catalysts supported on them showed activity in acid electrolytes and, in addition to this, they showed more stability than commercial catalysts supported on carbon black [1-133].

This study recommends therefore, that the home-prepared catalyst supported on multi-walled carbon nanotubes should be used as methanol tolerant oxygen reduction catalyst as they show both activity and durability. Heat treatment of the catalyst for ORR is also recommended as it improves the activity of the synthesized catalysts. Catalysts supported on titanium oxide show that they are more stable than commercial catalysts. However, their activity was not impressive, to the extent that it is recommended that titanium oxide should be used to modify

the carbon-based support material, with the overall objective of enhancing the durability of the fuel cell catalyst. MoO_2 is hereby recommended to be used as a co-catalyst more than being used as just support material because of its low surface area. Therefore, in terms of reducing the metal loading of the expensive platinum, the molybdenum oxide is not the support material of choice as this study discovered that more of the platinum salt had to be used when supporting on molybdenum during synthesis. Further studies are also recommended on the role of supporting materials as these materials have great influence on the cost, activity and durability of the fuel cell catalyst and, accordingly, the fuel cell system.

BIBLIOGRAPHY

1. A.B. Stambouli, Fuel cells: *The expectations for an environmental-friendly and sustainable source of energy*. Renewable and Sustainable Energy Reviews 2011. **15**: p. 4507-4520.
2. A. Midilli, I. Dincer, M. Ay, *Green energy strategies for sustainable development*. Energy Policy 2006. **34**: p. 3623-3633
3. S.J. Davis, K. Caldeira, and H.D. Mathews, *Future CO_2 Emissions and Climate Change from Existing Energy Infrastructure.*Science 2010. **329**: p. 1330-1333
4. J.A. Turner, *A Realizable Renewable Energy Future*. Science 1999. **285**: p. 687-689
5. N. Lior, *Energy resources and use: The present situation and possible paths to the future*. Energy 2008. **33**: p. 842-853
6. A. Kirubakuran, S. Jain, R.K. Nema, *A review on fuel cell technologies and power electronic interface*. Renewable and Sustainable Energy Reviews 2009. **13**: p. 2430-2440
7. *Benefits of fuel cell technology*. 11th August 2013]; Available from www.altenergy.org/renewables/fuel.cells.html
8. T.S Zhao, W.W. Yang, R. Chen, Q.X. Wu, *Towards operating direct methanol fuel cells with highly concentrated fuel*. Journal of Power Sources 2010. **195**: p. 3451-3462
9. H. Liu, C. Song, L. Zhang, J. Zhang, H. Wang, D.P. Wilkinson, *A review of anode catalysis in the direct methanol fuel cell.* Journal of Power Sources 2006. **155**: p. 95-110
10. T.S. Zhao and C.Xu, *Direct Methanol Fuel Cell:Overview Performance and Operational Conditions © 2009.* Elseiver B.V.
11. V.A. Paganin, E. Sitta, T. Iwasita and W. Vielstich, *Methanol crossover effect on the cathode potential of a direct PEM fuel cell*. Journal of Applied Electrochemistry 2005. **35**: p. 1239-1243
12. R.Z. Jiang, D.Y. Chu, J. Electrochem.Soc. 2007 **147**: p. 4605
13. P. Convert, C. Coutanceau, F. Claguen, C. Lamy. Journal of Appl. Electrochem. 2001 **31**: p. 945
14. T.J. Schmidt, U.A. Paulus, H.A. Gasteiger, N. Alonso-Vante, R.J. Behm, J. Electrochem. Soc. 2000 **147**: p. 2620
15. M. Bron, P. Bagdanoff, S. Fiechter, M. Hilgendorff, J. Electro-anal. Chem. 2001 **517**: p. 85
16. D.J. You, K. Kwan, C. Pak, H. Chang, *Platinum-antimony tin oxide nanoparticle as cathode catalyst for direct methanol fuel cell*. Catalysis Today 2009 **146**: p. 15-19
17. W. Yuan, K. Scott, H. Cheng. J. Power Sources 2006 163: p. 323
18. S. Siracusano, A. Stassi, V. Baglio, A.S. Aricó, F. Capitanio, A.C. Tavares, *Investigation of carbon supported Pt and PtCo catalysts for oxygen reduction in direct methanol fuel cells*. Electrochimica Acta 2009 **54**: p. 4844-4850
19. E. Antolini, *Review: Carbon Supports for low-temperature fuel cell catalysts*. Applied Catalysis B: Environmental 2009. **88**: p. 1-24

20. E. Antolini, E.R. Gonzalez, *Ceramic materials as supports for low-temperature fuel cell catalyst*. Solid State Ionics 2009. **180**: p. 746-763
21. Z. Liu, F. Peng, H. Wang, H. Yu, C. Chen, Q. Shi, *Design of Pt catalyst with high electrocatalytic activity and well tolerance to methanol for oxygen reduction in acidic medium*. Catalysis Communications 2012. **29**: p. 11-14
22. S.B. Yoon, B. Fang, M. Kim, J.H. Kim, and J.S Yu, *Nanostructured Supported Catalysts for Low-Temperature Fuel Cells*. Nanostructured Materials 2009. Chapter 4: p. 173-231.
23. C. Jehabharathi, P. Venkateshkumar, J. Mathiyarasu, K.L.N. Phani, *Platinum-tin bimetallic nanoparticles for methanol tolerant oxygen-reduction activity*. Electrochimica Acta 2008. **54**: p. 448-454
24. *History of fuel cells*. 05th May 2013]; Available from http://www.sae.org/fuel cells/fuel cells-history.htm
25. A.J. Appleby, *FUEL CELLS – OVERVIEW*. Elsevier B.V. © 2009
26. V. Ramani, *Fuel cells*. The Electrochemical Society Interface 2006.
27. Sir William Grove gaseous voltaic battery; Available from https://www.google.co.za
28. H.A. Gasteiger, S.S. Kocha, B. Sompappli, and F.T. Wagner. App.Catal.B-Environ. 2005. **56**: p.9
29. Fuel cells 2000-benefits. 11th August 2013]; Available from www.fuelcells.org/base.cgim?template=benefits
30. *Collecting the history of fuel cells*. Last updated December 2005]; Available from http://american history.si.edu/fuel cells/index.htm.
31. A. Kirubakaran, S. Jain, R. K. Nema, *A review on fuel cell technologies and power electronic interface.* Renewable and Sustanable Energy Reviews 2009. **13**: p. 2430-2440.
32. Basic fuel cell diagram]; Available from http://www.google.com
33. *Benefits of fuel cell technology*. 11th August 2013]; Available from www.altenergy.org/renewables/fuel.cells.html
34. M. Farooque, HC. Maru, *Fuel cells- the clean and efficient power generators*. IEEE. Proc. 2001. **89**: 1819-1829
35. U.S. Department of Energy. *Fuel cell hand book,* 7th ed., West Virginia: Office of Fossil fuel, National Energy Technology Laboratory; October 2000.
36. JB. O'Sullivan, Fuel cells in distributed generation. IEEE. Proc. 1999. p. 568-572
37. G. Coors W. Protonic, *Ceramic fuel cells for high efficiency operation with methane*. J. Power Sources 2003. p. 150-156.
38. KE. Swider-Lyons, RT. Carlin, RI. Rosenfeld, RJ. Nowak, *Technical issues and opportunities for fuel cell development for autonomous underwater vehicles*. In: Proceedings of the 2002 workshop on autonomous underwater vehicle. 2002. p. 61-64
39. N.S. Rosenthal, S.A. Vileka, R. Datta, *A comprehensive yet comprehensible analytical model for the direct methanol fuel cell*. Journal of Power Sources 2012. **206**: p. 129-143
40. T. S. Zhao, C. Xu, R. Chen, W. W. Yang, *Mass transport phenomena in direct methanol fuel cells*. Progress in Energy and Combustion Science 2009. **35**: p. 275-292
41. T. Maiyalagan, S. Pasuphathi, *Components for PEM fuel cells: An overview*; Materials Science Forum 2010. **657**: p.143 189;
42. H. Y. Yana, J. Inukai, H. Uchida, M. Watanabe, P.K. Babu, T. Kobayashi, J.H. Chung, E. Oldfield, A. Wieckowaki, Phys. Chem. Chem. Phys. 2006. **8**: p. 4932-493

43. S.S. Kocha, Chapter 3 – *Electrochemical Degradation: Electrocatalyst and Support Durability. Polymer Electrolyte Fuel Cell Degradation*. 2012 p. 89-214
44. G. Q. Lu and C. Y. Wang, *"Electrochemical and flow characterization of a direct methanol fuel cell"*. Journal of Power Sources 2004.**134**: p.33-40
45. K. Sundmarcher, T. Schultz, S. Zhou, K. Scott, M. Ginkel, and E. D. Giles, *"Dynamics of direct methanol fuel cell: experiment and model- based analyses".* Chemical Engineering Science 2001. **56**: p. 333-341
46. JH. Han and HT. Liu, *Real time measurements of methanol crossover in a DMFC*, Journal of Power Sources 2007. **164**: p.166-173
47. X. Ren, TE. Springer, S. Gottesfeld, *Water and methanol uptakes in Nafion membranes and membrane effects on direct methanol cell performance*. J. Electrochem. Soc. 2000.**147**: p. 92-98
48. JG. Liu, TS. Zhao, ZS. Liang, R. Chen, *Effect of membrane thickness on the performance and efficiency of passive direct methanol fuel cells*. J. Power Sources 2006.**153**: p. 61-67
49. J.B. Fernandas, Electrocatalysis, Department of Chemistry, University of Goa, Goa
50. H. Liu, C. Song, L. Zhang, J. Zhang, H. Wang, D.P. Wilkinson, *A review of anode catalysis in the direct methanol fuel cell*; Journal of Power Sources 2006.**155**: p. 95-110
51. C. Nitin, H. Bagkar, M. Chen, H. Parab, and R.S Liu, *Nanostructured Electrocatalyst Synthesis: Fundamental and Methods*. Published online 12th October 2009. Wiley-VCH Verlag GmbH & Co. KGaA
52. A.Vante, N. Cattarin, S. and Musian, M. Journal of Electroanalytical Chemistry 2000. **481**: p. 200-207
53. H. Liu, C. Song, L. Zhang, J. Zhang, H. Wang, D.P. Wilkinson, *A review of anode catalysis in the direct methanol fuel cell*. Journal of Power Sources 2006.**155**: p. 95-110
54. S. K. Kamarudin, F. Achmad, W. R. W. Daud, *Overview on the application of direct methanol fuel cell (DMFC) for portable electronic devices*. International Journal of Hydrogen Energy 2009. **34**:p. 6902-6916
55. D.H Lim, D.H Choi, W.D Lee, H.I Lee, *A new synthesis of highly dispersed and CO tolerant PtSn/C electrocatalyst for low-temperature fuel cell; its electrocatalytic activity and long term durability*. Applied Catalysis B: Environmental 2009. **89**:p. 484-493
56. T. Toda, H. Igarashi, M. Watanabe, *Enhancement of the electrocatalytic O_2 reduction on the Pt-Fe alloys*. Journal of Electroanalytical Chemistry 1999. **460**: p. 258-262
57. SH Bergens and MEP Markiewicz, University of Alberta, Edmonton, AB, Canada; Cathodes. Elsevier B.V. 2009
58. S.Y. Huang, P. Ganesan, B.N. Popov, *Titania supported platinum catalyst with high electroacatalytic activity and stability for polymer electrolyte membrane fuel cell*. Applied Catalysis B: Environmental 2011. **102**: p. 71-77
59. R. Balgis, G.M. Anilkumar, S. Sago, T. Ogi, K. Okuyama, *Nanostructured design of electrocatalyst support material for high-performance PEM fuel cell application*. Journal of Power Sources 2012 **203**: p. 26-33
60. J.H. Kim, B. Pang, M. Kim, J.S Yu. Catal. Today 2009 **146**: p. 25-30
61. JH. Han and HT. Liu, *Real time measurements of methanol crossover in a DMFC*, Journal of Power Sources 2007. **164**: p.166-173

62. S. Mukerjee, S. Srinvasan, M. P. Soriage. Journal of Physical Chemistry 1995. **99**:p. 4577-4589
63. S. Koh, M.F Toney and P.Strasser. Electrochim.Acta 2007. **52**:p. 2765
64. T. Toda, H. Igarashi, H. Uchida and M. Watanabe. J. Electrochem. Soc. 1999. **146**: p. 3750
65. M.T. Paffet, J.G. Berry and S. Gottesfield. J. Electrochem. Soc. 1988. **135**: p. 1431
66. A.A. Gerwith and M.S. Thorum; "*Electroreduction of Dioxygen for Fuel-Cell Applications: Materials and Challenges"*; Inorg.Chem 2010. **49**: p. 355
67. N. Tsiouvaras, M. A. Peńa, J. L. G. Fierro, E. Pastor, M. V. Martìnez-Huerta, *The effect of Mo precursor on the nanostructure and activity of PtRuMo electrocatalysts for proton exchange membrane fuel cell*, Catalysis Today 2010. **158**: p.12-21
68. M.M.P. Janssen, J. Moolhuysen; Electrochim. Acta 1976. **21**: p.861
69. A.S. Arico, V. Antonucci, N. Giordano, A.K. Shukla, M.K. Ravikumar, A. Roy, S.R. Barman and D.D. Sarma. J. Power. Sources 1994. **50**: p. 295
70. F. Colmati, E. Antolini, E.R. Gonzalez; Electrochim. Acta 2005. **50**: p.5496
71. Y. Takasu, T. Fujiwara, Y. Murakimi, K. Sasaki, M. Aguri, T. Asaki, W. Sugimota. J. Electrochem. Soc. 2000. **147**: p. 4421-4427
72. S. Sharma, B.G. Pollet, *Supported materials for PEMFC and DMFC electrocatalysts - A review*. Journal of Power Sources 2012. **208**: p. 96-119
73. M. Watanabe, M. Uchida, S. Motoo; J. Electroanal.Chem. 1987. **229**: p. 395-406
74. Z. Liu, J.Y. Lee, M. Han, W. Chen, L.M. Gan; J. Mater. Chem. 2002. **12**: p. 2453-2458
75. C.M Chen, M. Chen, Y.W. Peng, H.W. Yu, C.F. Chen, *High efficiency microwave digestion of multi-walled carbon nanotubes synthesized by thermal chemical vapour deposition.* Thin Solid Films 2006. **498**: p. 202-205
76. K.T Jeng, C.C Chien, N.Y. Hsu, S.C. Yern, S.D Chiou, S.H. Lin, W.M Huang, Performance of direct methanol fuel cell using carbon nanotube supported PtRu anode catalyst with controlled composition. Journal of Power Sources 2006.**160**: p. 97-10
77. S. Rojas, F.J. Garcia, S. Jaras, M.V. Huerta, J.L.F. Fierro, M. Boutonnet. Appl. Catal. A: Gen. 2005. **285**: p. 24-35
78. R.P. Raffaelle, B.J. Landi, J.D. Harris, S.G. Bailey, A.F. Hepp, *Carbon nanotubes for power applications*. Material Science and Engineering B 2005. **116**: p. 233-243
79. E. Antolini, E.R. Gonzalez, *Ceramic materials as supports for low-temperature fuel cell catalyst*. Solid State Ionics 2009. **180**: p. 746-763
80. S. Maass, F. Finsterwalder, G. Frank, R. Hartmann, C. Merten, *Carbon support oxidation in PEM fuel cell cathodes*. Journal of Power Sources 2008. **176**: p. 444-451
81. F. Rodrìguez-Reinosa, Carbon 1998. **36**: p.159-175
82. F. Danafar, A. Fakhrúl-Razi, M.A.M Salleh, D.R.A. Biak, *Fluidized bed catalytic chemical vapour deposition synthesis of carbon nanotubes - A review*. Chemical Engineering Journal 2009. **155**: p. 37-48
83. H. Lv, N. Cheng, S. Mu, M. Pani, *Heat-treated multi-walled carbon nanotubes as durable supports for PEM fuel cell catalysts*; Electrochimica Acta 2011. **98**: p. 736-742
84. C. Song and J. Zhang, *Electrocatalytic Oxygen Reduction Reaction*
85. C.J. Tseng, S.T. Lo, S.C. Lo, P.P. Chu, *Characterization of Pt-Cu binary catalysts for oxygen reduction for fuel cell applications*. Materials Chemistry and Physics 2006. **100**: p. 385-390

86. B.L. Dutrow, C.M. Clark. X-ray Powder Diffraction (XRD); Geochemical Instrumentation and Analysis Available at serc.carleton.edu/research_education/geochemsheet/techniques/XRD.html
87. S.M.S. Kumar, N. Hidyatai, J.S. Herero, S. Irusta, K. Scott, *Efficient tuning of the Pt nano-particles mono-dispersion on Vulcan XC-72R by selective pre-treatment and electrochemical evaluation of hydrogen oxidation and oxygen reduction reactions*. International Journal of Hydrogen Energy 2011. **36**: p. 5453-5465
88. X. Tang, B. Zhang, Y. Li, Y. Xu, Q. Xin, W. Shen, *Structural features and catalytic properties of Pt/CeO_2 catalyst prepared by the modified reduction-deposition techniques*. Catal. Lett 2004. **97**: p. 163-169
89. Y.C. Chiang, W.H. Lin, Y.C. Chang, *The influence of treatment duration on multi-walled carbon nanotubes functionalized by H_2SO_4/HNO_3 oxidation*. Applied Surface Science 2011. **257**: p. 2401-2410
90. S. Bruckenstein and B. Miller, *Unraveling reactions with rotating electrodes*. Acc.Chem.Res 1977. **10**: p. 54.61
91. "*Crystallite Size and Microstrain Analysis of Thin Films"*2005. Available at http://www.rigakumsc.com/contract/amia_res_TN-C01.htm
92. *Basics of X-ray Diffraction*: Chapter 7. Available at epswww.unm.edu/xrd/xrdbasics.pdf
93. R. Jenkins, J.L. de Vries., An Introduction to X-Ray Powder Diffractometry, Eindhoven, N.V. Philips Gloeilampenfabrieken, **2**:p. 8-10
94. H. Lipson, H. Steeple. Interpretation of X-ray Powder Diffraction Patterns; Lond, Macmillan and Company Ltd. 1970 **4**: p. 93-94, **5**: p.113-114
95. B.D. Cullity. Elements of X-ray Diffraction, 2nd Edition, Ontario, Addison-Wesley Publishing Company Inc. 1978. **7**: p. 188-226
96. *Electron microscope*- Ask.com Encyclopedia last modified on 20 July 2013 available at www.dstuns.iitm.ac.in/microscopy-instruments.php
97. Spence, John C.H. (1988) [1980]. *Experimental high resolution electron microscopy*. New York: Oxford U. Press. ISBN 0-19-505405-9
98. J. Prabhuram, T.S. Zhao, C.W. Wong, J.W. Guo. Journal of Power Sources 2004. **134**:p. 1-6
99. *High resolution electron microscopy (HRTEM)* available at http://en.wilkepedia.org/wiki/Transmissionelectronmicroscope
100. E. Suzuki, *"High-resolution scanning electron microscopy of immunogold-labelled cells by the use of thin plasma coating of osmium".* Journal of Microscopy 2002. **208**: p.153-157
101. *High resolution scanning electron microscopy (HRSEM)* available at http://en.wilkepedia.org/wiki/Scanningelectronmicroscope
102. E.S. Steigertwalt, G.A. Deluga, D.E. Cliffel, C.M. Lukewart. Journal of Physical Chemestry 2001. **105**: p. 8097-8101
103. Y. Garsany, O.A. Baturina, K.E. Swider-Lyons, S.S. Kocha, *Experimental Methods for Quantifying the Activity of Platinum Electrocatalysts for the Oxygen Reduction Reaction*. Analytical Chemistry 2010. **82**: p. 6321-6328
104. S.S. Kocha, Y. Garsany, D. Myers, *Testing Oxygen Reduction Reaction Activity with the Rotating Disc Electrode Technique*. 12th March 2013. Available at https://www1.eere.energy.gov.hydrogenandfuelcells/webinars.html

105. T.D. Jarvi, E.M. Stuwe, *Fundamental Aspects of Vacuum and Electrocatalytic Reactions of Methanol and Formic Acid on Platinum Surfaces*. Electrocatalysis, J. Lipkowski, P.N. Ross Jr. (Editors), New York, Wiley-VCH Inc. 1998. **3**: p. 75-153
106. S.K. Kamarudin, N. Hashim, *Materials, morphology and structures of MEAs in DMFCs*. Renewable and Sustainable Energy Reviews 2012.**16**: p. 2494-2515
107. I. Takahashi, S.S. Kocha, *Examination of the activity and durability of PEMFC catalysts in liquid electrolytes*. Journal of Power Sources 2010.**195**: p. 6312-6322
108. C.M Chen, M. Chen, Y.W. Peng, H.W. Yu, C.F. Chen, *High efficiency microwave digestion of multi-walled carbon nanotubes synthesized by thermal chemical vapour deposition*. Thin Solid Films 2006. **498**: p. 202-205
109. J. Chen, Q. Chen, Q. Ma, *Influence of surface functionalization via chemical oxidation on the properties of carbon nanotubes*. Journal of Colloid and Interface Science 2012. **370**: p. 32-38
110. C.T. Hsieh, J.Y. Lin, S.Y. Yang, *Carbon nanotubes embedded with PtRu nanoparticles as methanol fuel cell electrocatalysts*. Physica E 2009. **41**: p. 373-378
111. N.Y. Hsu, C.C. Chien, K.T. Jeng, *Characterization and enhancement of carbon nanotube-supported PtRu electrocatalyst for direct methanol fuel cell applications*. Applied Catalysis B: Environmental 2008. **84**: p. 196-203
112. E. Yoo, T. Okada, T. Kizuka, J. Nakamura, *Effect of carbon substrate material as a Pt-Ru catalyst support on the performance of direct methanol fuel cells*. Journal of Power Sources 2008. **180**: p. 221-226
113. G. An, P. Yu, L. Mao, Z. Liu, S. Miao, Z. Miao, K. Ding, *Synthesis of PtRu/carbon nanotube composite in supercritical fluid and their application as an electrocatalyst for direct methanol fuel cells*. Carbon 2002. **45**: p. 536-542
114. C.T. Hsieh, J.Y. Lin, S.Y. Yang, *Carbon nanotubes embedded with PtRu nanoparticles as methanol fuel cell electrocatalysts*. Physica E 2009. **41**: p. 373-378
115. W.Z. Li, C.H. Liang, WJ. Zhou, JS. Qiu, ZH. Zhou, GQ. Sun et al. *Preparation and characterization of multiwalled carbon nanotubes supported platinum for cathode catalysis of direct methanol fuel cells*. J. Phy. Chem. B 107 (2003) 6292-6299
116. S. Kim, H.J. Sohn, S. Park, *Preparation and characterization of carbon-related materials supports for catalysts of direct methanol fuel cells*. Current Applied Physics 2010. **10**: p.1142-1147
117. M. Williams, L. Khotseng, Q Naidoo, L. Petric, A. Nachaev, V. Linkov, *Applicability of analytical protocols for the characterisation of carbon-supported platinum group metal fuel cell electrocatalysts*. South African Journal of Science 2009. **105**: p. 285-289
118. M. Carmo, A.R. dos Santos, J.G.R. Poco, M. Linardi, *Physical and electrochemical evaluation of commercial carbon black as electrocatalysts supports for DMFC applications*. Journal of Power Sources 2007. **173**: p. 860-866
119. A.L. Ocampo, M. Miranda-Hernández, J. Morgado, J.A. Montaya, P.J. Sebastian, *Characterization and evaluation of Pt-Ru catalyst supported on multi-walled carbon nanotubes by electrochemical impedance*. Journal of Power Sources 2006. **160**: p. 915-924
120. J. Prabhuram, T.S. Zhao, Z.X. Liang, R. Chen, *A simple method for the synthesis of PtRu nanoparticles on the multi-walled carbon nanotube for the anode of a DMFC*. Electrochimica Acta 2007**. 52**: p. 2649-2656

121. E. Antolini, J.R.C. Salgado, E.R. Gonzalez, *Carbon supported Pt75M25 (M= Co, Ni) alloys as anode and cathode electrocatalysts for direct methanol fuel cells*. Journal of Electroanalytical Chemistry 2006. **580**: p.145-154

122. A.O. Neto, T.P.R. Vasconcelos, R.W.R.V. Da Silva, M. Linardi and E.V. Spinace, *Electro-oxidation of ethylene glycol on PtRu/C and PtSn/C electrocatalysts prepared by alcohol-reduction process*. Journal of Applied Electrochemistry 2005. **35**: p. 193-198

123. M. Zhu, G. Sun, Q. Xin, *Effect of alloying degree in PtSn catalyst on the catalytic behaviour for ethanol electro-oxidation*. Electrochimica Acta 2009. **54**: p. 1511-1518

124. D.M. Han, Z.P. Gao, R. Zeng, C.J. Kim, Y.Z. Meng, H.K. Liu, *Multiwalled carbon nanotube-supported Pt/Sn and Pt/Sn/PMo12 electrocatalysts for methanol electro-oxidation*. International Journal of Hydrogen Energy 2009. **34**: p. 2426-2434

125. Y. Shao, G. Yin, Y. Gao, *Understanding and approaches for the durability issues of Pt-based catalyst for PEM fuel cell*. Journal of Power Sources 2007. **171**: p. 558-566

126. H. Li, G. Sun, L. Cao, L. Jiang, Q. Xin, Comparison of different promotion effect of PtRu/C and PtSn/C electrocatalysts for ethanol electro-oxidation. Electrochimica Acta 2007. **52**: p. 6622-6629

127. S.Y. Huang, P. Ganesan, B.N. Popov, *Titania supported platinum catalyst with high electrocatalyst activity and stability for polymer electrolyte membrane fuel cell*. Applied Catalysis B: Environmental 2011. **102**: p. 71-77

128. V.A. Paganin, E. Sitta, T. Iwasita and W. Vielstich, *Methanol crossover effect on the cathode potential of a direct PEM fuel cell*. Journal of Applied Electrochemistry 2005. **35**: p. 1239-1243

129. J. Cho, W. Roh, D. Kim, J. Yoon, J. Choy, H. Kim. J. Chem. Soc. Faraday Trans 1998 **94**: p. 2835

130. E. Antolini, T. Lopez, E.R. Gonzalez, *Review- An overview of platinum-based catalysts as methanol resistant oxygen reduction materials for direct methanol fuel cells*. Journal of Alloys and Compounds 2008 **461**: p. 253-262

131. T. Iwasita, Electrochim. Acta2002 **47:** p. 3663.

132. N.M. Markovic, H.A. Gasteiger, P.N. Ross, X. Jiang, I. Villegas, M.J. Weaver, Electrochim. Acta1995 **40** p. 91.

133. P.A. Christensen, A. Hamnett, G.L. Troughton, J. Electroanal. Chem.1993 **362:** p. 207.

134. N. Jung, Y.H. Cho, M. Ahn, J.W. Lim, Y.S. Kang, D.Y. Chung, J. Kim, Y.H. Cho, Y.E. Sung, *Methanol-tolerant cathode electrode structure composed of heterogeneous composites to overcome methanol crossover effects for direct methanol fuel cell*. Inernational Journal of Hydrogen Energy 2011. **36**: p. 15731-15738